Remotely Activated Microcapsules for Oil Recovery Treatments

Mazurek, Malgorzata Natalia; Skov, Anne Ladegaard; Hvilsted, Søren

Publication date:
2016

Document Version
Publisher's PDF, also known as Version of record

Remotely Activated Microcapsules for Oil Recovery Treatments

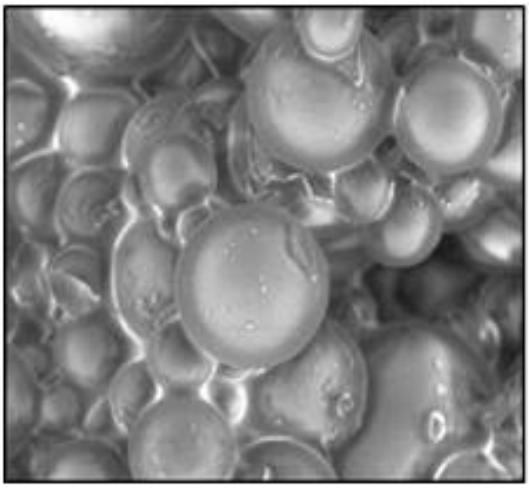

Malgorzata Kostrzewska

PhD Thesis

October 2016

DTU Chemical Engineering
Department of Chemical and Biochemical Engineering

Remotely Activated Microcapsules for Oil Recovery Treatments

Malgorzata Kostrzewska **October 2016**

Supervisor: Anne Ladegaard Skov

Co-supervisor: Søren Hvilsted

PhD Thesis

Danish Polymer Centre, DTU, Kgs.Lyngby

DTU Chemical Engineering
Department of Chemical and Biochemical Engineering

Preface

The work presented in this Ph.D. dissertation was carried out at the Danish Polymer Centre, Department of Chemical and Biochemical Engineering, Technical University of Denmark, between 15th of September 2013 and 15th of September 2016. The financial support of Mærsk Oil and Gas, Qatar is highly acknowledged.

First and foremost I would to thank my supervisor Anne Ladegaard Skov for being a real mentor during these years. I would like to thank you for encouraging my research and for your continuous support. I would also like to thank my co-supervisor Søren Hvilsted for his insightful comments and valuable advices.

My sincere thanks also go to Lidia Gonzalez for introducing me to a research world and to a DPC family. I am grateful for her guidance and friendly attitude. I am also indebted to Kim Chi Szabo, Irakli Javakhishvili and Liyun Yu for their assistance in the lab.

I am very thankful to my officemates. Working with you was a great experience. I enjoyed our meetings and discussions, and most of all your positive energy, which made DPC a great place to work.

A special thanks to my family and my friends. Words cannot express how grateful I am for your patience and support. This thesis would have never been possible without my loving husband Piotr - you were always around at times I thought that it is impossible to continue and you helped me to reach my goals - thank you.

Malgorzata Kostrzewska

October 2016
Kgs. Lyngby

Abstract

Water-flooding is a commonly used oil recovery method in mature reservoirs, because injected water enhances oil sweep efficiency and leads to increased oil production. Due to the occurrence of fractures in water-flooded reservoirs, excessive water production is observed. Hence, water shut-off treatments are extensively investigated, though currently applied materials still suffer from some disadvantages. The main drawback is lack of control over the setting of plugs in the fracture, and this may cause blocking of the injection well and the formation of the plug before placing the material in the fracture. Secondly, only a few developed materials prevent from blocking oil-rich pores, and yet they are not able to create a permanent plug, as they do not form a covalently bonded structure.

The aim of the project is to design a novel plugging material which can block fractures without affecting the pores and ensure permanent water shut-off treatment. To eliminate the danger of premature plug formation, stimulus-responsive materials were investigated. Considering that fractures are extremely hard-to-access places, the designed material should respond to a remotely applied stimulus, in order to achieve better control over plug formation.

The developed material consists of vinyl-functional polydimethylsiloxane (PDMS) microparticles and microcapsules with an encapsulated PDMS cross-linker. Due to reactions between the released cross-linker and vinyl groups on the PDMS microparticles' surface, a covalently bonded elastomer plug is formed. The size of both components is adjusted to allow for creating the plug without affecting the pores. Control over cross-linking is achieved through an encapsulation process. Microcapsules prepared via a phase separation method are impermeable at 50°C, thereby eliminating premature plug formation. It is shown that after heating microcapsules to 120°C, the cross-linker is released from a poly(methyl methacrylate) (PMMA) shell. Moreover, gamma irradiation of the microcapsules decreases the T_g of the polymeric shell, changing the permeability of the microcapsules. Due to the irradiation process, microcapsules become permeable at lower temperatures, and a remotely applied activation has been achieved. Applying the alternating magnetic field (AMF) was another activation method investigated as part of this research. Magnetic nanoparticles, which generate heat on exposure to the AMF, were encapsulated successfully within the polymeric shell, and as a result, heating microcapsules when they are subjected to the AMF is possible. As an alternative to remote activation methods, solvent-flushing was examined, allowing for an investigation into the plug being cross-linked under high-pressure. Compressed material created a uniform, void-less structure capable of withstanding harsh conditions in reservoirs.

Resume på dansk

Typisk benyttes kunstig vandoversvømmelse til at udvinde olie i modne reservoirer, da det injicerede vand forøger effektiviteten af oliefejningen og dermed leder til en øget olieproduktion. På grund af det tilstedeværelse af diverse frakturer i disse vandoversvømmede reservoirer bliver der produceret store mængde vand. Derfor undersøges der vidt spredt såkaldte water shut-off behandlinger ved hjælp af dannelse af kunstige propper i reservoiret. Ulempen ved disse behandlinger er som regel manglen på kontrol over hvor proppen sætter sig. Dette kan forårsage blokering af injektions-brønden eller også kan en præmatur prop dannes før frakturen. Desuden er det kun en fraktion af disse udviklede materialer, der ikke ligeledes blokerer olierige porer, og som hovedregel er de ikke baseret på kovalente bindinger.

Formålet med dette projekt er at designe et nyt propmateriale der kan blokere frakturer uden at influere porerne og sikre permanent water shut-off behandling. For at eliminere faren for præmatur propdannelse er stimulus-responderende materialer undersøgt. Taget i betragtning at frakturer findes i ekstremt utilgængelige områder, er det nødvendigt at materialet responderer på et fjernstyrnet stimulus for at have fuld kontrol over propdannelsen.

Det udviklede materiale består af vinyl-funktionel polydimetylsiloxan (PDMS) mikropartikler og mikrokapsler med en indkapslet PDMS krydsbinder. På grund af reaktionen mellem frigiven krydsbinder og vinylgrupperne på mikropartiklernes overflade dannes der en kovalent bundet elastomer-prop. Størrelsen af begge komponenter kan justeres for at tillade dannelsen af en prop, der ikke kan sætte sig i porerne. Kontrol over krydsbindingen opnås ved hjælp af indkapsling. Mikrokapsler fremstillet via faseseparation er uigennemtrængelige ved 50°C, og dermed kan der ikke dannes en prop. Når kapslerne opvarmes til 120°C, så frigives krydsbinderen fra poly(metyl metakrylate) (PMMA) kapslen. Ydermere kan gammastråling også bruges til at sænke glasovergangstemperaturen af kapslen og dermed ændre permeabiliteten af kapslen. Dette kan gøres fjernstyret. En anden metode til fjernstyret control er alternerende magnetfelt (AMF), som også er undersøgt i dette projekt. Magnetiske nanopartikler, som danner varme under et AMF, blev succesfyldt indkapslet i polymerkapslen, og som et resultat deraf blev det muligt at opvarme blandingen via AMF. Som et alternativ til fjernstyret aktivering blev solvent-oversvømmelse undersøgt, og betingelserne i frakturen blev efterlignet, hvormed det viste sig, at en komprimeret, krydsbunden prop blev dannet, som kunne modstå de skrappe betingelser i oliebrønden.

Abbreviations and symbols

AMF	Alternating magnetic field
APG	Aluminum phosphate gel
ATR-FTIR	ATR Fourier transform infrared spectroscopy
cSt	Centistokes
DBP	Dibutyl phthalate
DCM	Dichloromethane
DP	Degree of polymerisation
bpd	Barrels per day
DSC	Differential scanning calorimetry
EOR	Enhanced oil recovery
G’	Storage modulus
G’’	Loss modulus
HPAM	Hydrolysed polyacrylamide
MMA	Methyl methacrylate
MNP	Magnetic nanoparticles
mT	Militesla
NMR	Nuclear magnetic resonance
PAM	Polyacrylamide
PDMS	Poly(dimethylsiloxane)
PDI	Polydispersity index
PMAA	Poly(methacrylic acid)
PMMA	Poly(methyl methacrylate)
PPG	Preformed polymer gel
ppm	Parts per million
PVA	Poly(vinyl alcohol)
r	Stoichiometric imbalance
rpm	Rotations per minute
RT	Room temperature
SEC	Size exclusion chromatography
SEM	Scanning electron microscopy
SDS	Sodium dodecyl sulfate
TGA	Thermogravimetric analysis
THF	Tetrahydrofuran

Thesis structure

Objectives

The aim of this PhD project is to obtain and activate microcapsules with an encapsulated PDMS cross-linker in order to establish an elastomer plug for blocking of fractures in oil reservoirs. The encapsulation allows for a controlled reaction between the cross-linker and reactive microparticles. Occurrence of the fractures significantly decreases oil production due to extensive water production while applying water-flooding treatment. Currently employed materials do not guarantee permanent and selective blocking of the fracture (e.g. without affecting oil-rich regions) as well as their formation cannot be remotely controlled.

A novel elastomer plug, which is the result of the reaction between microcapsules with a hydride PDMS cross-linker and vinyl-functional PDMS microparticles, ensures permanent and selective blocking of the fractures in a controllable manner. Due to reaction between released cross-linker and the vinyl-functional PDMS microparticles, a covalently bonded plug is formed and partially shuts off the water flow. Thus, the extensive water production in the oil reservoir is eliminated. Microencapsulation of the cross-linker gives the control over the formation of plug, because the cross-linker is released only after activation of the microcapsules. Considering that fractures are hard-to-reach places, this work focuses on developing remotely applicable activation methods such as gamma irradiation and magnetic activation. Additionally, application of the ultrasound waves and so-called solvent-flushing activation were tested as alternative activation methods. For instance, the solvent-flushing activation allowed for obtaining cross-linked material under high pressure and a structure of the plug could be examined.

In this study, microcapsules with encapsulated PDMS cross-linker were prepared and characterized, as well as various activation methods for the release of the cross-linker from the capsule were examined. Preparation and characterisation of the vinyl-functional PDMS microparticles were done in the first stage of the project (mainly conducted by collaborators), and results are available in literature[1,2,3].

Thesis outline

The thesis is organised as follows. Chapter 2 deals with the preparation and characterisation of the microcapsules as well as optimisation of the phase separation technique utilized to prepare the microcapsules.

In Chapter 3, activation of the microcapsules by gamma irradiation is presented. Additionally, plasticised and fluorinated derivatives of PMMA are investigated as potential shell materials more susceptible to gamma irradiation than the pristine PMMA.

Chapter 4 deals with the so-called 'magnetic activation' of the microcapsules. By means of encapsulation of the magnetic nanoparticles, the microcapsules' shell can be melted when the microcapsules are exposed to the alternating magnetic field.

The topic of Chapter 5 is an investigation of ultrasound waves as an activating stimulus, whereas Chapter 6 describes the solvent-flushing method as a triggering method.

Finally, the conclusions of this thesis and opportunities for future work are discussed in Chapter 7.

The thesis is based on the manuscripts listed below, which can be found in the following appendices:

Appendices to Chapter 2

L. Gonzalez, M. Kostrzewska, B. Ma, L. Li, J. H. Hansen, S. Hvilsted, A. L. Skov, 'Preparation and Characterization of Silicone Liquid Core/Polymer Shell Microcapsules via Internal Phase Separation', *Macromolecular Materials and Engineering*, **299**, 2014, 1259-1267

Appendices to Chapter 3

M. Kostrzewska, B. Ma, I. Javakhishvili, J. H. Hansen, S. Hvilsted, A. L. Skov, 'Controlled release in hard to access places by poly(methyl methacrylate) microcapsules triggered by gamma irradiation', *Polymers for Advanced Technologies*, **26**, 2015, 1059-1064

1. Introduction

Nowadays, the oil industry needs new technologies in order to increase oil recovery from mature reservoirs. Water-flooded reservoirs suffer from extensive water production, due to the occurrence of fractures. This thesis deals with designing novel plugging materials which can permanently block these fractures and thus lead to increased oil recovery.

The introduction section describes existing problems and provides an overview of currently applied methods in fractured reservoirs. It also describes the need for new technologies. As an answer to this need, our idea is to use a PDMS elastomer material consisting of vinyl-functional PDMS microparticles and an encapsulated cross-linker which reacts with the vinyl groups. Due to the reaction, a strong, elastic network is formed inside the fracture. Remote control over the reaction is achieved due to microencapsulation.

1.1 Oil recovery in fractured reservoirs

Primary oil production methods recover only a small fraction of the oil originally placed in a producing formation, typically ranging from 10% to 25%[4], since reservoir pressure will fall over the lifetime of the well and at some point this pressure will be insufficient to force the oil to the surface. After the natural reservoir drive diminishes, secondary methods must be applied, in which external fluids or gases are injected into an oil field to increase reservoir pressure and displace any remaining oil towards the production well[5,6]. The injection of water, called 'water-flooding', is one of the most commonly used secondary techniques[7]. In general, secondary recovery projects produce an additional 10% to 30% oil. However, in naturally fractured fields, the oil production rate can be significantly decreased[8,9], because the fractures act as fast flow paths for the injected water, which is easily transported to a production well. As a comparison, pore sizes containing oil are estimated to be smaller than 1 μm[10], whereas fracture width, defined as the distance between the fracture walls, usually varies from 1 μm to 4 mm[11]. Fracture lengths range from just a few meters to thousands of meters, depending on the type of rock and reservoir pressure. As a result, the water bypasses oil-rich areas and the oil production rate is decreased. A water-flooding scheme in non-fractured and fractured reservoirs is presented in Figure 1.

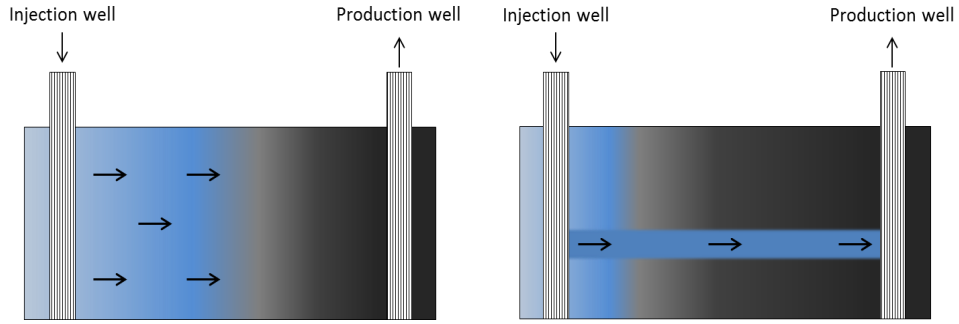

Figure 1. Schematic presentation of the water-flooding method. On the left side, a non-fractured reservoir is presented. Injected water passes through the reservoir uniformly, and due to induced high pressure it pushes out oil from the pores. On the right side, a fractured reservoir is shown. Injected water tends to flow through highly permeable fractures towards the production well, leaving behind unswept oil.

Water content in the producer may reach more than 90% over time[12]. Production costs for one water barrel are the same as for one oil barrel, and the annual costs incurred while disposing of excess water is estimated to be roughly 40 billion dollars worldwide. Therefore, water shut-off treatments need to be applied to maintain high pressure throughout the whole volume of the reservoir. Mostly, it is achieved through the utilisation of chemical methods that rely on injecting chemical materials into the fracture. The injected materials solidify or expand in the fracture, leading to the formation of a physical barrier. The material is pumped into the reservoir through the injection well in the form of a low-viscous aqueous mixture containing the plugging agent. When the fracture is blocked, water cut is eliminated and the oil recovery rate increases. In order to apply a successful water shut-off treatment in a reservoir, the plugging material has to fulfill many requirements.

1.2 Requirements for plugging materials

Fracture properties, such as width, length, orientation or intensity, vary greatly depending on the reservoir type. However, it is possible to make a list of universal features describing the perfect plugging system.

Firstly, the blocking material should have good mechanical strength. The plug is supposed to resist high pressure in the reservoir for a long time, as the water is injected under high pressure during water-flooding, and so the plug material should withstand high forces. Secondly, the material must be characterised by good durability at high temperatures, as the temperatures in reservoirs very often reach more than 100°C[5]. Thirdly, cations present in brine as Ca^{2+} should not negatively affect the mechanical strength of the material. The

presence of cations may lead to the undesired precipitation of some dissolved materials, resulting in unsuccessful treatment. As mentioned before, the plugging agent is mostly pumped into the fractures in the form of an aqueous mixture, so it is economically reasonable to use brine water instead of clear water. Hence, the properties of the plug should not be dependent on water composition.

Moreover, the material should solidify or expand in a controllable manner, in order to avoid plugging of the injection well before the material has set inside the fracture. Since the length of the injection wells very often reaches hundreds of meters[13], this is a very difficult task to perform. On the one hand, the setting time should be relatively short, to decrease treatment costs, but on the other hand, the material cannot block the injection well, due to premature solidification. This is frequently achieved through the usage of agents that delay activation, so-called 'retardants', but their performance depends strongly on many factors such as temperature, pH and concentration.

As mentioned before, the water shut-off treatment should not affect oil production, meaning that plugging should occur only in the fractures. The low viscosity of the injected mixture facilitates good transport through the well, but it also allows for penetrating the pores and blocking oil-rich regions. In this regard, the plugging process should be selective, meaning that the structure of the plugging agent should facilitate placing the material selectively into the fracture.

Another requirement is relatively low costs. The injection volume of blocking material adds up commonly to thousands of cubic metres, due to the dimensions of the fractures, and the water shut-off treatment should be economically feasible[14]. And last but not least, the applied material must be non-toxic and environmentally friendly.

Obviously, fulfilling all of the abovementioned requirements is a very complicated undertaking. The next section describes current methods applied in fractured oil fields, focusing on the advantages and disadvantages of each technique.

1.3 Current water shut-off methods in fractured reservoirs

This part focuses on the most commonly used materials in fractured reservoirs, namely hydrogels. In general, hydrogels are materials capable of absorbing large amounts of water. Swollen gels show fairly good elastic properties and are capable of withstanding high pressures[15]. They can be divided into three main categories: inorganic gels, polymer-based gels and preformed particle gels (PPG).

1.3.1 Inorganic gels

Conformance improvements in fractured reservoirs are very often achieved by injecting inorganic gels into the oil field[16,17,18]. Sodium silicate gel is one of the most frequently used[19] examples in this case. Silicates were the first oilfield conformance fluids utilised in water-flooding applications back in 1922[20]. Sodium silicate forms a strong gel after being activated, for instance through the usage of an inorganic salt[21]. Due to low, water-like viscosity before activation, the gel easily penetrates the reservoir and plugs fractures after activation. This kind of gel is known to be stable at high temperatures (up to 150°C) and the gel treatment is fairly economical[22].

However, this method suffers from some disadvantages. The biggest problem with silicate systems is the inability to retard the reaction and the occurrence of syneresis[20,21]. Rapid gelation time does not allow for precise setting of the plug and may lead to blocking of the injection well. Taking into consideration also the very low viscosity of the initial solution, there are justified concerns that oil-rich pores might be blocked as well. Syneresis is generally attributed to the formation of new bonds during gel development through the condensation of two silanol groups. Gel shrinkage occurs because the siloxane bond takes up less space than the two individual silanol groups. It was found that the more rapidly the gel sets, the larger the initial syneresis rates[23]. Syneresis may cause the blocked reservoir zone to recover a fraction of its original permeability[24].

1.3.2 Polymer-based gels

Polymer materials have gained attention due to their improved properties compared to inorganic gel systems, such as better elastic properties[20].

Polymer-based gels can be divided into two main categories: monomer gels and polymer gels. In both cases the gel is obtained thanks to a cross-linking reaction. In the first method, the cross-linker reacts with low-molecular weight monomers while the material is being injected into the fracture, whereas the second method utilises reaction between the cross-linker and high-molecular polymers with functional groups.

1.3.2.1 Monomer gels

Acrylamide monomer-based systems are the most applied monomer gels in the oil recovery industry[25,26,27,28]. The initial viscosity of the monomer and cross-linker mixture can be adjusted to some extent by using the proper concentration of these components in water. Therefore, the mixture penetrates into all regions, not only zones close to the well. It is also possible to use retardants, such as potassium ferricyanide, to prevent premature gelation[26].

Another advantage is that the cross-linked gel remains stable at temperatures of up to 150°C for one year[26].

Nevertheless, the polymer gel is still capable of penetrating low permeable pores, thus leading to a decrease in the oil recovery rate. Moreover, relatively high concentrations of the monomer are recommended, as the reaction mixture may be diluted with water during the injection process. For this reason, the treatment cost increases. Given that acrylamide is toxic and suspected to be carcinogenic, this method is considered as environmentally unfriendly.

1.3.2.2 Polymeric gels

The polymer gel system consists of high-molecular weight polymer, a cross-linker and other additivities. Polyacrylamide (PAM) gel is the most commonly used among other polymer gels and has been applied in many successful water shut-off treatments[26,29,30,31]. In oilfield applications PAM is usually cross-linked using Cr(III)[32]. For example, Demir et al.[12] reported the average water cut decreased from 97% to 45% after injecting Cr(III) cross-linked polymer gel, following which the oil rate increased from 12 barrels per day (bpd) to 80-90 bpd. The main advantages of polymer gels are good injectivity and good flow through the reservoir.

However, due to the fact that the reactive mixture is multi-component (polymer, cross-linker and additivities), final properties may vary, depending on the reaction conditions. For example, gelation is controlled by shear stress, temperature, dilution and pH, and so gel strength cannot be regulated easily[26,33]. Furthermore, plugging composition should be mixed with pure water, as partially hydrolysed polyacrylamides (HPAM) used in the oil industry are known to be sensitive to temperature and divalent ions. The amide groups present in these polymers can hydrolyse in aqueous solutions to an extent that depends on pH and temperature. Highly hydrolysed polyacrylamide may have a degree of hydrolysis sufficient to cause precipitation in the reservoir[34], which has a negative influence on the plug's properties. Since the usage of clean water is required, the technique is less environmentally friendly and contributes to higher treatment costs.

1.3.3 Preformed particle gels

Preformed particle gel is another type of widely used plugging material. Although PPG is mostly made from a similar polymer as the previously described polymer systems (HPAM), it is classified as a new kind of material, since it exhibits new properties compared to older polymer-based systems.

PPG is a particulate superabsorbent crosslinking polymer that swells up to 200 times its original size in brine[35,36]. The difference between the PPG and polymer gel systems is that the

PPG option is cross-linked before the injection process. In such a way, difficulties controlling the composition of the mixture are eliminated. PPG stability at low temperatures is not sensitive to reservoir minerals and the water salinity. Hence, a brine solution can be used during the injection process[37], which in turn reduces treatment costs and makes the method more environmentally friendly. Additionally, PPG is cut into smaller particles, with sizes on the micrometre or millimetre scale, depending on field application requirements. Particle size is tailored to be smaller than the fracture width but larger than the diameter of the pores so that the PPG preferably goes into the fractures. After swelling, the preformed particles fill the fracture volume, thereby preventing water from passing through easily. Yuzhang Liu et al.[38] reported that millimetre-sized polymer grain PPGs were applied in approximately 2,000 wells in China to reduce high fracture permeability. The PPG treatment was applied in sandstone reservoirs and in naturally fractured carbonate reservoirs, with temperatures ranging from 20 to 110°C. PPG treatment led to water shut-off and increased the oil production rate.

Although the PPG covers most of the requirements for the plugging material, some improvements are possible. First of all, the interaction between the particles has a physical nature, as swollen preformed particle gels are not covalently bonded together. This means that the particles can be separated due to the high pressure of the injected water, which may lead to damage of the plug and secondary water cut phenomena[37]. Secondly, HPAM polymers are known to be unstable at elevated temperatures, if divalent cations are present[39,40,41]. For temperatures above 60°C, acrylamide groups within the hydrolysed polyacrylamides polymer experience hydrolysis and form acrylate groups. If significant concentrations of divalent cations are present, HPAM polymers precipitate, which in turn limits the utility of HPAM polymers for many potential enhanced oil recovery (EOR) applications in warmer reservoirs[42]. Furthermore, the swelling process can be controlled to some extent and is based mostly on direct interaction of the polymer with other chemicals. Remotely controlled systems have not been reported in the literature.

1.4 Novel elastomer system

To overcome existing problems in blocking fractures in oil reservoirs, a novel silicone material has been developed. Poly(dimethylsiloxane) (PDMS) is the most commonly used of the polymeric organosilicon compounds, generally referred to as silicones, and it has been chosen for this project because of its unique properties. For instance, the siloxane bonds (-Si-O-Si-) which form the backbone of silicone are highly stable. This binding energy is higher than that of carbon bonds (C-C), and thus silicones have higher stability and heat resistance than other organic polymeric rubbers. Due to low intermolecular force, PDMS elastomers are highly

elastic and have excellent compressibility properties. Moreover, PDMS is hydrophobic and has outstanding resistance to oil at high temperatures[43,44].

To fulfill the requirements for the plugging material mentioned in chapter 1.2, the developed plug consists of microcapsules containing a hydride PDMS cross-linker and vinyl-functional PDMS microparticles. Both components are prepared before the injection of the material into the fracture. They are mixed in a silicone oil containing the Platinum (Pt) catalyst, which acts as a suspension medium and makes the material pumpable. In the presence of a Pt catalyst, the hydride groups react with vinyl groups on the microparticles' surface through a hydrosilylation reaction, and a covalently bonded network is formed. Due to microencapsulation process, the cross-linker is released on demand allowing for controlled formation of the network. Figure 2 shows a schematic presentation of the plug before and after release of the cross-linker.

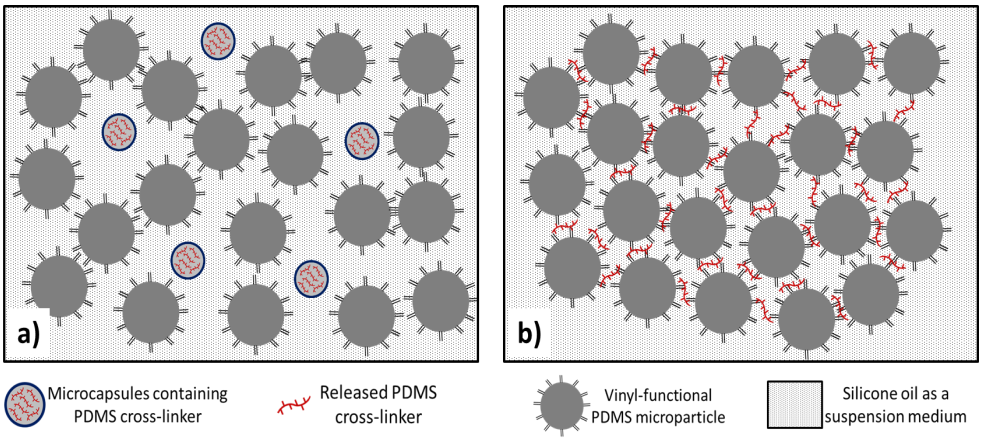

Figure 2. A schematic presentation of the elastomer plug consisting of the microcapsules containing a hydride PDMS cross-linker and vinyl-terminated PDMS microparticles. The components are mixed in a silicone oil, which acts as a suspension medium. Figure 2a) presents the system before activation of the microcapsules – the cross-linker is protected by the shell and unwanted plug formation is prevented. Figure 2b) shows the plug after activation of the microcapsules – the released PDMS cross-linker reacted with vinyl groups on the microparticles' surface, resulting in a covalently bonded plug.

1.4.1 Comparison between elastomer system and known plugging materials

Firstly, the mechanical strength of the PDMS network is higher than for the commonly used PAM polymers. For example, the elastic modulus of swollen preformed particle gel, synthesised from polyacrylamide and potassium salt, was 100 Pa[36]. The measurement was performed at room temperature, using a dynamic oscillatory rheometer with a frequency

equal to 1 Hz. The elastic modulus of the PDMS network is much higher and varies between 10^4-10^6 Pa[45,46]. Hence, the PDMS material should withstand higher pressure than the PPG.

Secondly, PDMS is known to be stable at elevated temperatures. For instance, silicone rubber can be used long term at 150°C with almost no change in its properties[47], whereas the PPG is stable for approximately 1 year at 150°C[14].

Thirdly, PDMS is injected into the fracture in the form of pre-crosslinked microparticles. Such prepared microparticles, in contrast to PPG, do not swell in contact with water, and hence the danger of blocking the injection well, due to the premature swelling of the particles, is eliminated. The size of the PDMS microparticles can be also designed to be smaller than the fracture width but larger than the pore diameter. In this way, the material will form only in the fracture, without blocking the pores. As the PDMS particles are less deformable than hydrogels, they will not penetrate into pores even under high pressure. Fracture widths range between 1 µm to 4 mm, but it is known that fractures larger than 10 µm significantly increase the permeability of the rock[48]. Hence, the size of microparticles should fall between 10 µm and 4 mm. However, to ensure good transport of the PDMS microparticles through the fractures, microparticles with a diameter up to 1 mm are of particular interest in this project.

Moreover, in contrast to PPG, the PDMS microparticles have reactive vinyl groups on the surface. These vinyl groups are capable of reacting further with the multi-functional cross-linker. After the reaction inside the fracture, each microparticle is covalently connected with other microparticles with a cross-linker as a joining agent, following which a strong barrier is created. This makes the material even more durable and resistant to high pressure. In this way, the macroscopic PDMS elastomer cannot be washed away due to the injection of water and should result in the long-term validity of the treatment[49]. For instance, the interaction between swollen PPG is based on physical phenomena; therefore, the mechanical strength of the plug is much lower, and cases have been reported in which water has broken through the swollen PPG plug.

Finally yet importantly, another innovation implemented in our system is the microencapsulation of the cross-linker, in order to achieve better control over the cross-linking reaction. As long as the liquid cross-linker is coated within an amorphous polymer shell, it is separated from the environment and the reaction cannot take place. The mixture of PDMS microparticles and microcapsules can be then stored and transported without the formation of the plug material, which means that the material can be placed precisely in the fracture, before the reaction takes place. As the plug system was designed for a particular type of oil reservoir in which the temperature reaches 50°C, the microcapsules should be

stable at a given temperature, and so this fact was taken into account while investigating the thermal stability of the microcapsules.

Only after the so-called activation of the microcapsules is the inner part released, leading to the reaction between the cross-linker and PDMS particles. Activation is a process in which the shell's permeability increases upon the application of an external stimulus. Many polymeric delivery systems are triggered by various stimuli, such as ultrasound[50,51], pH[52,53,54], temperature[52,55] or mechanical damage[56,57]; however, in this project emphasis is placed on remotely applicable activation methods.

1.5 Activation of the microcapsules

In order to trigger the release of the cross-linker from the microcapsules, the microcapsules must be activated. In this project, emphasis was put on remotely applicable activation methods since fractures are hard-to-reach places, however other activation ways were also examined.

1.5.1 Thermal activation

Thermal activation is one of the most popular activation methods. When the shell consists of thermoplastic amorphous polymer, the microcapsules collapse upon heating to temperatures higher than the glass transition temperature (T_g) of the polymer. Among many available polymers, a poly(methyl methacrylate) (PMMA) has been chosen as a shell. It is hard and brittle below the T_g but soft and flowable above the T_g. Therefore, heating the microcapsules above the T_g of the PMMA will initiate the cross-linking reaction, as the microcapsules will disintegrate. Hence, the T_g of the shell should be higher than 50°C, but the system should respond to the given stimuli relatively quickly and efficiently.

This method requires heating large amounts of the plug material placed in the fracture, and simple thermal activation cannot be initiated from a distance. Remote activation would provide the advantage of precisely setting the plug and would decrease the danger of blocking either the injection well or the pores.

1.5.2 Gamma irradiation activation

Gamma irradiation is high-frequency electromagnetic radiation, which consists of high-energy photons. This kind of irradiation is widely used in sterilising medical equipment[58]; for example, whole pallets can be sterilised in a relatively short time[59]. Gamma rays penetrate through many materials, even when applied from a distance, and hence this activation method can be used in oil reservoirs.

It is commonly known that upon gamma irradiation, polymers may undergo either chain scission or cross-linking[60]. The occurrence of each of these phenomena depends on many factors, such as polymer structure, irradiation dose and time. At small doses, PMMA undergoes mainly chain scission[61,62], and a decrease in molecular weight leads to a decrease in T_g. Hence, when the T_g of the microcapsules' shell becomes lower than the temperature inside the fracture, the PMMA shell will collapse and the cross-linker will be delivered into the environment.

1.5.3 Alternating magnetic field activation

Another idea involves incorporating into the microcapsules structure magnetic nanoparticles (MNPs) and applying an alternating magnetic field (AMF). At high frequencies the nanoparticles generate large amounts of heat. This activation method, in contrast to the previously described, does not influence the T_g of the shell. The idea is to increase the temperature inside the microcapsules to reach temperature above the T_g of the shell. As the PMMA becomes soft and pliable at those temperatures, the cross-linker is released into the environment, due to the collapse of the microcapsules. At elevated temperatures, the cross-linking reaction between the PDMS microparticles will accelerate and the time formation of the permanent plug should decrease.

Heat dissipation from magnetic particles is caused by a delay in the relaxation of the magnetic moment through either rotation within the particle (Néel mechanism) or rotation of the particle itself (Brownian mechanism), when they are exposed to an alternating magnetic field[63,64,65]. The Néel relaxation process is determined by the anisotropy energy of the particle, whereas the Brownian mechanism is characterised by a rotational Brownian motion of the nanoparticle itself. Since the heat dissipated by Brownian relaxation depends on the local environment, such as viscosity of the medium, the use of magnetic particles that dissipate heat through Néel relaxation, which is not influenced by the local environment, provides better control over the behavior of the nanoparticles. However, any distinction between the relative contribution of heat by both mechanisms has not been discussed in detail, and still the amount of generated heat by the nanoparticles dispersed in a particular medium is mostly found experimentally rather than estimated based on theoretical models[66].

1.5.4 Ultrasonic activation

Ultrasound waves are sound waves with frequencies higher than the upper audible limit of human hearing. They have found applications in many areas, for example in medicine[67,68] and in the food industry[69]. Ultrasonication is also used in the process employed to grind micro- and nano-particles[70]. Particle reduction size upon ultrasonication is caused by a phenomenon

called ‘ultrasound cavitation’. When sonicating liquids at high intensities, the sound waves that propagate into the liquid media result in alternating high-pressure (compression) and low-pressure (rarefaction) cycles. During the low-pressure cycle, high-intensity ultrasonic waves create small vacuum bubbles or voids in the liquid. When the bubbles attain a volume at which they can no longer absorb energy, they collapse violently during a high-pressure cycle. This phenomenon is termed ‘cavitation’[71], and since it may cause damage to the PMMA shell, ultrasound has been tested as a potential activating stimulus for the microcapsule system.

1.5.5 Solvent-flushing activation

Solvent methods for enhanced oil recovery and heavy-oil recovery have been studied and implemented in many oil fields[72,73]. The principle is based on injecting the solvent into a reservoir, in order to displace oil trapped inside the pores. Mostly, light hydrocarbon is employed; however, there are also known examples of using other solvents, such as methyl ethyl ketone[72]. Considering this point, a solvent-flushing activation of the microcapsules system was also tested. Although this method cannot be remotely applied, this activation approach was tested as an alternative to other activating techniques; moreover, this approach could provide additional information about the cross-linked plug. The idea was to use a good solvent for the PMMA and flush the system consisting of the PDMS microparticles and the microcapsules under high pressure. The dissolved PMMA shell would be washed away from the system, allowing for uniform spreading of the cross-linker, which in turn would lead to the formation of a covalently bonded PDMS microparticle system.

2. Preparation and characterisation of PMMA-coated microcapsules containing a PDMS cross-linker

This chapter describes the preparation process and characterisation techniques for the microcapsules. It is based on the article '*Preparation and Characterization of Silicone Liquid Core/Polymer Shell Microcapsules via Internal Phase Separation*', published in *Macromolecular Materials and Engineering Journal*. The manuscript contains experimental details and it is included in the appendices assigned to Chapter 2.

2.1 Introduction

Microcapsules are micro-sized particles generally composed of an inner active agent defined as a core, and a polymer wall defined as a shell[74]. The usage of microcapsules allows for better control over where and when a core substance is released into the surrounding environment. The release rate from microcapsules depends on many factors, such as size of the microcapsules, shell material, core/shell content, activating stimulus, etc[75,76,77]. Their properties are determined during the preparation process, and hence the choice of the proper preparation technique is essential. Among many known techniques, an internal phase separation method has been chosen for this study, as it allows for obtaining microcapsules with relatively narrow size distribution and it has been already employed on a large scale in fields such as agriculture and self-healing materials[78]. Moreover, the preparation of liquid core microcapsules with a PMMA shell has been reported in the literature, and so the method could be adapted easily for our purposes[79,80].

The procedure involves dissolving a cross-linker (core material) and the PMMA (shell material) in highly volatile organic solvent, in this case dichloromethane (DCM). This prepared oil phase is then added to an aqueous emulsifier solution under vigorous stirring. As a result, an emulsion with tiny oil droplets is obtained. When the organic solvent is removed, the previously dissolved shell polymer separates from the cross-linker (due to their immiscibility) and creates a coating around the liquid core. The phase separation scheme is presented in Figure 3.

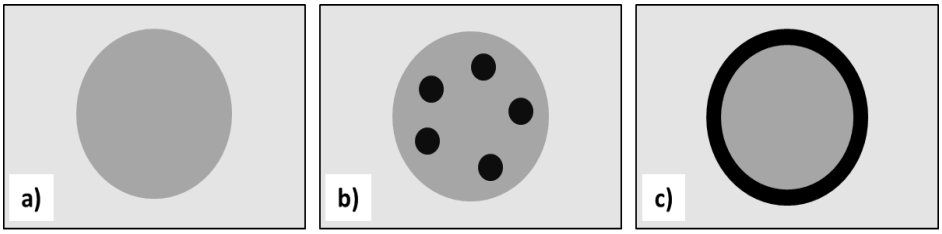

Figure 3. Schematic diagram of the microcapsule formation mechanism: a) an oil phase drop containing dissolved PMMA and the cross-linker in DCM, b) DCM begins to evaporate; size of the droplet decreases and the PMMA starts phase separating and migrating towards the edge of the droplet, c) after the DCM is removed, the PMMA creates a solid coating around the liquid cross-linker.

2.2 Results and discussion

This chapter presents the preparation of microcapsules containing the commercially available 7-functional hydride cross-linker HMS-301 (M_w=2000 g/mol, viscosity 25-35 cSt). PMMA (M_w=15000 g/mol) was employed as a shell material. The optimisation process of the phase separation technique and the characterisation of obtained material are also described.

2.2.1 Studied factors

In order to investigate the influence of various factors on microcapsule properties, microcapsules were prepared under various conditions, employing the phase separation technique. Table 1 presents the studied systems. The influence of factors such as type of emulsifier, the addition of acetone to the oil phase and core/shell concentration in the oil phase were investigated.

Table 1. Studied compositions of the oil and aqueous phases. Factors as type of emulsifier (E), the addition of acetone (Acetone) to the oil phase (DCM) and core/shell masses in the oil phase (PMMA and HMS-301, respectively) were investigated.

Number	DCM	PMMA	HMS-301	E	Acetone
	[g]	[g]	[g]	(1%)	(5%)
1	100	1	1.5	PVA	No
2	100	1	1.5	PVA	No
3	100	1	1.5	PVA	No
4	100	1	1.5	PVA	Yes
5	100	2.55	3.9	PVA	No
6	100	2.55	3.9	PVA	Yes
7	100	1	1.5	PMAA	Yes (2.5)
8	100	1	1.5	PMAA	No
9	100	1	1.5	PMAA	Yes
10	100	2.55	3.9	PMAA	No
11	100	2.55	3.9	PMAA	Yes
12	7.05	0.255	0.386	PMAA	Yes

2.2.2 Influence of studied factors

It was found that regardless of the type of the emulsifier used in the aqueous phase and the concentration of components in the oil phase, microcapsules with a core-shell morphology were prepared. Scanning electron microscopy (SEM) images, shown in Figure 4, proved that the PMMA created a continuous coating around the cross-linker when the phase separation technique was applied. This indicates that the liquid core is well-protected by PMMA, and microencapsulation provides good separation of the cross-linker from the environment. According to the interfacial theory, an acorn morphology was expected to be observed when the PMAA emulsifier was used[81], though experimental data are not in agreement with the theory.

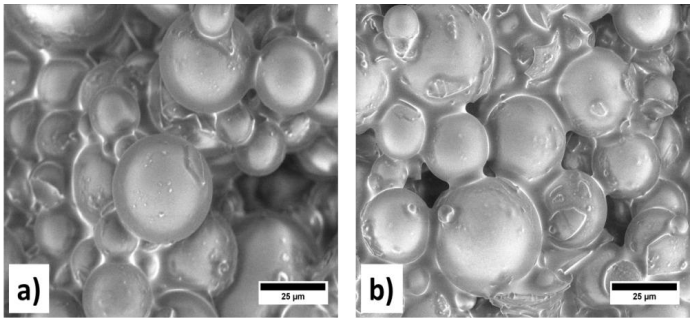

Figure 4. SEM images of the microcapsules prepared by the phase separation technique with DCM as the oil phase. The used emulsifiers are a) PVA (numbers 1-3 as shown in the Table 1) and b) PMAA (number 8 as shown in Table 1). In order to check the reproducibility of the process, microcapsules were prepared three times under the same conditions (number 1-3 in Table 1).

Size distribution of the microcapsules was analysed by Uthsca Imagine Tool 3.0 software, as described by Lavergne et al.[82] Baum et al.[83] reported that the addition of a water-soluble co-solvent to the oil phase resulted in smaller droplets when the solution was emulsified. They also claimed that the addition of the co-solvent led to a narrower size distribution of the microcapsules. However, the experiments we conducted allowed us to conclude that the addition of the acetone and the type of emulsifier used in the oil did not affect the size of the microcapsules significantly. As acetone has no impact on microcapsule size, it was not added in further experiments. Figure 5 presents the size distribution of microcapsule formulations 1-3 from Table 1. The diameter of microcapsules falls between 3 and 40 µm, with an average size around 20 µm.

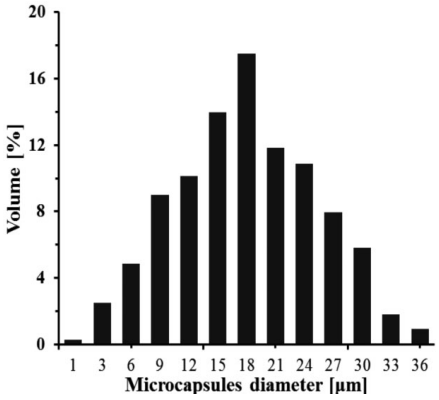

Figure 5. Size distribution of the microcapsules (Table 1, samples 1-3).

As mentioned in the Introduction section, the plug material should selectively plug fractures. Hence, microcapsules cannot enter oil-rich pores. As the size of the microcapsules is bigger than the size of the pores (>1μm), this requirement has been accomplished.

The composition of PMMA microcapsules with a silicone liquid core was confirmed by employing ATR-FTIR spectroscopy. In Figure 6, spectra for commercial PMMA, commercial HMS-301 and the PMMA microcapsules synthesised, by using 1% PVA as an emulsifier, are shown. In the PMMA microcapsule spectrum, a carbonyl-stretching absorption band at 1726 cm^{-1} of the ester group of PMMA is observed. Bands at 1483, 1435 and 1387 cm^{-1} are also related to PMMA as well as the band at 1146 cm^{-1}, which corresponds to the C—O (ester bond) stretching vibration of PMMA. A peak at 2156 cm^{-1} is also observed, which is attributed to hydride vibrations (Si—H) and corresponds to the silicone liquid core (HMS-301). In addition, the bands at 1412 and 1259 cm^{-1} are related to the asymmetric and symmetric deformations of the methyl group attached to the silicone atom (Si—CH_3) of the HMS-301, respectively. Finally, the peak at 1024 cm^{-1} corresponds to Si—O—Si stretching vibrations, and the peak at 797 cm^{-1} is ascribed to Si—C stretching vibrations. As peaks attributed to both compounds were observed in the microcapsules spectra, two cases were possible. The first hypothesis was that the PMMA shell is thin enough that light could pass through the capsules, and hence the peaks assigned to the cross-linker were detected. The second hypothesis was that the cross-linker could be present on the PMMA surface and the observed peaks did not provide evidence that the cross-linker was being encapsulated inside the shell successfully. To verify whether the cross-linker was enclosed within the PMMA shell, the microcapsules were washed with heptane, which is a good solvent for the cross-linker and a poor solvent for the PMMA. After the washing step, peaks attributed to the cross-linker were still recognisable in the spectra. Henceforth, it was proved that the cross-linker was encapsulated within the polymer shell.

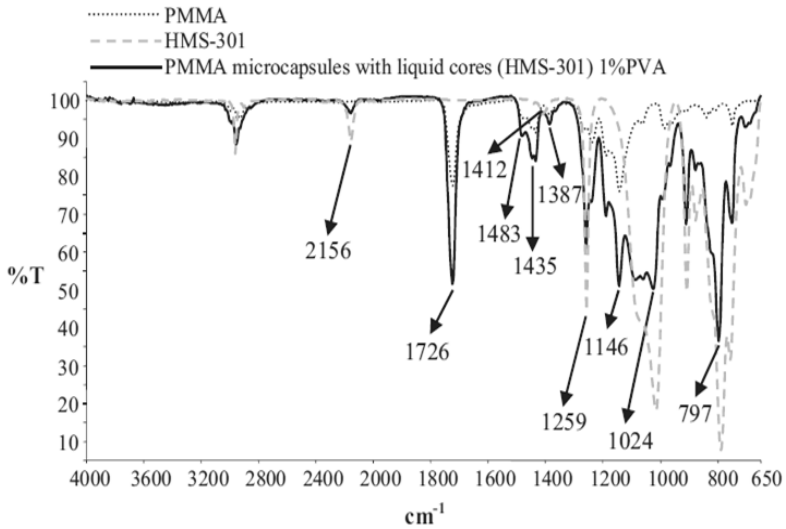

Figure 6. ATR-FTIR spectra of PMMA, HMS-301 and microcapsules obtained when using 1% PVA solution as the aqueous phase (Table 1, samples 1-3).

No evidence of hydroxyl groups (OH) in the region of 3300 cm^{-1} from the emulsifier (PVA) was detected via ATR-FTIR spectroscopy, meaning that the emulsifier was not incorporated into the microcapsules structure and had been fully washed away.

Three methods for determining the core and the shell content were employed, namely a thermogravimetric (TGA) method, an extraction method and a nuclear magnetic resonance (NMR) method. The methods are described in the article *'Preparation and Characterization of Silicone Liquid Core/Polymer Shell Microcapsules via Internal Phase Separation'*[84]. As the NMR is the fastest and most accurate of all three methods, it is described herein.

The core/shell content in the NMR method was evaluated using a peak integration approach. Firstly, the microcapsules were dissolved in the d-chloroform and tested with ^{1}H NMR analysis. Physical mixtures consisting of pure HMS-301 and PMMA with various component ratios were also prepared and used as reference samples. Figure 7 presents ^{1}H NMR spectra of the microcapsules listed in the Table 1 as numbers 1-3. The PMMA gives four main resonances in the ^{1}H NMR spectrum. Signals at 0.7 and 1 ppm correspond to the protons of the methyl groups attached to the carbon of the backbone of the PMMA. The peak at 1.7 ppm is attributed to the protons of the methylene groups from the backbone, and the peak at ~3.5 ppm refers to the protons of the methyl groups attached to the ester groups of the side chains of the PMMA. A spectrum of the cross-linker shows a peak at 4.7 ppm, which is assigned to the hydrogens attached to the silicon atom, while the peak at 0 ppm corresponds to the protons of the methyl groups linked to the silicone atom.

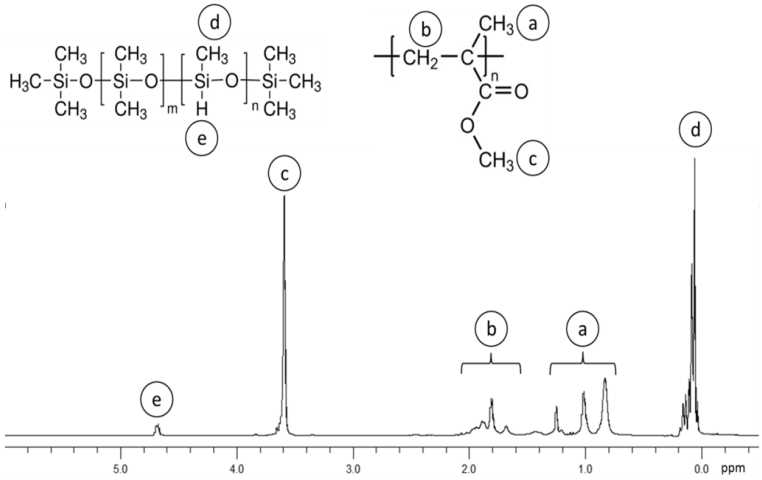

Figure 7. The ^{1}H NMR spectrum of the microcapsules (Table 1, samples 1-3) with an indication of the characteristic peaks.

Thanks to the integration of peaks at 3.5 ppm and 4.7 ppm, it was possible to determine the mass percentage of each component. Obtained results are presented in Table 2. The same approach was applied in analysing the physical mixtures of the HMS-301 and PMMA. Knowing the real mass content of the mixture, it was shown that the ^{1}H NMR method is accurate, with a possible error rate of 2%. Again, no signal coming from the –OH groups of the PVA emulsifier were detected in the spectra.

It is obvious that when PVA is used as the emulsifier, microcapsules contain more cross-linker than microcapsules prepared in 1% PMAA as the aqueous phase. The reason for this is not clear, as previous analyses have not shown significant differences between these two emulsifiers. One possible explanation may be that although the acorn morphology was not observed, the usage of 1% PMAA solution lowers encapsulation efficiency, and some part of the cross-linker is washed away during the washing step. Due to that fact, microcapsules prepared with the PVA emulsifier solution as the aqueous phase (Table 1, samples 1-3) will be subjected in further experiments.

Table 2. Studied microcapsule formulations and content of the cross-linker determined by the ^{1}H NMR method. Factors as type of emulsifier (E), the addition of acetone (Acetone) to the oil phase (DCM) and core/shell material masses in the oil phase (PMMA and HMS-301, respectively) are presented.

Number	DCM	PMMA	HMS-301	E	Acetone	The cross-linker content
	[g]	[g]	[g]	(1%)	(5%)	[mass %]
1	100	1	1.5	PVA	No	-
2	100	1	1.5	PVA	No	40
3	100	1	1.5	PVA	No	53
4	100	1	1.5	PVA	Yes	55
5	100	2.55	3.9	PVA	No	42
6	100	2.55	3.9	PVA	Yes	58
7	100	1	1.5	PMAA	Yes (2.5)	16
8	100	1	1.5	PMAA	No	26
9	100	1	1.5	PMAA	Yes	43
10	100	2.55	3.9	PMAA	No	50
11	100	2.55	3.9	PMAA	Yes	32
12	7.05	0.255	0.386	PMAA	Yes	36

One of the application requirements is stability of the microcapsules at 50°C, meaning that the cross-linker is supposed to be confined within the shell at that temperature, and thereby the cross-linking reaction is hindered. Rheology allows for monitoring changes in the storage and loss moduli of the sample, i.e. structural changes. When the cross-linker reacts with the vinyl groups and thereby forms a three-dimensional elastic network, the storage modulus increases. In order to investigate at which temperature the cross-linker is released, the microcapsules were mixed with vinyl-terminated DMS-V35 (M_w=49 500 g/mol, viscosity 5000 cSt) containing 5 ppm of the Pt catalyst. Substituting the PDMS microparticles with vinyl-terminated PDMS was dictated by the fact that the reaction between the cross-linker and the vinyl-terminated DMS-V35 is easily detectable rheologically. For the microparticle-based systems the rheology changes significantly less and is thus difficult to detect with precision and overall vinyl-functional DMS-V35 was used instead. To examine under what conditions the network was formed, the mixture prepared from the microcapsules and the vinyl-terminated DMS-V35 was analysed by shear rheology. The sample was kept at different temperatures, for three hours at each temperature. Changes in the storage modulus were

analysed and the results are presented in Figure 8. The microcapsules did indeed react with vinyl-terminated PDMS at 100°C, since a significant increase in the storage modulus was observed at the given temperatures. The PMMA passes through a phase change transition at 95°C, following which microcapsules become permeable. Below 100°C, the microcapsules were relatively stable, because only minor changes in G' were observed in our test – the remaining cross-linker on the surface of the shell could be a reason for this result. Although the storage modulus increased below the T_g of the PMMA, it is obvious that the cross-linking reaction took place mainly at 100°C. This experiment evidences the stability of the microcapsules at 50°C and confirms the possibility of thermally activating the system.

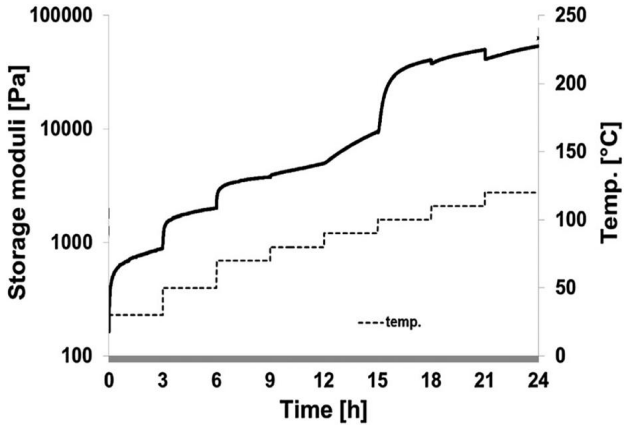

Figure 8. Reactivity of the microcapsules (Table 1, samples 1-3) with vinyl-terminated DMS-V35 at various temperatures. The mass ratio between the compounds was 1:10, respectively. The utilized DMS-V35 contained 5 ppm of the Pt catalyst.

2.2.3 Optimisation of the preparation process

From previous experiments, the following conclusions can be drawn:

1) The type of emulsifier does not influence the size and the morphology of microcapsules; however, higher cross-linker content is obtained when PVA is used, and so PVA should be used in further experiments.
2) The addition of acetone does not affect the size and the size distribution of microcapsules, and so the addition of co-solvent can be omitted.
3) Various cross-linker and PMMA concentrations in the oil phase do not influence the preparation process; hence, even higher concentrations should be examined, in order to make the process more efficient.

Further experiments were performed in which the following factors were investigated: the oil phase/aqueous phase ratio, the concentration of components in the oil phase, various core/shell ratios and mixing time. The studied systems are presented in Table 3.

Dichloromethane is a good solvent for both cross-linker and PMMA. It is also highly volatile and water-immiscible, and therefore it is a good candidate for microcapsule preparation. However, DCM is known to be toxic and is suspected of being carcinogenic. Decreasing its volume in the preparation process is thus desired. The microcapsules were prepared when only 50 g of the DCM was used (Table 3, number 1). Initially, the oil phase consisted of 100 g of the organic solvent (Table 1), and reducing the needed amount of solvent was a valuable improvement. Although the concentration of the dissolved components was higher than in previous experiments, the phase separation of the PMMA was successful. Subsequently, even higher concentrations of the oil phase were tested (listed in Table 3 as samples 1, 2 and 3), but it was found that only microcapsules listed as number 1 were successfully prepared. Too high content of dissolved components in the DCM resulted in the rapid phase separation of PMMA and led to a disturbed formation of microcapsules.

In order to increase the content of cross-linker, a higher amount of the cross-linker was used in respect to PMMA (Table 3, number 4). Optical microscopy images confirmed the formation of microcapsules; however, during the washing step, the microcapsules created a thin layer on the filter paper. Presumably, the PMMA shell was too thin and the microcapsules collapsed, so any further increases of the cross-linker ratio to the PMMA were discontinued.

Table 3. Studied systems in order to optimise the preparation process of the microcapsules.

Number	**DCM**	**PMMA**	**HMS-301**	**1% PVA solution**
	[g]	**[g]**	**[g]**	**[mL]**
1	50	1	1.5	150
2	50	2	3	150
3	50	3	4.5	150
4	50	1	3	150
5*	50	1	1.5	150

** mixing time was decreased from three to two hours*

Subsequently, the mixing time was decreased from three to two hours (Table 3, number 5). A shorter preparation time is preferred, as it makes the technique more cost-effective. Both optical and scanning electron microscopy images demonstrated microcapsules with characteristic single-hole defects in the PMMA shell. Additionally, the optical microscopy

images showed a residual DCM encapsulated in the microcapsules. As DCM and the cross-linker have different reflection indexes, DCM could be observed as light spots inside the microcapsules. It was concluded that DCM was not removed completely from the oil phase, due to the decreased mixing time. Dichloromethane dissolves PMMA, and the presence of unremoved solvent led to obtaining damaged microcapsules. The process of encapsulating of the DCM and dissolving the PMMA shell is presented in Figure 9.

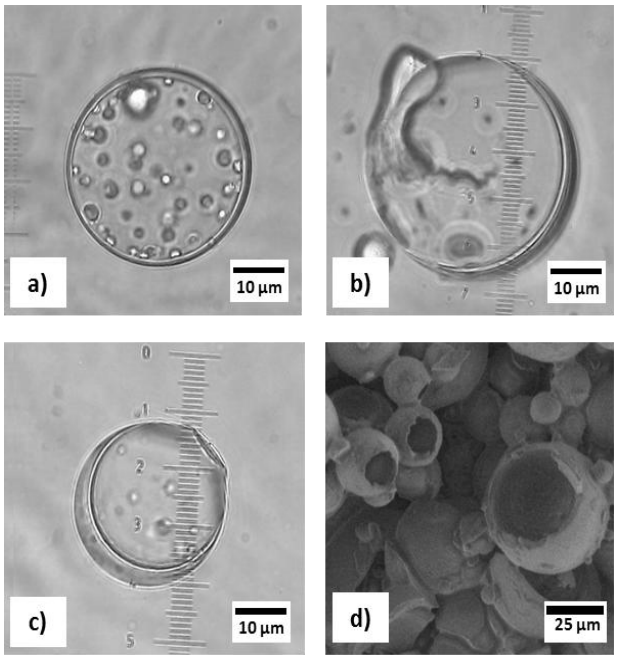

Figure 9. Microscopy images showing the effect of residual DCM inside the microcapsules (Table 3, number 5) a) bright spots inside the microcapsules represent DCM, b) the DCM starts to dissolve the PMMA shell leading to the release of the crosslinker, c) the hole-defected microcapsules in a water solution, d) SEM image of washed and dried microcapsules.

The preparation process was optimised, and the new procedure thereafter is as follows: 1 g of PMMA and 1.5 g HMS-301 dissolved in 50 g of DCM. The oil phase is then added drop-wise to 150 mL of 1% PVA solution under virgorous strirring. The obtanied emulsion is then mixed for 3 hours at room temperature. Subsequently, the obtained microcapsules are washed with deionised water, using vacuum filtration, and dried at room temperature for one day.

2.2.4 Encapsulation of high-molecular weight PDMS cross-linkers

The phase separation technique was also adapted for preparing microcapsules with a high-molecular weight PDMS cross-linker. The applied preparation procedure is described in section 2.2.3. The properties of the high-molecular weight cross-linkers HMS-064 and HMS-

082 and the cross-linker HMS-301 are presented in Table 4. Higher molecular weight results in higher cross-linker viscosity, and all the cross-linkers have different degrees of polymerisation and functionality. Functionality is the number of hydrides attached to the silicone atoms in one molecule. The type of cross-linker employed might have an impact on the final properties of the plug material, and hence attempts were made in order to encapsulate various kinds of cross-linker.

Table 4. Comparison of properties of various PDMS cross-linkers, which subsequently were encapsulated by the phase separation technique.

Name	Viscosity [cP]	Molecular weight [g/mol]	Mole% (MeHSiHO)	Functionality	DP*
HMS-064	8000 - 11000	55000 - 65000	5-7	50	850
HMS-082	110-150	5500-6500	7-8	6	82
HMS-301	25 - 35	1900 - 2000	25 - 30	7 - 8	28

* degree of polymerisation

Due to the significantly higher viscosity of the cross-linkers HMS-064 and HMS-082, the prepared microcapsules were more deformed and agglomerated than microcapsules with HMS-301. Higher cross-linker viscosity leads to higher oil phase viscosity and changes the formation process of the oil droplets. Hence, dried microcapsules were more agglomerated and irregular in shape, as presented in Figure 10.

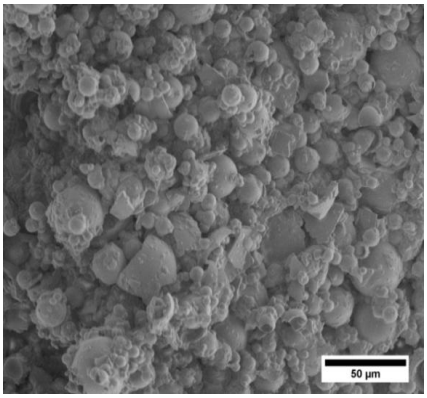

Figure 10. Microcapsules containing the HMS-082 cross-linker prepared via the phase separation technique.

The ATR-FTIR method proved that the microcapsules consisted of PMMA and the PDMS cross-linker. The mass percentage composition of the capsules was determined by using the ^{1}H NMR method. The mass contents of HMS-064 and HMS-082 were found to be 37% and

29%, respectively. Compared to the core content when HMS-301 was used, the values for highly viscous cross-linkers were rather low. Nevertheless, it was proved that the phase separation technique allows for preparing microcapsules with highly viscous PDMS cross-linkers (confirmed by the SEM, ^{1}H NMR and ATR-FTIR methods), although further optimisation of the preparation process is required.

2.2.5 Microcapsules with a pre-crosslinked core

The phase separation technique was employed to prepare microcapsules containing the pre-crosslinked core. The idea was to encapsulate mixtures consisting of vinyl-terminated PDMS reacted with an excess of cross-linker, albeit the mixture should remain liquid. Due to the excess cross-linker, a significant amount of the unreacted hydrides will be still present inside the microcapsules and capable of reacting further with PDMS microparticles, in order to create a permanent plug inside the fracture. Presumably, the pre-crosslinked cores would contribute to better mechanical properties of the plug material, though it should stay liquid-like and flowable, to ensure proper release from the PMMA shell.

Firstly, mixtures consisting of DMS-V35 (containing 5 ppm of the Pt catalyst) and the HMS-301 cross-linker were prepared with a stoichiometric imbalance 'r' equal to 5, 10, 15, 20 and 30. The stoichiometric imbalance 'r' is defined as:

$$r = \frac{[\text{hydride}]}{[\text{vinyl}]} \quad \text{(eq. 1)}$$

where [hydride] and [vinyl] are cross-linker and PDMS concentrations, respectively. All mixtures contained 3 ppm of Pt catalyst.

The sample with r=5 became solid at room temperature, shortly after mixing. The sample with r=10 remained liquid at room temperature; however, at 60°C it became solid after 1 hour. The sample with r=15 remained liquid at 60°C for 1 hour, whereas the samples with r=20 and r=30 created an inhomogeneous mixture after mixing, which consisted of cross-linked lumps and unreacted cross-linker. Therefore, the mixture with r=15 was chosen for further investigation.

In order to prove that the sample did not become solid at room temperature (RT) and at 60°C, frequency sweep tests were performed. Figure 11 presents storage moduli (G') and loss moduli (G'') of samples which were kept for 1 hour at both temperatures (RT and 60°C) prior to the measurement. It can be seen that the G'' was higher than the G' over time for both samples. Although the storage modulus of the sample stored at 60°C was higher than for the

sample kept at room temperature, indicating that the cross-linking reaction did occur to some extent, the sample remained liquid.

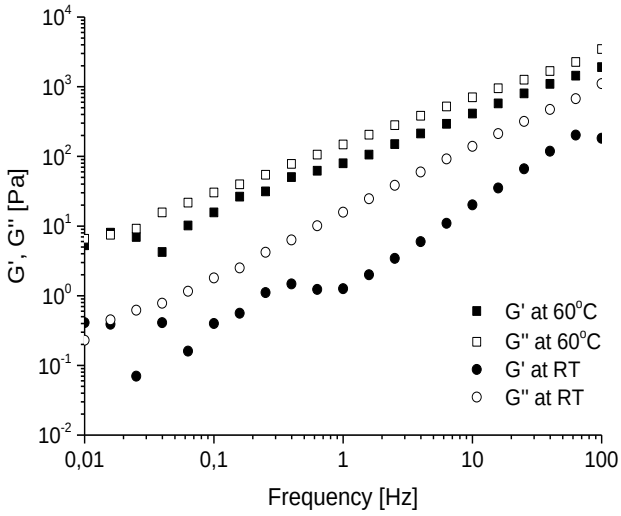

Figure 11. Storage modulus (G') and loss modulus (G'') of the mixtures with r=15 kept at room temperature and at 60°C for 1 hour prior to measurement.

In order to prepare the microcapsules, the sample with r=15 was prepared and kept at 60°C for 1 hour, to ensure cross-linking between the components. Then, the correct amount of pre-crosslinked core material was added to DCM, followed by the addition of PMMA. Subsequently, the oil phase was mixed with 1% PVA solution and vigorously mixed. Obtained material was washed and dried.

Microcapsules with pre-crosslinked cores were not obtained. The PMMA and the pre-crosslinked mixture merged together and created lumps and agglomerations. Perhaps the migration of the PMMA towards the edge of the droplet was disturbed due to a different core structure. As it was not possible to prepare a less viscous pre-crosslinked mixture that would remain liquid at elevated temperatures, the preparation of this kind of the microcapsule was discontinued.

2.3 Conclusions

The phase separation technique was found to be a universal method for preparing microcapsules containing a PDMS cross-linker. Microcapsules with relatively narrow size distribution, falling within the required limits, were obtained. The mass content of the

encapsulated cross-linker reached 50%. The cross-linker was effectively protected from the environment at wide temperature ranges, thus preventing any reaction between the cross-linker and other substances. Heating microcapsules to a temperature higher than the T_g of the PMMA shell was shown to be an efficient activation method. At 100°C the cross-linker was released and the reaction between the cross-linker and the vinyl-terminated PDMS took place, which subsequently proved the possibility of thermally activating the system.

Moreover, the preparation method was optimised by decreasing the amount of organic solvent and minimizing the preparation steps. Additionally, the phase separation technique was adapted for preparing microcapsules containing high-molecular weight PDMS cross-linkers.

3. Microcapsules activated by gamma irradiation

This chapter is based on the article '*Controlled release in hard to access places by poly(methyl methacrylate) microcapsules triggered by gamma irradiation*', published in *Polymers for Advanced Technologies*. The manuscript describes experimental details and can be found in appendices assigned to this chapter. This part describes an impact of gamma irradiation on PMMA properties. Besides commercially available PMMA, other shell materials were examined, such as lab-synthesised PMMA with low molecular weight (M_w), fluorinated derivatives of PMMA and plasticised PMMA.

3.1 Introduction

One of the requirements for the successful microcapsules application in the plugging of fractures in offshore reservoirs is the possibility of remotely activating the system. Gamma irradiation was considered one of the most promising stimuli in this regard. Gamma rays are electromagnetic radiation and the most energetic form of electromagnetic radiation, with a very short wavelength of less than one-tenth of a nanometer. Gamma radiation penetrates through many materials, and hence it interacts with other materials even when it is applied from a distance. Gamma radiation has sufficient energy to ionise polymers, and therefore it may be used in changing the properties of polymer materials.

Polymers upon gamma irradiation undergo chain scission, or cross-linking, as mentioned in the Introduction section. Since PMMA is considered a polymer undergoing mainly chain scission, it was chosen for this study and various types of PMMA were examined as potential shell materials susceptible to chain scission upon gamma irradiation. Due to the fact that the molecular weight and glass transition temperature of the shell polymer decrease after irradiation, microcapsules should collapse at lower temperatures than prior to irradiation. To enhance the impact of irradiation, polymers with purposely-low selected M_w were examined, since the glass transition temperature of short chain polymers changes significantly, even when minor changes are induced in relation to the length of the chain. Hence, low-molecular weight polymers were investigated, namely commercially available PMMA with M_w=15000 g/mol and lab-synthesised PMMA with M_w=2000 g/mol.

The plasticisation of PMMA, also described in this chapter, is another method that helps modify the T_g of the polymer. Plasticisers reduce interactions between polymer chain segments, thereby decreasing T_g, melt viscosity and the elastic modulus. Plasticisers are usually selected as non-volatile materials and must have good compatibility with the desired

polymer. Dibutyl phthalate (DBP) was used in this study, and the impact on PMMA properties upon gamma irradiation and the microcapsule preparation process was investigated.

Furthermore, fluorinated derivatives of PMMA (poly(2,2,2-trifluoroethyl methacrylate)) at various molecular weights were also synthesised and examined as potential shell material. Fluorinated polymers are supposed to degrade faster than non-fluorinated polymers upon exposure to gamma irradiation[85].

3.2 Results and discussion

Five kinds of PMMA were investigated. The sample denoted as 'PMMA_1' was a commercially available polymer with M_w=15000 g/mol, the sample labeled 'PMMA_2' was a lab-synthesised polymer with M_w=2000 g/mol and 'PMMA_3' refers to a plasticised commercial PMMA. Samples named '3F-PMMA_4' and '3F-PMMA_5' were fluorinated derivatives with M_w=10000 g/mol and 22000g/mol, respectively.

3.2.1 PMMA plasticisation

Firstly, the addition of plasticiser was explored as an easy and fast method of adjusting the T_g. Figure 12 presents the T_g of plasticised PMMA_1 with different amounts of DBP. As expected, plasticised PMMA possess results in decreasing the T_g with an increasing amount of plasticiser. Since the sample with 15% of the DBP showed the T_g=59°C, it was selected for further investigation, including gamma irradiation tests and the preparation of microcapsules (hereafter denoted as sample 'PMMA_3'). As stated in the Introduction section, the T_g=59°C should ensure good microcapsule stability in the reservoir, and as the difference between the reservoir temperature and the T_g is not significant, the response of the system to the applied activating stimulus ought to be relatively fast.

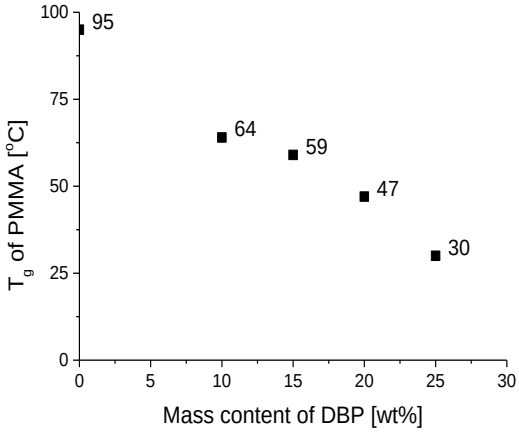

Figure 12. T_g of PMMA_1 containing various plasticiser concentrations. T_g of the polymer decreased with increasing content of the plasticizer within the investigated range.

3.2.2 Polymer gamma irradiation

All samples were exposed to different irradiation doses, and Table 5 shows the T_g, molecular weights and polydispersity of the studied polymers.

Table 5. Glass transition temperatures and molecular weight of non-irradiated and irradiated polymers with doses up to 10 kGy. The irradiation rate was 1 Gy/s.

Absorbed dose [kGy]	**PMMA_1**		**PMMA_2**		**PMMA_3**		**3F-PMMA_4**		**3F-PMMA_5**	
	T_g [°C]	**M_w [g/mol]**	**T_g [°C]**	**M_w [g/mol]**	**T_g [°C]**	**M_w [g/mol]**	**T_g [°C]**	**M_w [g/mol]**	**T_g [°C]**	**M_w [g/mol]**
0	95	15000 PDI 2.3	58	2000* PDI 1.6	59	15000* PDI 2.3	62	10000* PDI 2.5	71	22000* PDI 2.1
0.3	92	14 500	53		-		-		-	
0.5	90	15 000	54		-		-		-	
0.8	86	14 000	47		69		62		63	
1.6	83	13 500	46		52		49		74	
10	89	13 500	53		57		47		74	

**SEC calibration was undertaken for standard PMMA molecular weights. Therefore, SEC results are presented only for PMMA_1, since sample PMMA_2 has very low molecular weight and the plasticised sample is a mixture of two components, while fluorinated derivatives have different structures.*

Samples PMMA_1 and PMMA_2 had lower glass transition temperatures after irradiation, due to induced chain scission. Scission is a two-stage process initiated at unsaturated chain ends, and it is followed by random scissions of the backbone[86]. Therefore, in the first stage,

the molecular weight does not change significantly, because pendant and end group cleavage takes place. Scission of the main backbone causes observable changes in chain length. Since the molecular weights of irradiated samples did not change significantly, it was assumed that mainly end-chain degradation took place.

Figure 13 presents ^{1}H NMR spectra of sample PMMA_1, before and after irradiation. Peaks characteristic for protons derived from PMMA are described in section 2.2.2. Peaks attributed to a double bond of the monomer – methyl methacrylate (MMA) – were also observed in the spectrum at 5.5 and 6.0 ppm for both irradiated and non-irradiated samples. Integration of the signals indicated that the amount of monomer in the sample decreased during irradiation, presumably due to the volatility of methyl methacrylate. This means that the presence of the residual monomer did not cause any decrease in the T_g. ^{1}H NMR spectra of non-irradiated and irradiated polymers showed the same peaks, meaning the structure of PMMA did not change noticeably, and this confirmed our assumptions that a slight change in chain length was sufficient to influence polymer properties.

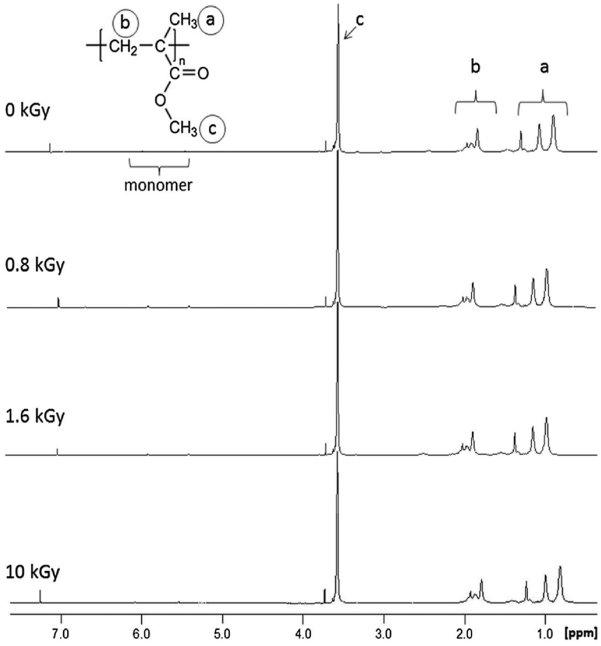

Figure 13. ^{1}H spectra of PMMA_1 exposed to various irradiation doses.

At the highest irradiation doses, the T_g started to increase slightly because of a cross-linking reaction[87]. When the concentration of degradation products increases, the possibility of macro-radicals recombining with each other also increases. Since PMMA monomers are very susceptible to free radical polymerisation, products formed during the degradation process

recombine and cross-link with each other. Therefore, the glass transition temperature of the PMMA increased.

Irradiated sample PMMA_3 behaved similarly to the non-plasticised sample. In both cases, the lowest T_g was observed at the dose of 1.6 kGy and started to increase at higher doses. Nevertheless, the influence of irradiation was less evident for the plasticised samples. It was found that plasticisers protect polymer compositions against chain scission. For instance, aromatic groups have the ability to absorb energy and increase the radiation stability of a mixture[88,89]. Furthermore, plasticisers act as lubricants between adjacent polymer chains and allow for greater molecular movement. This increased chain mobility leads to a higher rate of free radical migration, which in turn increases the possibility of radical collision. Therefore, the impact of irradiation on the T_g was less noticeable for the plasticised sample, although the data presented herein indicate that PMMA degradation did take place.

Fluorinated polymers showed slightly different behavior. On the one hand, the lowest T_g for sample 3F-PMMA_4 was observed at a dose of 10 kGy, indicating that chain scission dominated over cross-linking, even at higher doses, in contrast to non-fluorinated PMMA. On the other hand, the T_g of sample 3F-PMMA_5 decreased at lower doses, but at 10 kGy the T_g was higher than initially, meaning that cross-linking took place with higher efficiency than in the case of PMMA. The ^{1}H NMR method was used to investigate the structure of the irradiated polymer, but no new peaks were observed. It was assumed that gamma irradiation did not affect the structure of the polymers significantly. Therefore, there is no conclusive evidence that the fluorination process increases the sensitivity of PMMA to chain scission at given gamma irradiation doses.

3.2.3 Activation of microcapsules using gamma radiation

Microcapsules with a non-plasticised PMMA_1 and a plasticised PMMA_3 shell were prepared using the phase separation technique. Adding plasticiser did not influence the preparation process of the microcapsules, and because dibutyl phthalate is soluble in DCM and miscible with PMMA, plasticised PMMA microcapsules were successfully prepared. The ^{1}H NMR analysis confirmed the presence of DBP in the microcapsules. Fluorinated derivatives of the PMMA, due to their high hydrophobicity, were found to be unsuitable as a shell. Attempts were made in order to prepare the fluorinated microcapsules, the results for which are presented later in this chapter.

Due to that fact that plasticiser hinders the effects of gamma irradiation, only microcapsules with shell denoted as PMMA_1 (M_w=15000 g/mol) were exposed to irradiation. In order to

compare reactivity of the non-irradiated and irradiated microcapsules, microcapsules described in Chapter 2 (Table 1, entry 1-3) were used.

Firstly, microcapsules with a PMMA_1 shell were exposed to a 1.6 kGy dose, and then their reactivity with the vinyl-terminated DMS-V35 (containing 5 ppm of the Pt catalyst) was compared with reactivity of the non-irradiated microcapsules. The dynamic moduli of the mixture were measured at different temperatures, the results of which are presented in Figure 14. Non-irradiated microcapsules reacted with DMS-V35 at 100°C, as a significant increase in the storage modulus was observed. PMMA passes through a phase change transition at 95°C, and consequently microcapsules become permeable. Below 100°C, the microcapsules are relatively stable, because only minor increases in G' were observed. On the other hand, a dramatic increase in G' was observed at 30°C for irradiated microcapsules despite the fact that the T_g of the irradiated PMMA_1 was around 80°C, which means that not only does the T_g of polymer change during irradiation, but also local heating effects resulting from the delivered irradiation energy may affect the PMMA shell locally.

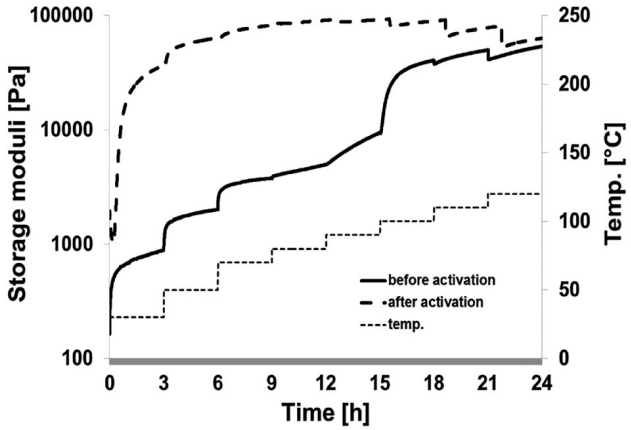

Figure 14. The reactivity of microcapsules (PMMA_1 as a shell) with vinyl-terminated DMS-V35, before and after irradiation. The mass ratio between the compounds was 1:10, respectively. DMS-V35 contained 5 ppm of the Pt catalyst.

3.2.4 Preparation of microcapsules with fluorinated derivatives of PMMA as a shell

In order to prepare the microcapsules with a fluorinated shell the phase separation method was also employed. The fluorinated derivatives of PMMA are highly hydrophobic, and so the interaction between the oil and the aqueous phases was expected to change. The composition of the oil phase (the ratio between the core and shell components as well as

their concentration in the organic solvent) remained unchanged, whereas various types and concentrations of emulsifiers were investigated. The studied systems are presented in Table 6.

Table 6. Studied systems for preparing microcapsules with fluorinated shell. In each experiment, 150 mL of the aqueous phase and 50 mL of the organic were used. The ratio between the core and the shell components was kept constant (0.75 g and 0.5 g of the HMS-301 and 3F-PMMA_4 were added, respectively).

Number	Composition of the aqueous phase	Organic solvent
1	1% PVA	DCM
2	3% PVA	
3	1% PMAA	
4	3% PMAA	
5	1% SDS	
6	1% PMAA + 15% gelatin	
7	1% PVA	chloroform
8	1% PVA	THF

Regardless of the aqueous phase composition used, the microcapsules were not successfully prepared. Mostly, agglomerations and lumps were formed, and optical microscopy images did not provide evidence for the formation of microcapsules. Moreover, the solution after evaporating the organic solvent was hazy, which might indicate that the non-encapsulated cross-linker remained in the aqueous phase. One idea for improving capsule formation was to increase the viscosity of the aqueous phase, in order to prevent the formation of agglomerations; however, once again, microcapsules were not obtained. Even when other organic solvents were used – chloroform and tetrahydrofuran (THF) – microcapsule preparation was not successful. Therefore, another preparation method was investigated, namely a spray technique.

The spray technique is widely used large-scale microencapsulation method, mainly employed in the food industry[90,91,92]. This technique also requires dissolving microcapsule components in organic solvent, but in contrast to the phase separation technique, the oil phase is sprayed into a poor solvent for the PMMA. Due to the atomisation of the oil phase, tiny droplets containing PMMA precipitate after being added to the poor solvent, which leads to the formation of microcapsules. Methanol was used as the poor solvent and three solvents were examined as the oil phase – DCM, chloroform and tetrahydrofuran (THF). Experimental details are described in the appendix assigned to this chapter.

Regardless of the organic solvent used, microcapsules with fluorinated shells were not obtained. As no clear evidence was found that fluorination of the PMMA enhances chain scission after exposure to small doses of gamma irradiation, further attempts to prepare the microcapsules were discontinued.

3.3 Conclusions

Gamma irradiation was examined for potential use as an activating stimulus for PMMA microcapsules. It was found that PMMA undergoes chain degradation following small doses of gamma irradiation, and therefore the glass transition temperature decreases. The effect of chain degradation is more noticeable for PMMA with a relatively low molecular weight. Moreover, physical modification of the microcapsule shells, by adding plasticiser, allows for the easy and fast control of the initial T_g of the microcapsule shell.

Secondly, the cross-linking reaction between the microcapsules and DMS-V35 takes place in a highly efficient manner after gamma irradiation activation. Before activation, microcapsules are stable at a wide range of temperatures, but when they are exposed to gamma irradiation, an encapsulated cross-linker is released at lower temperatures, and an elastomer network is created. Therefore, two main advantages of using gamma irradiation stimulus are the possibility of remotely activating microcapsules in unreachable places and a significant decrease in activation temperature.

Fluorinated derivatives of PMMA were also exposed to gamma irradiation, but no evidence was found to support the notion that the fluorination of polymers enhances the impact of irradiation. Many attempts were made to prepare microcapsules with the fluorinated shell, but the goal was not achieved. Due to high hydrophobicity of the polymer, the microcapsules were not prepared by neither the phase separation technique nor the spray method.

4. Microcapsules activated by an alternating magnetic field

The magnetic field penetrates through materials, so it can be used as a remotely applied activating stimulus. Prior to activation, magnetic nanoparticles are incorporated into a microcapsule structure. In a high-frequency magnetic field, nanoparticles generate heat, which causes melting of the PMMA shell and thereby releases cross-linker.

Four kinds of magnetic nanoparticles were investigated and encapsulated within the PMMA shell. The obtained materials were investigated across a wide range of frequencies, in order to find optimal conditions for the magnetic activation of microcapsule.

4.1 Characterisation of nanoparticles

Magnetic nanoparticles are a class of nanoparticle that can be manipulated using a magnetic field. When nanoparticles are exposed to a magnetic field they align with the direction of the field. Heat generation in the alternating magnetic field is caused by heat dissipation from magnetic nanoparticles, due to the Néel mechanism (independent of environmental viscosity) or the Brownian mechanism (dependent on environmental viscosity), when they are exposed to the AMF with magnetic reversal times shorter than the magnetic relaxation times of the nanoparticles[66]. Distinguishing between which mechanism occurs in a certain sample is not straightforward, but it is known that heat dissipation for smaller nanoparticles is mainly caused by the Néel mechanism[93,94]. In this study, nanoparticles of different sizes, namely between 10 and 50 nm, were examined, to investigate the impact of size on the heating properties of the nanoparticles. Moreover, nanoparticles with and without surfactant were tested. The role of surfactant is to prevent nanoparticles from creating agglomerations, but nowadays surfactant-free nanoparticles are gaining more attention, as they are environmentally friendly[95]. Table 7 summarises the properties of the tested particles. Three kinds of tested nanoparticles (EMG 1400, Fe_3O_4 and PDMS coated MNP) had the same chemical structure, namely Fe_3O_4, which is called 'magnetite'. Nanoparticles with a different structure, i.e. $MnFe_2O_4$, were also examined. EMG 1400 and $MnFe_2O_4$ are commercially available nanoparticles described in the literature as nanoparticles with potential usage in hyperthermia treatment[96,97,98], whereas PDMS-coated nanoparticles and Fe_3O_4 were synthesised according the reported reference[99], the experimental details for which are presented in the appendices assigned to this chapter. The sample labelled 'Fe_3O_4' was used without surfactant, whereas the sample denoted as 'PDMS-coated MNP' was coated with a silicone polyether copolymer, and therefore they differed in size.

Table 7. Properties of the examined magnetic nanoparticles.

Name of MNP	Size [nm]	Type of the used surfactant
EMG 1400	10	Unknown
PDMS coated MNP	50	Non-reactive PDMS
Fe_3O_4	10	No surfactant
$MnFe_2O_4$	50	No surfactant

4.2 Alternating magnetic field experiments

The AMF tests were performed using a MagneTherm instrument (purchased from Nanotherics), which operates at a wide range of frequencies. Figure 15 presents the device, which consists of a coil enclosure, a power supply, a function generator and an oscilloscope. The coil is connected to a cooling system, in order to avoid overheating. Hence, any temperature increase would be attributed only to the heating effect of the nanoparticles. Prior to the AMF tests, a glass vial with the nanoparticle mixture was placed in a polystyrene sample holder, to ensure good isolation and prevent any heat losses. A thermocoupled data logger (EL-USB-TC-LCD) was inserted into the glass vial, in order to monitor temperature changes to the mixture during the AMF measurements. Then, the polystyrene sample holder was placed inside a coil located in a coil enclosure. Before placing the polystyrene holder inside the coil, a required frequency was set and the experiments were performed.

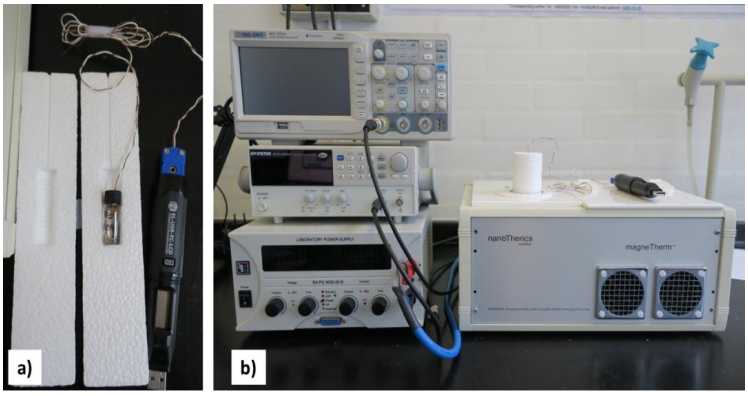

Figure 15. The set-up for the AMF tests. Figure 15a) shows the polystyrene holder with the glass vial. The data logger was inserted into the vial, thus enabling monitoring of temperature changes. In Figure 15b), the MagneTherm apparatus is presented. The polystyrene holder is placed in the coil, which is located inside the coil enclosure. A cooling system prevents the coil from overheating. A power supply, a function generator and an oscilloscope are also presented in Figure 15b).

Table 8. Tested AMF frequencies and maximum achievable field strength for given frequencies.

Frequency [kHz]	Maximum field strength [mT]
110	25
164	17
263	23
328	17
465	11
525	20
620	9
774	16
993	12

4.2.1 Investigation of aqueous mixtures in the AMF

Firstly, aqueous mixtures with 5% mass content of the MNP were prepared and exposed to AMF for 10 minutes at different frequencies. The results are presented in Figure 16. Figure 16a) presents the data obtained directly from the thermocouple data logger, while Figure 16b) summarises the highest temperature for each sample at all tested frequencies.

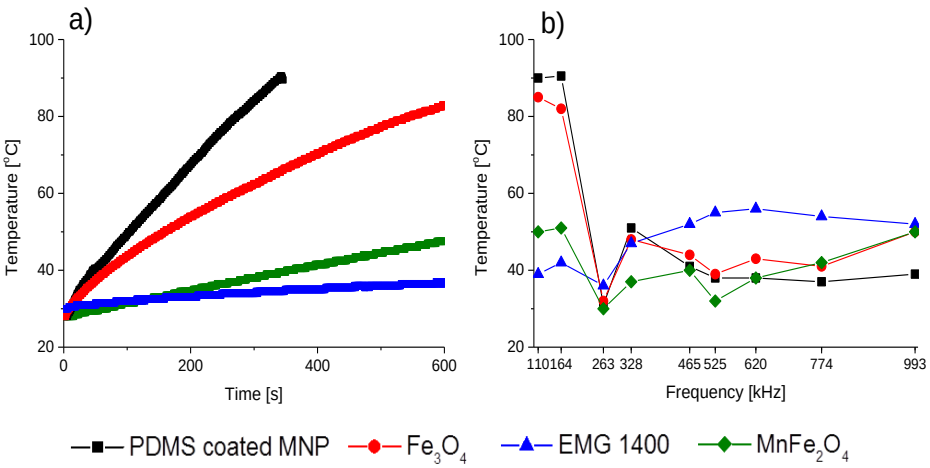

Figure 16.The relationship between the type of magnetic nanoparticle and temperature changes while exposed to the AMF. Figure 16a) presents temperature changes over time at 110 kHz for the tested nanoparticles, whereas Figure 16b) summarises the highest temperature reached by the tested nanoparticles at all examined frequencies.

The PDMS-coated nanoparticle mixture reached the highest temperature at 110 and 164 kHz. At given frequencies the temperature reached 90°C after 6 minutes of applying the AMF. The experiments were stopped to avoid boiling the sample. At other higher frequencies the nanoparticle mixture did not heat up so significantly. Starting from 328 kHz, the temperature decreased in line with increased frequency.

The Fe_3O_4 nanoparticle mixture exhibited similar heating properties to the PDMS-coated MNP. The highest temperature was observed at 110 and 164 kHz. At other frequencies, the observed temperature was significantly lower. When both kinds of nanoparticle are compared (PDMS-coated and Fe_3O_4 nanoparticles), it can be seen that at lower frequencies the nanoparticles with a surfactant generated more heat, whereas at higher frequencies non-coated nanoparticles showed better heating properties.

Although the EMG 1400 had the same chemical structure as the previously described nanoparticles, their mixtures did not heat up as significantly at the tested frequencies. The highest temperature was observed at 620 kHz (56°C), which means that the type of surfactant employed had a significant impact on the magneto-thermal properties of the nanoparticles.

The $MnFe_2O_4$ nanoparticles showed the weakest heating properties, indicating that the magnetite structure of the nanoparticles was favorable for obtaining high temperatures. Nevertheless, it was shown that at 164 kHz a 5% nanoparticle mixture could reach more than 50°C in 10 minutes.

4.2.2 Investigation of various mixtures in the AMF

In order to examine the impact of viscosity, magnetic nanoparticles were additionally examined in HMS-301 (viscosity 25-35 cSt) and in a vinyl-terminated DMS-V31 (M_w=28000 g/mol, viscosity 1000 cSt) medium. 5% mixtures of the EMG 1400 nanoparticles were prepared and tested at all frequencies for 10 minutes. Due to the limited amount of other kinds of nanoparticle, only PDMS-coated nanoparticles in more viscous liquids were tested at 110 kHz. A graph showing the results obtained for EMG 1400 nanoparticles is presented in Figure 17.

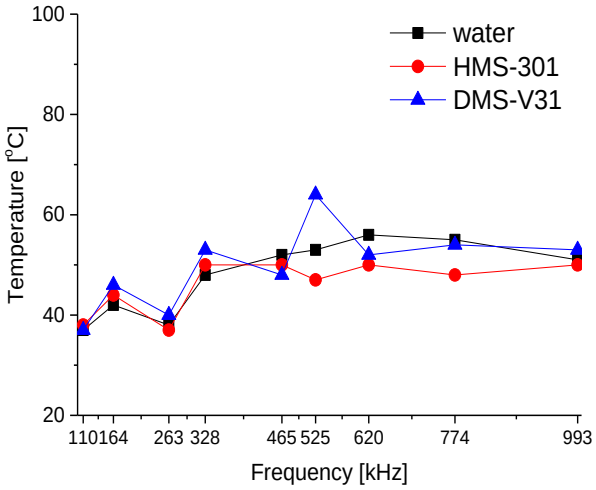

Figure 17. The highest recorded temperatures for 5% EMG 1400 mixtures in water, HMS-301 and in DMS-V31 at the tested frequencies.

When more viscous liquids were used as a medium, the temperature of the mixture at certain frequencies did not vary significantly from the temperature of the water mixtures. The difference in the temperatures for the tested liquids was not greater than just a few degrees. The exception was the DMS-V31 mixture at 525 kHz, when the mixture heated up 11°C more than the aqueous mixture. It is evident that the DMS-V31 mixtures mostly reached higher temperatures than the HMS-301 samples, but this finding cannot be related to viscosity, as aqueous mixtures at very few frequencies reached higher temperatures than the DMS-V31 mixtures.

PDMS-coated nanoparticle mixtures reached temperatures similar to the aqueous mixture: 90°C in less than 10 minutes, thus indicating that the viscosity of the medium did not change the heating properties of the nanoparticles.

From the data presented herein, it was concluded that the type of liquid used did not influence significantly the magnetothermal properties of the nanoparticles. No relationship between the viscosity of the liquid and the heating process of the nanoparticles was found, and so no conclusion about the heat dissipation mechanism could be made.

4.3 Preparation and characterisation of microcapsules with magnetic nanoparticles

After investigating the heating properties of the magnetic nanoparticles in various liquids, microcapsules with magnetic nanoparticles were prepared via solvent phase separation. The magnetic microcapsules were analysed in terms of their morphology, while the mass content

of the nanoparticles and the reactivity of the microcapsules, before and after exposure to the AMF, were also examined.

4.3.1 Microcapsules containing PDMS-coated nanoparticles

PDMS-coated nanoparticles are hydrophobic and miscible with the PDMS cross-linker. Hence, the phase separation method was suitable for preparing the magnetic microcapsules. An oil phase was prepared by adding the proper amount of PMMA, HMS-301 and magnetic nanoparticles to an organic solvent. The PMMA and the HMS-301 masses were kept constant at 0.25 g and 0.37 g, respectively. The prepared oil phase was placed in an ultrabath for 2 hours, to ensure good dispersion of the MNP. Afterwards, approximately 150 mL of aqueous emulsifier solution was charged to a 250 ml conical flask and the aqueous phase was mechanically stirred at 2000 rpm for 2–5 min. The oil phase was then added drop-wise over 60 s to form an oil-in-water emulsion. The agitation was kept for a further 2 hours at around 750 rpm. The dispersion of microcapsules was filtered by using a filtration pump. Finally, the product was washed with deionised water (~1.5 L) and dried at room temperature. Table 9 summarises the conducted experiments.

Table 9. Studied compositions for preparation of microcapsules containing PDMS-coated nanoparticles. Type and amount of the organic solvents and composition of aqueous phases as well as preparation temperature are given in the table.

No.	MNP [g]	Organic solvent	Aqueous phase [150 mL]	Temperature [C°]	Microcapsules formation
1	0.037	20 mL of DCM	1% PVA		a
2	0.037	10 mL of DCM	1% PVA		a
3	0.075	20 mL of DCM	1% PVA		a
4	0.037	20 mL of DCM	1% PVA, 3% SDS	20	b
5	0.037	20 mL of DCM	10% PVA		b
6	0.037	20 mL of chloroform	1% PVA		a
7	0.037	20 mL of toluene	1% PVA		c
8	0.037	20 mL of toluene	1% PVA	35	c
9	0.037	20 mL of toluene	5% PVA	20	c

[a] Formation of microcapsules without MNP enclosed within the PMMA shell

[b] Microcapsules did not form

[c] Formation of microcapsules with MNP enclosed within the PMMA shell

As presented in Chapter 2, non-magnetic microcapsules were obtained when the oil phase consisted of 20 mL of the DCM, 0.25 g of the PMMA and 0.37 g of the HMS-301. Using the

same oil phase composition, albeit with the addition of MNP (Table 8, no.1), did not lead to the formation of microcapsules containing MNP. Some nanoparticles were dispersed in the aqueous phase, but most of them settled on the bottom of the flask. In order to decrease formation time of the PMMA shell and to prevent the unwanted spreading of MNP into the aqueous phase, a lower amount of the DCM was used (Table 8, no.2); however, the MNP was not enclosed within the PMMA shell. An increased amount of MNP in the oil phase (Table 8, no.3) did not lead to the encapsulation of the nanoparticles within the polymer shell, and so further experiments were conducted. Subsequently, the composition of the aqueous phase was changed, whereby a 1% PVA and 3% SDS solution was used (Table 8, no.4), which resulted in the dispersion of all components in the aqueous phase and microcapsules were not obtained. Afterwards, the viscosity of the aqueous phase was increased to prevent the MNP diffusing into the aqueous phase (Table 8, no.5), but this did not cause the encapsulation of MNP. Since all experiments with DCM as the oil phase were unsuccessful, other organic solvents were examined – chloroform and toluene. When chloroform was used (Table 8, no.6) microcapsules were formed, but they did not contain MNP. Employing toluene as an organic solvent resulted in the formation of microcapsules which contained MNP (Table 8, no.7). In order to examine if the presence of the nanoparticles influenced the impermeable nature of the microcapsules, the magnetic microcapsules containing PDMS-coated MNP were mixed with vinyl-functional DMS-V31, which was less viscous than the previously used DMS-V35. The change of DMS was due to that the microcapsules could be more uniformly dispersed in lower-viscous media. The viscosity of DMS-V35 was simply too high for this purpose, and hence DMS-V31 with 5 ppm of the Pt catalyst was used in the subsequent work. The DMS-V31 mixture with 5wt% of the microcapsules became a gel at room temperature due to the overly high permeability of the PMMA shell. Hence, further experiments were conducted, in order to improve the impermeability of the shell. The next experiment was carried out at 35°C instead of 20°C (Table 8, no.8). The increased temperature of the aqueous phase should increase the evaporation rate of the organic solvent and facilitate the rapid formation of the polymer shell. Moreover, rapid solidification of the PMMA ought to prevent incorporating MNP into the shell structure and lead to non-porous microcapsules. In order to reach the required temperature, a flask with the aqueous and the oil phases was immersed in a water bath and heated up to 35°C by a hot plate. Dissolved PMMA in toluene created a layer on the surface of the aqueous phase, and microcapsules were not obtained. In the next synthesis, a 5% PVA solution was utilised as the aqueous phase (Table 8, no.9). A higher concentration of the emulsifier resulted in higher viscosity of the phase. In the more viscous medium, the organic solvent droplets were immobilised further, and the diffusion of MNP into the aqueous phase was limited. This led to the formation of spherical microcapsules with

a high amount of MNP. The prepared microcapsules, which are presented in Figure 18, had a distinct shell and the magnetic nanoparticles remained enclosed within the PMMA shell.

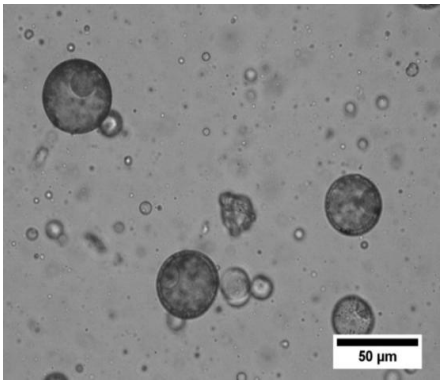

Figure 18. Optical microscopy images of the microcapsules containing the PDMS-coated nanoparticles (Table 8, no.9).

TGA analysis allowed for determination of the MNP content in the microcapsules (Figure 19). Firstly, the PDMS-coated nanoparticles were examined. Residue from the nanoparticles at 800°C was found to be 79.2%, which was equal to inorganic part of the nanoparticles. It means that almost 21% of the nanoparticles mass was the PDMS coating. Subsequently, the magnetic microcapsules containing the PDMS-coated MNP were analysed. It is known that PMMA and HMS-301 decompose almost without any residue[84]. Hence, residue at 800°C was equal to the inorganic part of the PDMS-coated MNP, which was 13,5%. In order to determine the real content of the PDMS-coated MNP, the identified residue was increased by 21%, and the total content of the nanoparticles, including the PDMS coating, was estimated to be 16.3%.

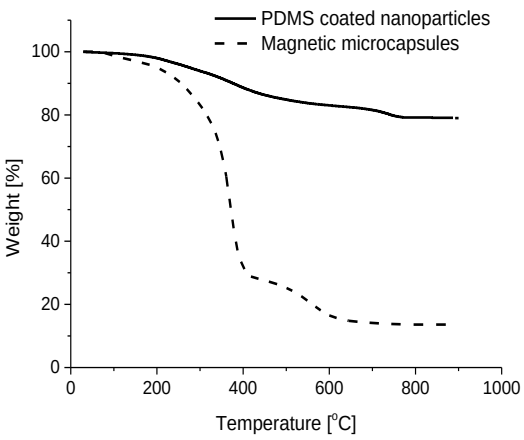

Figure 19. TGA curves of pure PDMS-coated MNP and magnetic microcapsules with encapsulated PDMS-coated nanoparticles.

The mass content of the core and shell components was determined by the peak integration method using the NMR method. Firstly, the microcapsules were dissolved in chloroform-d, and then the solution was decanted in order to remove any MNP. This prepared solution was examined by ^{1}H NMR analysis. PMMA and HMS-301 content was found to be 47% and 53%, respectively. Taking into consideration TGA and NMR analysis, it was established that 1 g of the microcapsules consisted of 0.16 g of MNP, 0.39 g of PMMA and 0.44 g of HMS-301.

Subsequently, the microcapsules (Table 8, no.9) were mixed with vinyl-terminated DMS-V31. A 5wt% mixture of the microcapsules in the DMS-V31 become a gel at room temperature after approximately 20-30 minutes, denoting that the encapsulation of the cross-linker was improved compared to the previously characterised microcapsules (Table 8, no.7).

It was shown that the PDMS-coated nanoparticles heated up to 120°C at 110 kHz in 10 minutes when they were dispersed in the PDMS cross-linker. Similar behavior was expected for the nanoparticles encapsulated within the PMMA shell. A 5wt% microcapsule water solution was prepared and exposed to the AMF for 30 minutes at 110 kHz. The temperature of the mixture was then measured during the experiment, with Figure 20 showing temperature changes over time.

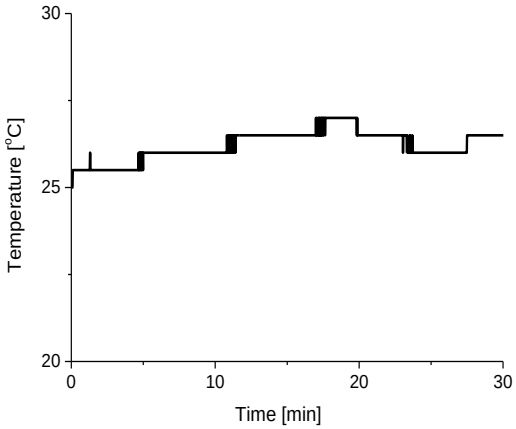

Figure 20. Temperature of the 5% microcapsule mixture in water while subjecting the mixture to AMF at 110 kHz for 30 minutes. The microcapsules contained PDMS-coated nanoparticles.

When the 5% microcapsule mixture in water was exposed to the AMF, its temperature did not increase significantly. Only minor changes were observed, and the temperature did not exceed 30°C, possibly because the total concentration of the magnetic nanoparticles in the mixture was very low, in which case the amount of MNP was not sufficient to heat up the whole mixture. However, the concentration of MNP inside the PMMA shell was estimated at 16%. It was shown previously in Chapter 3 that local heating effects can lead to changes in the PMMA shell and enhance the release of the cross-linker. Therefore, optical microscopy images were taken and the appearances of the microcapsules, before and after exposure to the AMF, were compared (Figure 21).

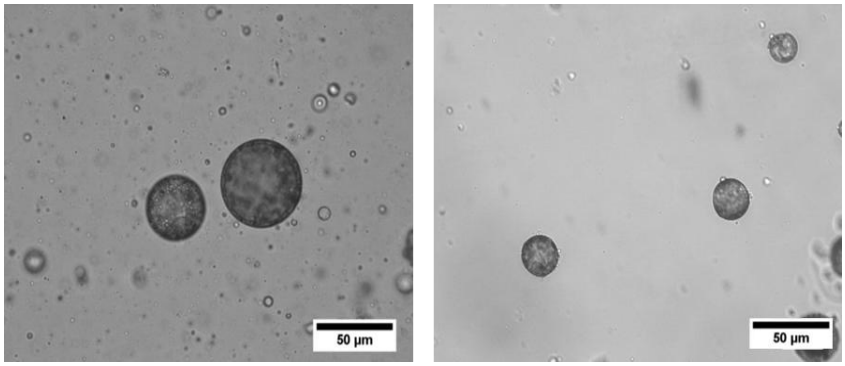

Figure 21. Optical microscope images of the magnetic microcapsules containing PDMS-coated nanoparticles, before (left) and after (right) exposure to the AMF, at 110 kHz for 30 minutes.

In both images, the microcapsules looked similar. The PMMA shell was not ruptured after the AMF tests and the microcapsules still had a round shape, which indicated that the nanoparticles did not generate enough heat to cause physical changes in the PMMA shell.

Subsequently, a 25% microcapsule mixture was tested at 110 kHz, but again the temperature did not rise significantly and no noticeable changes in the microcapsules structure were observed under the microscope. The experiment was performed at other frequencies, and in all experiments the mixture temperature did not exceed 30°C and the structure of the microcapsules remained unchanged.

4.3.2 Microcapsules containing Fe_3O_4 nanoparticles

The preparation of the microcapsules with Fe_3O_4 magnetic nanoparticles was straightforward, and the procedure was as follows. An oil phase was prepared by adding 0.25 g of the PMMA, 0.37 g of the HMS-301 and 0.037 g of the Fe_3O_4 magnetic nanoparticles to 20 mL of the DCM. The mixture was then sonicated for 2 hours in an ultrasound bath. Subsequently, the oil phase was added to 150 mL of 1% PVA emulsifier solution. This oil-in-water emulsion was mechanically stirred for further 2 hours at around 750 rpm. After that time, microcapsules consisting of PMMA shell and a liquid HMS-301 core with magnetic nanoparticles were washed with 1L of DI water and dried overnight in a fume hood.

The microcapsules presented in Figure 22 are spherical in shape and the magnetic nanoparticles are encapsulated within the polymer shell.

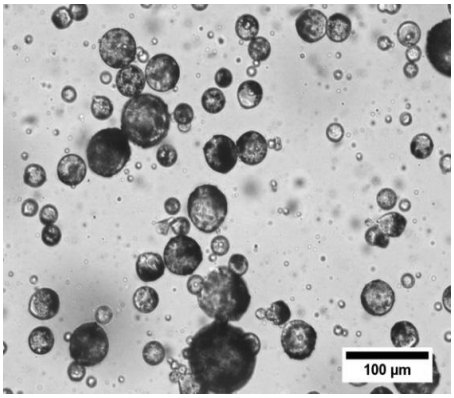

Figure 22. Optical microscopy image of microcapsules containing Fe_3O_4 magnetic nanoparticles.

The mass content of the magnetic nanoparticles was found to be 20%. Figure 23 presents TGA curves of the Fe_3O_4 nanoparticles and the magnetic microcapsules containing these MNP. By employing peak integration of the ^1H NMR spectra, PMMA and HMS-301 mass

content was found to be 45% and 55%, respectively. Hence, 1 g of the magnetic microcapsules consisted of 0.2 g of the magnetic nanoparticles, 0.36 g of the PMMA and 0.44 g of the HMS-301.

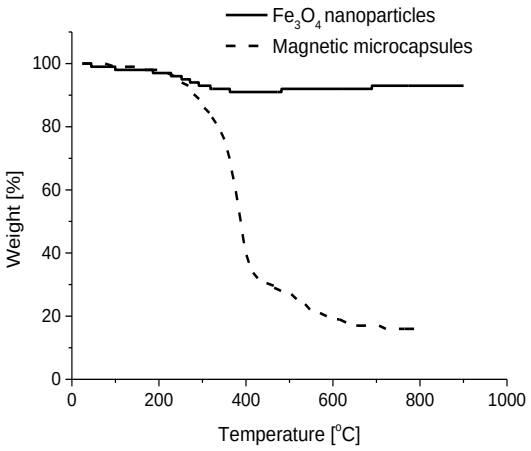

Figure 23. TGA curves of pure Fe_3O_4 nanoparticles and magnetic microcapsules with Fe_3O_4 MNP.

After mixing the microcapsules with the vinyl-terminated DMS-V31, the mixture did not become a gel at room temperature, thereby implying that the PMMA shell was impermeable. To investigate the stability of the microcapsules at 50°C, time sweep tests were perfored using the rheometer. Firstly, the microcapsules were mixed with DMS-V31 with a mass ratio of 1:10. In Chapter 2 it was shown that using the given mass ratio ensured the formation of the PDMS network between the DMS-V35 and the microcapsules at 120°C. Subsequently, the sample was tested at two temperatures – 50°C (below the T_g of the PMMA) and at 120°C (above the T_g of the PMMA). The results are presented in Figure 24. The performed tests showed that the microcapsules were impermeable at 50°C for 1 hour, as both moduli remained unchanged over time, and the G'' (loss modulus) was higher than the G' (storage modulus) during the entire measurement phase. At 120°C, as expected, the PMMA became soft and pliable and the microcapsules collapsed, thereby releasing the cross-linker. This led to the formation of the three-dimensional network and a subsequent increase in the storage modulus, which became higher than the loss modulus, thus confirming the formation of the PDMS network.

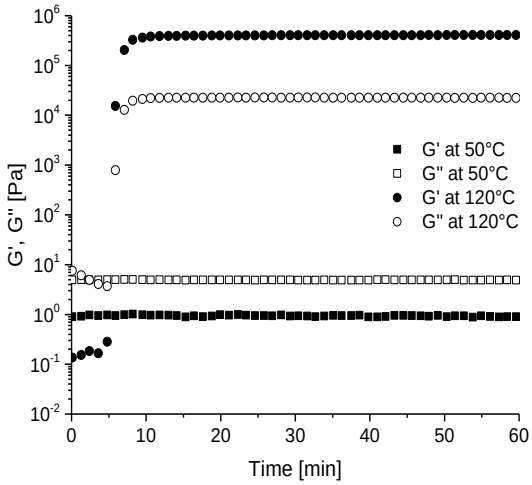

Figure 24. Storage and loss moduli (G' and G'') of the microcapsules containing Fe_3O_4 nanoparticles with DMS-V31. The mass ratio between the compounds was 1:10. The utilized DMS-V31 contained 5 ppm of the Pt catalyst and the measurements were performed at 50°C and 120°C, respectively, for 1 hour.

The presented data in Figure 24 differs slightly from the results shown in Figure 8. In Figure 8, the storage modulus at 50°C increased to some extent, whereas in Figure 24 the storage modulus remained constant at certain temperature. This divergence may result from the fact, that different microcapsules were tested – with and without the magnetic nanoparticles. The fact that the G' of the mixture with the magnetic microcapsules did not increase at 50°C, in contrast to the sample with non-magnetic microcacules, implies that microcapsules with the magnetic nanoparticles were more impermeable than the non-magnetic microcapsules.

The magnetic microcapsules with Fe_3O_4 nanoparticles were tested at 110 kHz, as the aqueous mixture with the nanoparticles reached the highest temperature among the tested frequencies. Moreover, in contrast to microcapsules containing the PDMS-coated MNP, the microcapsules with Fe_3O_4 were impermeable, and a mixture with DMS-V31 did not solidify at 50°C. Therefore, two samples were prepared – in water and in the DMS-V31 as a medium. The mass content of the magnetic microcapsules in both samples was equal to 5%. The solidification of the DMS-V31 sample after exposing it to the magnetic field ought to be assiged to the release of the cross-linker and the formation of the network. Figure 25 presents an evaluation of temperature while applying the alternating magnetic field. The temperatures of both samples did not increase, and in fact they even slightly decreased, which means that no nanoparticle heating effects were noted. In the optical microscopy

images, microcapsules which were mixed with water look the same before and after exposure to the AMF. In addition, the DMS-V31 mixture did not solidify after 30 minutes of the AMF experiment, which means that the PMMA shell remained intact and the cross-linker was not released into the surrounding environment. Tests performed at other frequencies led to similar results.

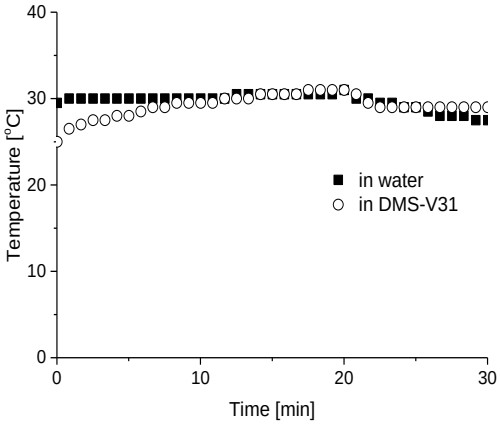

Figure 25. Temperature of the 5% microcapsules mixtures in water and in DMS-V31 while subjecting the mixtures to AMF at 110 kHz for 30 minutes. Microcapsules with enclosed Fe_3O_4 nanoparticles were tested.

4.3.3 Microcapsules containing EMG 1400 nanoparticles

The preparation procedure for the microcapsules with EMG 1400 magnetic nanoparticles was as follows. An oil phase was prepared by adding 0.25 g of the PMMA, 0.37 g of the HMS-301 and 0.037 g of the EMG 1400 magnetic nanoparticles to 20 mL of DCM. The mixture was then sonicated for 2 hours in an ultrasound bath. Subsequently, the oil phase was added to 150 mL of a 1% PVA emulsifier solution. The oil-in-water emulsion was mechanically stirred for further 2 hours at around 750 rpm. After that time, microcapsules consisting of the PMMA shell and the liquid HMS-301 core with the magnetic nanoparticles were washed with 1L of DI water and dried in a fume hood overnight.

Figure 26a) presents an SEM image of the microcapsules with a PMMA shell. All the microcapsules were spherical and their diameter fell between 5 and 50 µm. Optical microscopy images (Figure 26b) showed that the MNPs were mainly present in the core, as the inner part of the microcapsules was black. Additionally, the presence of nanoparticles was confirmed by scanning electron microscopy accompanied by X-ray microanalysis (EDS). Figure 26c) shows obtained data, where the colour purple represents iron atoms. It is obvious

that MNP were mainly located in the core. The analysis also allowed for characterising the polymeric shell, which was mainly non-porous with only a few voids. It was concluded that the PMMA coating successfully protected the encapsulated cross-linker, and the presence of the EMG 1400 nanoparticles did not influence the shell structure negatively.

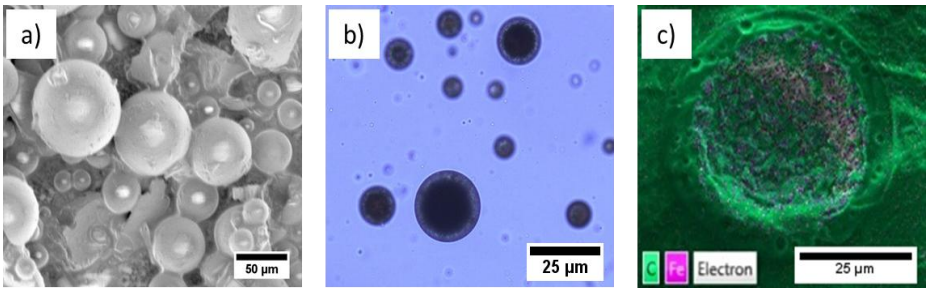

Figure 26. Microscopic images of the microcapsules with magnetic nanoparticles. Figure 26a) presents SEM images of the dried microcapsules, whereas Figure 26b) shows microcapsules in a water solution. Distribution of the magnetic nanoparticles (Figure 26c) was performed by EDS analysis. Purple colour represents iron atoms.

Commercially available EMG 1400 nanoparticles are coated with surfactant, which prevents particle agglomeration. The chemical structure of the surfactant used herein was unknown, and from the TGA analysis it was found that the mass content of the surfactant was 22%; hence, the inorganic part of the nanoparticles was found to be 78%. In order to determine the content of the EMG 1400 nanoparticles inside the microcapsules, the magnetic microcapsules with EMG 1400 nanoparticles were also analysed and the residue value of the magnetic microcapsules at 800°C was increased by 22%, to determine the mass content of the nanoparticles, including the coating. It was concluded that the total content of the nanoparticles was 28%. The TGA curves are shown in Figure 27.

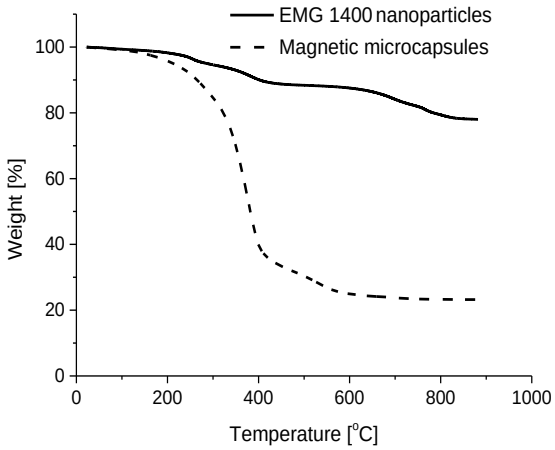

Figure 27. TGA curves of the EMG 1400 nanoparticles and the magnetic microcapsules with encapsulated EMG 1400 nanoparticles.

By employing the peak integration of the ^{1}H NMR spectra, PMMA and HMS-301 mass content was found to be 47% and 53%, respectively. Hence, 1 g of the magnetic microcapsules consisted of 0.28 g of the magnetic nanoparticles, 0.34 g of the PMMA and 0.38 g of the HMS-301.

Subsequently, the microcapsules were mixed with DMS-V31 (with 5 ppm of the Pt catalyst) and examined in terms of their impermeability at room temperature. This prepared sample remained stable at room temperature for a long time. Surprisingly, even when the mixture was heated up to 120°C, a reaction between the cross-linker and the vinyl-terminated PDMS did not take place, whereas the physical mixture of the four components (EMG 1400, PMMA and HMS-301 and DMS-V31) created a network at elevated temperatures. This indicated that the encapsulation process of the nanoparticles induced interaction between the particles and the cross-linker. After the literature study, it was found that one of the most popular surfactants used to coat nanoparticles is an oleic acid, which has a double bond in the structure[100,101]. Hence, it is very likely that the surfactant used in EMG 1400 is similar to oleic acid and also has a double bond. Encapsulated nanoparticles were dispersed in the cross-linker, and hence the interaction between them was strong. When the microcapsules collapsed, the platinum catalyst was delivered to the inner part of the microcapsules, thereby enabling the hydrosilylation reaction between the nanoparticles and the cross-linker. This led to the formation of covalent bonds between the nanoparticles and the cross-linker, and as a result the cross-linker could not react further with the vinyl-terminated PDMS compound. The spatial distribution of the components in the physical mixture was uniform, and so the

cross-linker was able to react equally with the nanoparticles and with DMS-V31, which explained the formation of the solid network at 120°C.

Microcapsules containing EMG 1400 nanoparticles could not be applied in this project, as the nanoparticles react with the cross-linker and hinder the hydrosilylation reaction between the cross-linker and the PDMS microparticles. Nevertheless, it was shown that the preparation procedure is not complicated, and the presence of the magnetic nanoparticles did not influence the microcapsules' structure.

Microcapsules with $MnFe_2O_4$ nanoparticles were also prepared and characterised, but since magnetic activation was not achieved, the obtained results are presented in the appendix assigned to Chapter 4.

4.4 Impact of the organic solvent and ultrasonication on nanoparticle properties

The previous study illustrated that the behavior of encapsulated nanoparticles differs from unprocessed particles, since encapsulated nanoparticles tend to lose the ability to generate heat in an alternating magnetic field. Two potential reasons were investigated – the influence of organic solvent and the impact of ultrasonication. Firstly, 5% PDMS-coated nanoparticle mixtures in water and in toluene were prepared, following which temperature changes while exposed to the AMF at 110 kHz of the non-ultrasonicated mixtures were compared. Then, the toluene mixture was ultrasonicated in an ultrasound bath for 2 hours. The samples were collected in 10-minute intervals and subjected to the AMF for 10 minutes, in order to investigate the impact of ultrasonication time on the heating properties of the nanoparticles. The results are presented in Figure 28.

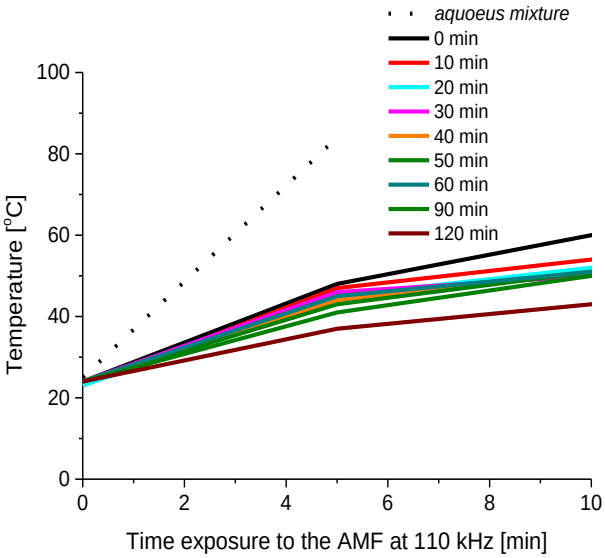

Figure 28. The relationship between ultrasonication time and the heating properties of the PDMS-coated nanoparticles in the AMF at 110 kHz. The straight lines represent the 5wt% toluene mixture of the nanoparticles. The dotted line denotes the 5% aqueous mixture of the PDMS-coated nanoparticles, which was not ultrasonicated (the measurement was stopped after 6 minutes, in order to avoid boiling the sample).

The usage of toluene as a solvent had a negative impact on MNP heating properties. The temperature of the aqueous mixture reached 90°C in 6 minutes, whereas the toluene mixture reached only 60°C in 10 minutes, although it was not ultrasonicated. From the previous tests it was also known that when PDMS-coated nanoparticles are mixed with the cross-linker and subjected to the AMF, the mixture reaches 120°C in 10 minutes, which means that the usage of the toluene was the factor which decreased the heating properties of the nanoparticles. Additionally, the toluene mixture of the Fe_3O_4 nanoparticles was tested at 110 kHz. The toluene sample heated up significantly less than the aqueous mixture (60°C and 83°C, respectively), thereby confirming the negative impact of toluene. Although microcapsules containing Fe_3O_4 and EMG 1400 nanoparticles were prepared by using DCM as the oil phase, tests with DCM were not performed, as the boiling point of DCM is only 39.6°C. Nevertheless, the poor heating properties of these magnetic microcapsules could be also assigned to the preparation procedure, which involves using an organic solvent. Organic solvent can influence the surface properties of nanoparticles, thus leading to significant changes in nanoparticle properties.

Additionally, it can be seen that the ultrasonication process influences the heating properties of MNP. The toluene mixture, before ultrasonication, heated up to 60°C in 10 minutes, whereas after 120 minutes of ultrasonication the temperature reached 43°C. It was found that 10 minutes of oil ultrasonication was not sufficient to disperse the nanoparticles in the organic solvent. Microcapsules obtained from this prepared oil phase varied, but most did not contain MNP, and only a few microcapsules with encapsulated MNP were observed. A great part of the MNP remained on the bottom of the flask. Therefore, another way to disperse nanoparticles needs to be developed.

4.5 Magnetic microcapsules and PDMS microparticles

Although magnetic activation was not achieved, the magnetic microcapsules with the PDMS-coated MNP were mixed with PDMS microparticles, in order to obtain a cross-linked material. A reaction between the cross-linker and PDMS microparticles is possible, due to the presence of the vinyl groups on the surface of the microparticles. To ensure good contact between the microparticles, the samples were prepared under high pressure, using a hot press. In total, 1 g of PDMS microparticles was mixed with microcapsules at different ratios (10-1, 20-1 and 30-1) and transferred to a metal mould, following which 0.1 g of the non-reactive silicone oil with 5 ppm of a platinum catalyst was also added. The mould was then placed for 3 hours in the hot press under 100 bars, and the temperature was set at 120°C. Cross-linked samples were then demoulded and analysed. Figure 28 shows SEM images of the cross-linked plug samples at different ratios. Since the microcapsules contained the MNP, it was easy to distinguish them from the PDMS microparticles. It is evident that the microcapsules were uniformly dispersed within the sample, without the occurrence of agglomerations, thereby resulting in the homogeneous distribution of a released cross-linker and therefore the formation of a uniform network. Moreover, due to high pressure, the microparticles were tightly packed and the reaction between the cross-linker and the vinyl groups led to good bonding between the PDMS microparticles.

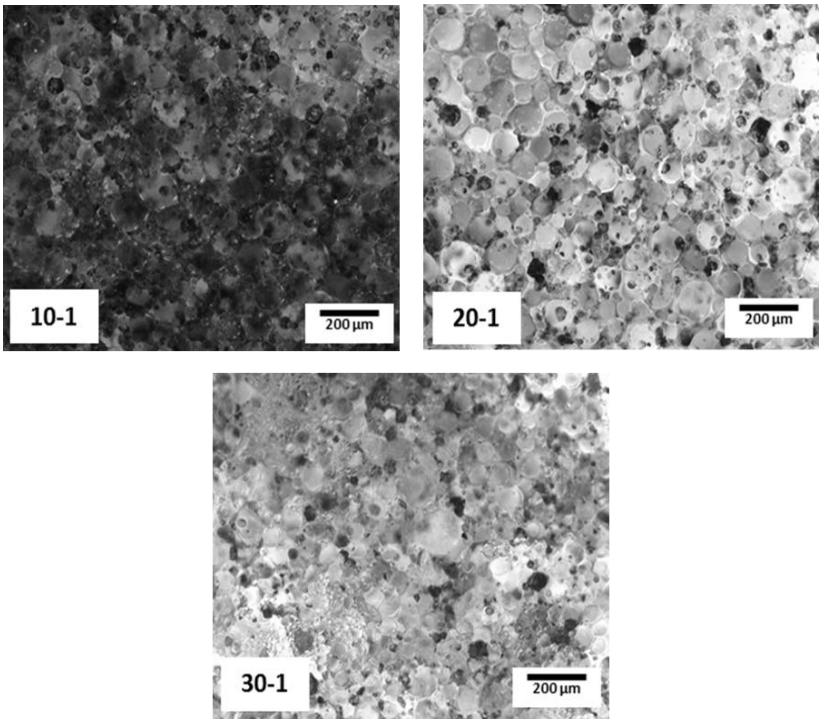

Figure 29. SEM images of the cross-linked plug samples containing magnetic microcapsules and vinyl-functional PDMS microparticles. The ratio between the microcapsules to the microparticles is stated on the picture. The microcapsules contained PDMS-coated MNP.

Viscoelastic properties of the cross-linked samples were investigated using a rheometer. Figure 30 presents frequency sweep results for the three samples at various ratios. Samples with the ratios 10-1 and 20-1 had an almost identical storage modulus (G'). The sample with the 30-1 ratio had a slightly lower G', but the difference was not significant. What is important is that the storage modulus of all the samples was independent of frequency, as would be expected from a structured material. The measurements proved that samples with tested mass ratios showed constant elastic properties. This conclusion is highly valuable, because while injecting material into a fracture, the composition of the components cannot be controlled precisely. The data presented herein demonstrate that deviations in ratios between components (within the tested range) will not have a negative impact on plug properties.

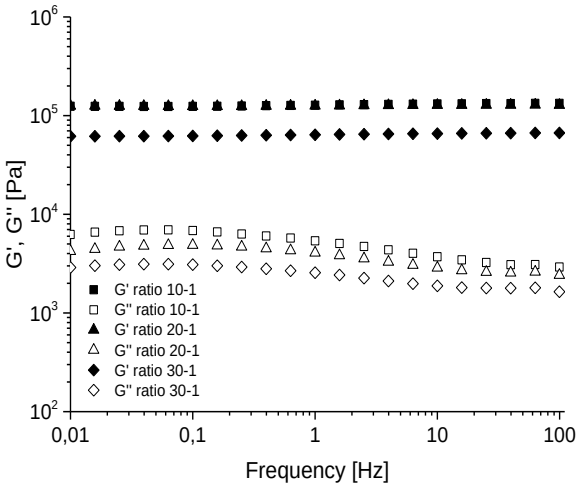

Figure 30. The storage (G') and the loss (G'') moduli of the cross-linked plug samples containing magnetic microcapsules and vinyl-functional PDMS microparticles. The ratio between the microcapsules to the microparticles is stated in the graph. The microcapsules contained PDMS-coated MNP.

4.6 Conclusions

An alternating magnetic field was tested as a potential activating stimulus for microcapsules. Firstly, aqueous nanoparticle mixtures were exposed to the AMF at various frequencies. The mixture with the PDMS-coated nanoparticles exhibited the best heating properties at 110 kHz, reaching 90°C in 6 minutes. When the nanoparticles were mixed with the cross-linker, the mixture reached 120°C in 10 minutes. The Fe_3O_4 nanoparticles also showed good heating properties at the mentioned frequency. The mixture with the nanoparticles heated up to 80°C in 10 minutes. Samples with the EMG 1400 nanoparticles showed fairly good properties at 620 kHz, reaching 56°C and proving the ability of the particles to generate heat at a certain frequency. The maximum temperature reached for the $MnFe_2O_4$ nanoparticles was 50°C, meaning that these particles possessed the weakest heating properties among the tested nanoparticles.

All of the magnetic nanoparticles were successfully encapsulated within the PMMA shell, using the phase separation technique. The mass content of the nanoparticles varied between 16 and 28%. The presence of the nanoparticles did not cause any increase in the size of the microcapsules; moreover, it was shown that the impermeability of microcapsules containing Fe_3O_4 nanoparticles remained unchanged, as the cross-linker was not released at 50°C. The optical microscopy images and SEM images confirmed that the nanoparticles were located mainly in the liquid core, without affecting the PMMA shell. Moreover, by applying EDS

analysis, it was shown clearly that the EMG 1400 nanoparticles were mainly encapsulated in the inner part of the microcapsules.

When microcapsules with encapsulated PDMS-coated nanoparticles and with Fe_3O_4 nanoparticles were exposed to the AMF at 110 kHz, the temperature of the mixture did not rise and the structure of the microcapsules remained unchanged. Two potential reasons were investigated – the usage of organic solvent during the preparation of the microcapsules, and the application of ultrasound waves to disperse the nanoparticles in the solvent. Both factors were found to decrease the heating ability of the nanoparticles. Therefore, the preparation technique needs to be modified. One idea involves using nanoparticles which are stable in organic solvent. Additionally, these nanoparticles cannot be coated with a double-bonded surfactant. As oleic acid and its derivatives are commonly used surfactants, not many commercial products fulfill this requirement. Hence, it would be reasonable to develop the synthesis of nanoparticles coated with a well-known surfactant. Another solution could be to replace the PMMA with a more temperature-sensitive polymer. Although magnetic nanoparticles heat up less after mixing with organic solvents, they are still capable of heating the mixtures. Hence, the usage of polymers which are more thermosensitive and exhibit good encapsulation properties at 50°C could solve the problem. Perhaps, in this regard, microcapsules with the plasticised PMMA shell could be magnetically activated. As presented in Chapter 3, plasticised PMMA is suitable as a shell material. Therefore, the next step would be to encapsulate magnetic nanoparticles within the plasticised PMMA shell.

5. Ultrasonic activation

Ultrasound waves were tested as an activating stimulus for microcapsules. PMMA is known to be brittle and hard below the T_g, and when treated with ultrasound waves the PMMA shell should break, thereby leading to the microcapsules collapsing and thus releasing the cross-linker.

5.1 Ultrasonic experiments

In order to investigate how ultrasonic treatment affects the structure of microcapsules (Table 3, no.1), and to examine whether this activation method is appropriate for oilfield applications, the experiments were divided into two parts. Firstly, the ultrasound waves were directly applied to the mixtures containing microcapsules – an ultrasound probe was immersed in the mixture in order to investigate whether microcapsules can be damaged by the ultrasonication. Subsequently, tests were designed to examine the impact of indirectly applying ultrasound waves. Foil was located on top of the vial, placed in the water bath, which should give an overview of the efficiency of indirect application in a reservoir. Figure 31 presents both approaches. All samples were ultrasonicated using a Hielscher UP200S ultrasonic processor at 24 kHz. Amplitude was set at 100%, as it is needed to obtain high ultrasonication intensity and promote cavitation in more viscous liquids[102].

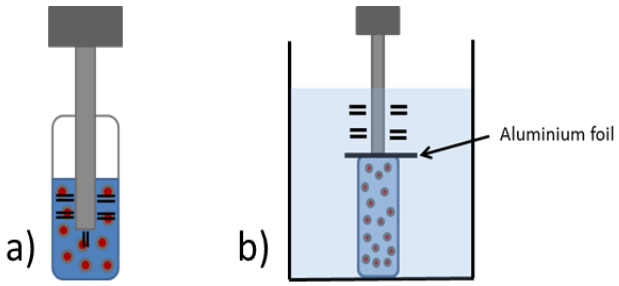

Figure 31. Schemes of the two applied ultrasonication approaches. Figure 30a) shows the direct application of ultrasound waves, whereas in Figure 30b) indirect application is presented, where aluminium foil was used as an obstacale to the ultrasound waves.

5.1.1 Direct application of ultrasound waves

Firstly, 2.5 mL of an 18% aqueous microcapsule mixture was subjected to ultrasound waves for 30 minutes. During ultrasonication, the microcapsules moved vigorously inside the vial, indicating that the ultrasound waves were strongly influencing the microcapsules. The

samples were taken in 10-minute time intervals. Subsequently they were dried and analysed by SEM, and the results are shown in Figure 32.

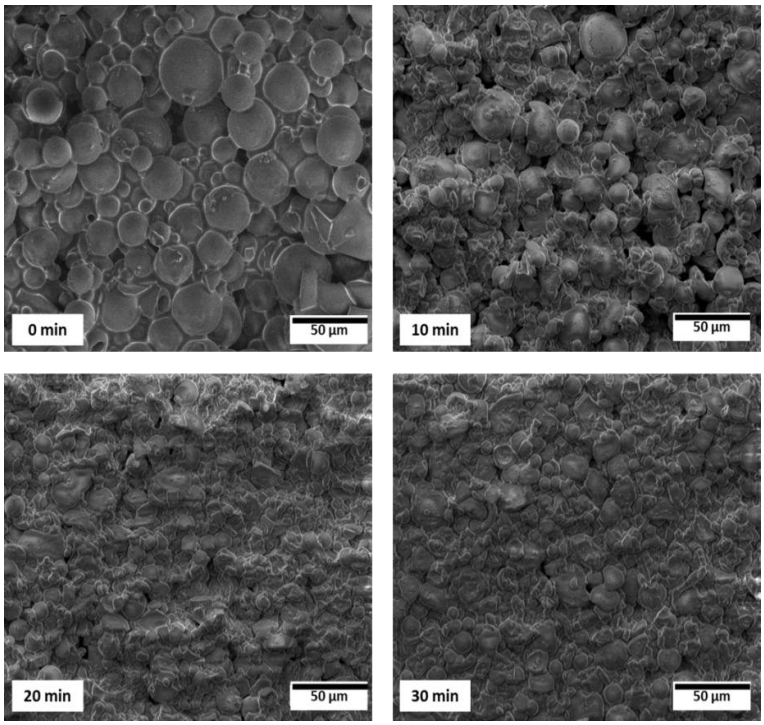

Figure 32. SEM images showing the microcapsules before and after ultrasonication where the ultrasound waves were applied directly to the mixture. It can be noted that with increasing ultrasonication time, the microcapsules became more damaged.

The ultrasound waves acted destructively on the microcapsules. From the SEM images it is evident that after 10 minutes of ultrasonication most of the microcapsules cracked, and after 20 minutes almost all of them broke completely. There was no obvious difference between the samples ultrasonicated for 20 and 30 minutes. Hence, 20 minutes of ultrasonication in water was sufficient to release the cross-linker from the microcapsules.

Subsequently, the experiment was repeated using DMS-V31 (containing 5 ppm of the Pt catalyst) instead of water. The concentrations of microcapsules and the sample volume were unchanged. SEM images could not be taken, since the sample had to be cleaned and dried prior to examination. Hence, the platinum catalyst was added to DMS-V31 and the progress of the cross-linking reaction was observed. After 30 minutes of ultrasonication, the mixture did not become solid, meaning that the microcapsules remained intact. Probably due to higher viscosity of the mixture, the ultrasound waves could not propagate and their impact

on the microcapsules' structure was negligible. Thus, another mixture was examined which was diluted with heptane. 2 mL of heptane were added to 2.5 mL of the mixture in order to decrease viscosity. Subsequently, the sample was ultrasonicated for 10 minutes. Thereafter, rheological measurement was made at 50°C, to determine whether the microcapsules had been destroyed. The non-ultrasonicated sample was also tested as a reference sample. The results, presented in Figure 33, showed that the cross-linking reaction hardly occurred in the ultrasonicated sample, as the storage modulus slightly increased over time and the mixture remained liquid. The fact that the storage modulus was higher than the loss modulus resulted from the high number of microcapsules added to the tested sample. The PMMA shell at 50°C was brittle and hard, and this contributed to high storage modulus values. Moreover, typical storage modulus values assigned to the cross-linked PDMS network were in the range between 10^4 and 10^6 Pa, implying that the cross-linking reaction did not occur at a satisfactory rate. However, there was a clear difference between the non-ultrasonicated and the ultrasonicated samples. The moduli of the non-ultrasonicated mixture remained almost constant over time, whereas the moduli for the ultrasonicated sample increased during measurement. This proves that some parts of the microcapsules did break, but ultrasonication efficiency was not sufficient to destroy the required number of microcapsules.

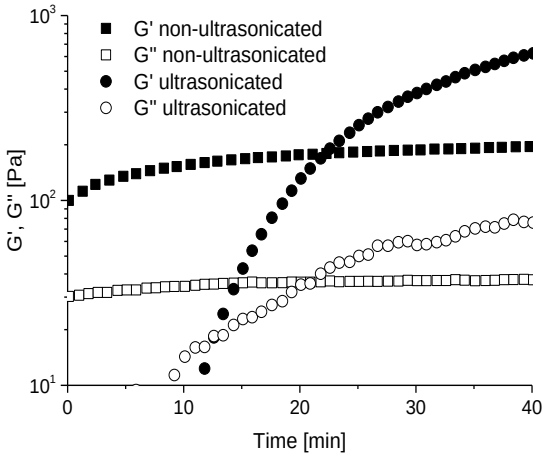

Figure 33. The graph shows storage G' and loss moduli G'' of the microcapsules and DMS-V31 mixture diluted with heptane. The moduli of the non-ultrasonicated mixture remained unchanged, whereas a slight change was observed for the ultrasonicated sample.

5.1.2 Indirect application of ultrasound waves

From the previously conducted experiments, it was observed that increased mixture viscosity negatively influences ultrasound's impact on the cracking process of microcapsules. The next

step was to perform experiments where the ultrasound waves were not directly applied to the mixture. The glass vial with the aqueous microcapsule mixture was placed in a water bath to check if the propagated ultrasound waves could break the microcapsules inside the glass vial. The ultrasound probe was located on top of the vial, which was sealed with aluminum foil. The concentration of microcapsules and sample's volume were identical, as in the previous experiments.

While applying the ultrasound waves very closely to the aluminum foil (still in the water bath), the microcapsules inside the vial hardly moved, meaning that only very few ultrasound waves could pass through the aluminum foil and hit the microcapsules. Although foil can be destroyed when exposed to ultrasonication (e.g. in a ultrasound bath), in the performed experiments it was a sufficient barrier for the ultrasound waves, and so the microcapsules stayed intact. This implies that this activation method would not be efficient in reservoir conditions, as the ultrasound probe would be placed inside the injection pipe.

5.2 Conclusions

Microcapsule ultrasonication led to PMMA shells breaking when the low-viscous mixture was tested. The higher viscosity of the mixture inhibited the propagation of ultrasound waves and led to a reduced effect of ultrasonication on microcapsules. The number of broken microcapsules in the ultrasonicated DMS-V31 mixture was not sufficient to release enough of the cross-linker to obtain the cross-linked material. Moreover, indirectly applied ultrasound waves did not affect the aqueous mixture of the microcapsules. Therefore, this method does not qualify as an activation method for microcapsules placed in an oil reservoir; however, the ultrasonication of microcapsules in a low-viscous medium is an excellent way of mixing and breaking microcapsules.

6. Solvent-flushing activation

The idea behind solvent-flushing activation involves flushing plug material with a good solvent so that solvent can dissolve the shell and allow the cross-linker to spread. The ideal solvent ought to dissolve PMMA while being immiscible with the cross-linker. As no such a solvent is available, it was decided to use acetone, which is a fairly good solvent for both components. PMMA in contact with the acetone does not dissolve immediately but swells first, which means that the cross-linker cannot be washed out of the system, as it will be delivered into the environment gradually from swollen microcapsules. The usage of the acetone was perceived as a rational choice, since other ketones were studied as displacement solvents for applications in oil reservoir.

6.1 Solvent-flushing experiments

In order to examine the solvent-flushing activation method, experiments were divided into two parts. Firstly, samples consisting of the microcapsules (Table 3, no. 1) and the vinyl-functional PDMS microparticles were flushed with acetone at low pressure. In such a way, required amounts of solvent, the mass ratio of the components and the required reaction time could be estimated. Subsequently, the system was activated at high pressure using a core-flooding setup, and the properties of the obtained final cross-linked plug samples were compared.

6.1.1 Low-pressure solvent-flushing experiments

In order to examine the properties of the material flushed at low pressure, simple experiments using a syringe were performed. The microcapsules and the PDMS microparticles were first placed in the syringe and compressed with a plunger, in order to ensure good surface contact between the microparticles. Afterwards, the plunger was removed and an acetone mixture with a 5 ppm platinum catalyst was added in portions. Following the addition of the acetone, the sample was again compressed with the plunger and placed in an oven at 50°C overnight. Different mass ratios between the PDMS microparticles and the microcapsules were examined as well as various volumes of added acetone. The mass of the PDMS microparticles was kept constant at 0.3 g, whereas different microcapsule masses were added. In total, five experiments were performed, and these are summarised in Table 10.

Initially, the mass ratio between the PDMS microparticles and the microcapsules was 10:1. This mass ratio assure the formation of cross-linked samples (as presented in Chapter 4).

Then, the acetone was added in 1 mL portions. All of the PDMS microparticles swelled after adding 3 mL of the solvent, and this volume was considered sufficient to saturate the sample. The next step involved squeezing the sample with the plunger and thus removing the acetone.

Table 10. Tested compositions of vinyl-functional PDMS microparticles and the microcapsules in low-pressure solvent-flushing experiments.

	Mass ratio	**Acetone [mL]**
1	10:1	3
2	5:1	3
3	3:1	3
4	3:1	2
5	3:1	1

After maintaining the sample at a ratio of 10:1 and at 50°C overnight, the PDMS microparticles did not create a macroscopic network, in contrast to the sample with an identical mass ratio, prepared using the hot press. This was assigned to the fact that probably some of the cross-linker had been washed away together with the solvent, and the remaining amount of cross-linker was not sufficient to obtain a cross-linked sample. Additionally, the PDMS microparticles swelled in contact with the acetone, and therefore the cross-linker could be easily absorbed by these swollen microparticles. As vinyl groups were present in the whole volume of the PDMS microparticles, the absorbed cross-linker reacted with inner vinyl groups, which in turn led to weaker surface binding between the PDMS microparticles. Hence, in following experiments, the microcapsule fraction increased. When a ratio of 5:1 was used, the macroscopic network did not form, as the PDMS microparticles remained separated. Increasing the amount of microcapsules further resulted in the formation of a soft network when the ratio was equal to 3:1. Figure 34 shows photographs of the sample.

Figure 34. The physical appearance of the plug sample, which was prepared at low pressure. The mass ratio between the vinyl-functional PDMS microparticles and the microcapsules was 3:1, respectively.

It is evident that the PDMS microparticles created a network; however, the sample was fragile and susceptible to damage. SEM images were taken with the aim of investigating the structure of the sample on the microscopic level. Figure 35 presents the obtained results. Although a cross-linked material was obtained, many voids were present in the sample's structure (Figure 35a), and these may ultimately result in poor plugging properties and poor mechanical strength of the cross-linked plug. Additionally, some marks were visible on the surface of the PDMS microparticles (Figure 35b). It seems that smaller microparticles were attached to bigger ones, but due to weak binding they detached, leaving characteristic marks.

Furthermore, not all of the microcapsules were dissolved. The microcapsules presented in Figure 35c) created agglomerations and their structure remained intact. Figure 35d) shows an enlarged image of the microcapsule agglomeration presented in Figure 35c). It is evident that some part of the cross-linker was not released while flushing with acetone, and therefore a cross-linked sample was not obtained when a lower amount of microcapsules was used.

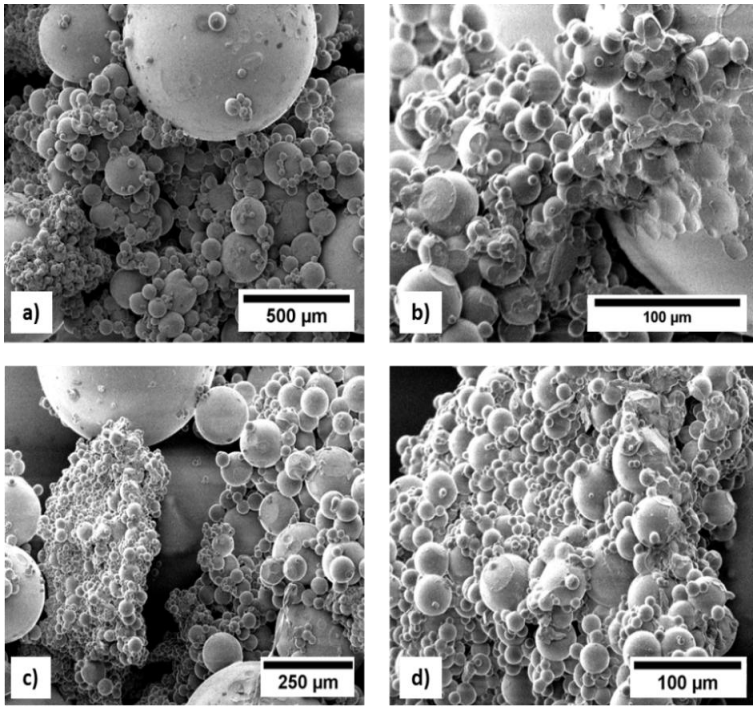

Figure 35. SEM images of the plug sample cross-linked at low pressure. The mass ratio between the vinyl-functional PDMS microparticles and the microcapsules was 3:1.

The low-pressure solvent-flushing experiments proved that it is possible to obtain a cross-linked system by applying this activation technique. The main conclusion is that the mass fraction of microcapsules in the plug material must be higher than in the case of other activation methods. This is caused in three ways. Firstly, some of the cross-linker was probably washed out of the system along with the acetone. Secondly, some part of the microcapsules remained intact and created agglomerations, and finally the cross-linker could be absorbed by the swollen PDMS microparticles.

6.1.2 High-pressure solvent-flushing experiments

The cross-linked plug sample, obtained thanks to the flushing with acetone at high pressure, was investigated. The plug material was placed in a fractured core sample (a description of core sample preparation is presented in the appendices assigned to Chapter 6), in order to reproduce conditions inside the fractured reservoir rock. Core sample dimensions and the drilled fracture are presented in Figure 36.

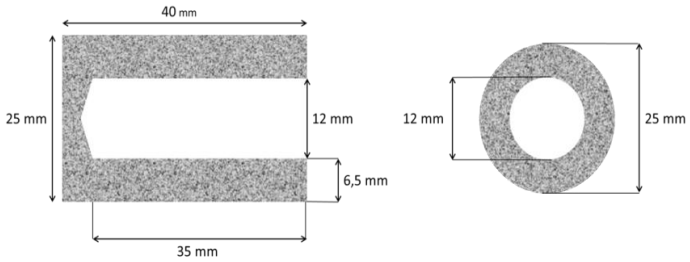

Figure 36. Schematic presentation of the fractured core samples showing the dimensions of the fracture.

The scheme for the equipment used for this experiment is presented in Figure 37. Firstly, 3 g of PDMS microparticles and 1 g of microcapsules were transferred to the core sample, followed by placing the filled core sample into the core holder. By pumping water into the system, sleeve pressure inside the core holder increased to 15 bar, and the pressure was kept constant during the experiment. When pressure was stabilised, the system was heated up to 50°C. Subsequently, an acetone mixture containing 5 ppm of platinum catalyst was injected into the core sample over 1 hour at a flow rate of 0.5 mL/min. The volume of the injected acetone was proportional to the volume used in the low-pressure experiments concerning the mass of the sample. After 30 mL of acetone mixture passed through the core sample, the system was kept at 50°C overnight at a given sleeve pressure. Afterwards, the sample was removed from the core holder and investigated.

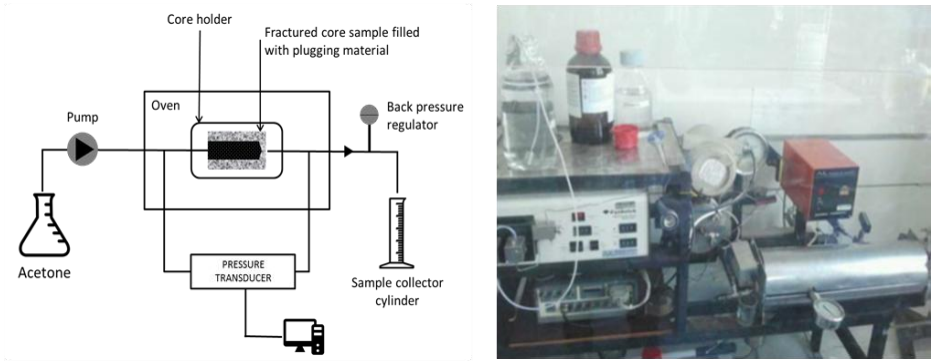

Figure 37. Schematic diagram (left) and physical appearance (right) of the core-flooding setup.

After removing the core sample from the holder, it was found that the core sample broke, due to high sleeve pressure, but the PDMS microparticles created a strong and elastic network which withstood the pressure. The physical appearances and SEM images of the cross-linked sample are shown in Figure 38.

The core sample was placed in such a way that the acetone was injected from a fractured side of the core, and thus the top of the cross-linked sample was narrower than the bottom part, as the microparticles were probably pushed due to high injection pressure. The cross-linked material was characterised by a tight and durable structure. The sample, which was flushed at high pressure, had a different appearance compared to the sample flushed at low pressure. From the SEM images (Figures 38c and 38d), it can be seen that the PDMS microparticles were tightly packed and created a uniform structure in which it is hard to distinguish the microparticles between each other. This means that they were strongly linked and the binding between them was sufficient to hold the connected microparticles. Secondly, no voids were observed. Thanks to the high injection pressure, the PDMS microparticles were compressed and the contact surface area was much higher than for the sample flushed at low pressure. A larger surface area resulted in a higher number of covalent bonds, which contributed to obtaining a stronger material. Thirdly, agglomerations of undissolved microcapsules did not occur in the sample. The flow of injected acetone was uniform within the sample and the PMMA shell was dissolved. At the same time, the cross-linker was not washed away, since the PDMS microparticles created a macroscopic network. Taking into consideration all of these observations, it was evident that high pressure is advantageous for obtaining the cross-linked plug material. However, it should be considered that the core sample was not fractured along the whole length of the core, and the PDMS microparticles could not be washed away. If the core sample had fractured along the whole length, there was a possibility that the PDMS microparticles would be pushed out of the core.

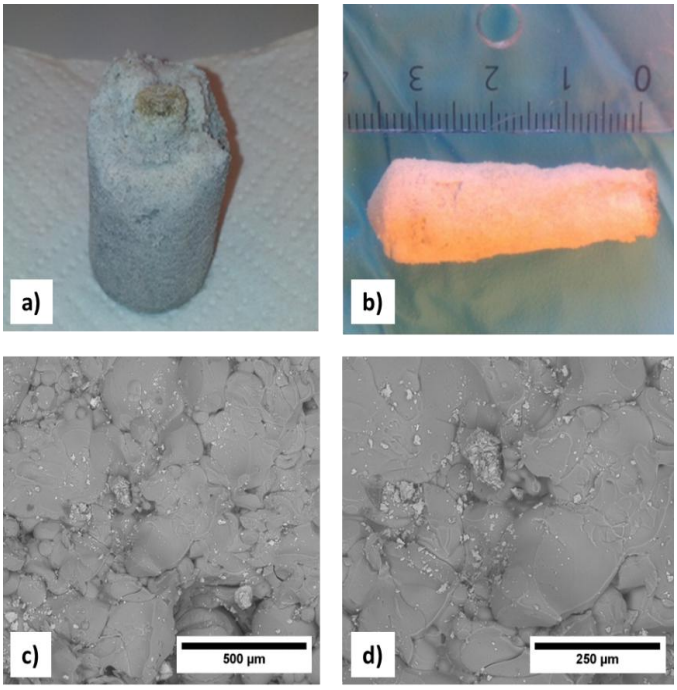

Figure 38. The physical apperances (a and b) and SEM images (c and d) of the plug sample cross-linked at high pressure. The mass ratio between the vinyl-functional PDMS microparticles and the microcapsules was 3:1, respectively

6.2 Conclusions

Solvent-flushing was tested as an activation method for a plug system. It was proved that this method allows for obtaining a cross-linked system. Samples flushed at high pressure were characterised by a highly cross-linked and packed composition which resulted in achieving a material without voids in its structure, in which all PDMS microparticles were strongly bonded with each other and the cross-linker was evenly spread within the system. A material with such a structure should provide good barrier properties against water while water-flooding a fractured oil reservoir. Moreover, as solvent-flushing is used to displace oil from pores, this activation should be relatively easy to apply, using already developed equipment.

7. Conclusions and future work

7.1 Conclusions

The aim of the project was to develop a material consisting of PDMS microparticles and microcapsules which would facilitate the plugging of fractures located in oil reservoirs. Encapsulation of the cross-linker provided control over the cross-linking reaction between the PDMS microparticles. Due to poor fracture accessibility, remote activation methods were preferred.

In the first stage of the project, the preparation of impermeable microcapsules was achieved. A phase separation technique was shown to be a universal method for obtaining microcapsules of a required size. The PMMA shell protected the liquid core across a wide range of temperatures, preventing a cross-linking reaction before activation. With this method, microcapsules with various cross-linkers and microcapsules containing magnetic nanoparticles were obtained, without compromising on the impermeable nature of the shell. Moreover, by adding plasticiser to the oil phase, microcapsules were prepared with a plasticised shell, thereby making T_g shell adjustment possible.

Although remotely inapplicable, a thermal activation method was tested, and it was shown that when microcapsules were exposed to temperatures higher than the T_g of the PMMA shell, the cross-linker was released into the environment, thus allowing for a cross-linking reaction. These thermoplastic properties of the PMMA shell were use in remotely applied activation methods, namely gamma irradiation and magnetic activation.

At small doses of gamma irradiation, PMMA undergoes chain scission, and thereby the T_g of the polymer decreases. It was found that irradiated microcapsules became permeable at lower temperatures, as the properties of the PMMA shell were modified, thereby allowing for remotely triggering the release of the cross-linker.

Using an alternating magnetic field was also considered as a remotely applicable stimulus. Our investigation of liquid magnetic nanoparticle mixtures showed that high temperatures were reachable in a relatively short time, and encapsulated nanoparticles could lead to melting the PMMA shell. However, magnetic nanoparticle treatment prior to microcapsule preparation caused changes in the nanoparticles' heating properties. Nevertheless, the idea of exposing microcapsules to a magnetic field was found to be a promising activation method.

As an alternative to remote activation methods, solvent-flushing was also investigated. The possibility of conducting experiments in a core-flooding setup provided an important insight into the properties of a cross-linked plug under high pressure. The obtained material was characterised by a durable and well-packed structure. High pressure led to good surface contact between the PDMS microparticles, which in turn resulted in obtaining a material with a uniform and void-less structure. Moreover, it was shown that small deviations between the microparticles and microcapsules ratio did not negatively influence the elastic properties of the plug. Therefore, the properties of the settled plug should be significantly affected by the injection process.

Summarising, in comparison to currently used plugging materials, such as hydrogels, an elastomer system consisting of PDMS microparticles and microcapsules provides the possibility remotely activating a material, thereby eliminating the danger of plugging the injection well. Moreover, thanks to being able to define the size of the components, the fracture will be plugged selectively, meaning that oil-rich pores remain unaffected. The ability to prepare components prior to injection into a reservoir reduces the influence of injection conditions on the final properties of the plug. As covalently bonded PDMS microparticles create a uniform, elastic structure, a permanent water shut-off treatment has been accomplished.

7.2 Future work

Although encapsulating magnetic nanoparticles was successful, magnetic activation was not achieved. Thus, further investigation is required in this regard. As referred to in Chapter 4, nanoparticles, which are stable in organic solvent, ought to be used during the preparation of microcapsules. The high mass content of nanoparticles encapsulated within the PMMA shell should allow for generating a sufficient amount of heat and cause melting of the PMMA while exposed to the AMF.

Furthermore, only a few solvent-flushing tests were performed, and as these clearly demonstrated, PDMS microparticles cross-linked at high pressure create a durable and long-lasting structure. Nonetheless, this method was not optimised. The influence of factors such as solvent flow rate, sleeve pressure and temperature was not investigated. Moreover, properties of the cross-linked plug could be modified by using other kinds of cross-linker and PDMS microparticles. As shown in Chapter 2, highly viscous cross-linkers were encapsulated via the phase separation technique. Testing them would provide an overview on how to adjust the final properties of the plug. In addition, various vinyl-terminated PDMS can be used to prepare PDMS microparticles. By varying the molecular weights of PDMS,

microparticles with different properties could be prepared, and hence the obtained cross-linked plug could exhibit new properties.

Bibliography

1 B. Ma, A. L. Skov and S. Hvilsted, PhD thesis, Technical University of Denmark, 2014.

2 B. G. Ma, J. H. Hansen, S. Hvilsted and A. L. Skov, *Rsc Adv.*, 2014, **4**, 47505–47512.

3 L. González, M. Baoguang, L. Li, J. H. Hansen, S. Hvilsted and A. L. Skov, *Macromol. Mater. Eng.*, 2014, **299**, 729–738.

4 R. A. Dawe, *J.Chem.Tech.Biotechnol.*, 1991, **51**, 361–393.

5 S. Sajjadian, V. M. Ataabadi, M. D. National and I. Oil, 2012.

6 M. V. Kok, *Energy Sources, Part A Recover. Util. Environ. Eff.*, 2011, **33**, 377–382.

7 P. A. C. Marescalco, *Int. J. Numer. Methods Fluids*, 2008, **61**, 768–779.

8 D. J. Ligthelm, P. J. Hoek, P. Hos, M. J. Faber and R. C. Roeterdink, in *SPE Europec/EAGE Annual Conference and Exhibition held in Vienna, Austria*, 2006, pp. 1–13.

9 F. Muhammed, B. Bai, A. Imqam and A. O. Almansour, in *SPE Heavy Oil Conference-Canada held in Alberta, Canada*, 2014, pp. 1–15.

10 N. A. Solano, C. R. Clarkson, F. F. Krause, S. Aquino and A. Wiseman, *CSEG Rec. - Focus Artic.*, 2013, 42–47.

11 B. Yadali Jamaloei, *Oil Gas Sci. Technol. – Rev. IFP Energies Nouv.*, 2011, **66**, 991–1004.

12 M. Demir, N. N. Topgüder, M. Yılmaz, Y. Karakeçe, Y. Ince and U. Karabakal, in *SPE Russian Oil & Gas Technical Conference and Exhibition held in Moscow, Russia*, 2008, pp. 1–11.

13 J. Gale, in *SPE/PS-CIM International Conference on Horizontal Well Technology, Calgary, Canada*, 2002, pp. 266–272.

14 B. Bai, M. Wei and Y. Liu, in *SPE Production and Operations Symposium held in Oklahoma City, USA*, 2013, pp. 1–17.

15 R. Ryles and J. Cicchiello, in *SPE/DOE Fifth Symposiumon Enhanced Oil Recovery of the Society of Petroleum Engineers of the Department of Energy held in Tulsa, USA*, 1986, pp. 301–305.

16 F. E. Fragachan, F. Cazares-Robles, J. J. Gutierrez and G. Herrera, in *Petroleum Conference and Exhibition of Mexico held in Villahermosa, Mexico*, 1996, pp. 195–200.

17 I. Lakatos and J. Lakatos-Szabo, in *SPE Annual Technical Conference and Exhibition held in San Antonio, USA*, 2012, pp. 1–13.

18 D. G. Hatzignatiou, R. Askarinezhad, N. H. Giske and A. Stavland, in *SPE Bergen One Day*

Seminar, Bergen, Norway, 2016, pp. 1–14.

19 H. A. Nasr-El-Din and K. C. Taylor, *J. Pet. Sci. Eng.*, 2005, **48**, 141–160.

20 K. D. Oglesby, D. D'Souza, C. Roller, R. Longsdon, L. D. Burns and B. J. Felber, in *SPE Improved Oil Recovery Conference held in Tulsa, USA*, 2016, pp. 1–25.

21 A. A. Hamouda and H. A. Amiri, *Energies*, 2014, **7**, 568–590.

22 S. Bauer, P. Gronewald, J. Hamilton and A. Mansure, in *SPE International Symposium on Oilfield Chemistry held in Houston, USA*, 2005, pp. 1–6.

23 J. Ferguson and M. P. Applebey, *Trans. Faraday Soc.*, 1930, 642–655.

24 B. Vinot, R. S. Schechter and L. W. Lake, *SPE Reserv. Eng.*, 1989, **4**, 391–397.

25 A. Z. Abidin, T. Puspasari and W. A. Nugroho, *Procedia Chem.*, 2012, **4**, 11–16.

26 B. Bai, J. Zhou and M. Yin, *Pet. Explor. Dev.*, 2015, **42**, 525–532.

27 E. Larry, G. Funkhouser and C. Mike, in *SPE International Symposium on Oilfield Chemistry held in Houston, USA*, 1999, pp. 1–13.

28 K. S. M. El-Karsani, G. A. Al-Muntasheri and I. A. Hussein, *SPE J.*, 2014, **19**, 135–149.

29 S. F. Hassan, M. Han, X. Zhou, D. Krinis, B. Zahrani and S. Aramco, in *SPE Annual Technical Symposium and Exhibition held in Khobar, Saudi Arabia*, 2013, pp. 1–11.

30 M. Simjoo, A. D. Koohi, M. Vafaie-Sefti and P. L. J. Zitha, in *SPE European Formation Damage Conference held in Scheveningen, The Netherlands*, 2009, pp. 1–8.

31 G. A. Al-Muntasheri, L. Sierra, F. O. Garzon, J. D. Lynn and G. Izquierdo, in *SPE Improved Oil Recovery Symposium held in Tulsa, USA*, 2010, pp. 1–24.

32 T. M. Klaveness and P. Ruoff, *J. Phys. Chem.*, 1995, **98**, 10119–10123.

33 H. Jia, Q. Ren, Y. Li and X. Ma, *Petroleum*, 2016, **2**, 90–97.

34 A. Moradi-Araghi and P. H. Doe, *SPE Reserv. Eng.*, 1987, 189–198.

35 B. Bai, L. Li, Y. Liu, H. Liu, Z. Wang and C. You, in *SPE/DOE Symposium on Improved Oil Recovery, Tulsa, USA*, 2007, pp. 415–422.

36 F. A. Muhammed, B. Bai and A. Brahim, in *SPE Improved Oil Recovery Symposium held in Tulsa, USA*, 2014, pp. 1–18.

37 H. Zhang and B. Bai, *Preformed Particle Gel Transport Through Open Fractures and its Effect on Water Flow*, 2010.

38 Y. Liu, B. Bai and Y. Wang, *Oil Gas Sci. Technol. – Rev. IFP Energies Nouv.*, 2010, **65**,

859–878.

39 A. Zaitoun and B. Potie, in *International Symposium on Oilfield and Geothermal Chemistry held in Denver, USA*, 1983, pp. 143–148.

40 P. H. Doe, A. Moradi-Araghi, J. E. Shaw and G. A. Stahl, *SPE Reserv. Eng.*, 1987, **2**, 461–467.

41 P. Davison and E. Mentzer, *Soc. Pet. Eng. J.*, 1982, **22**, 353–362.

42 A. Moradi-Araghi and I. J. Westerman, in *SPE International Symposium on Oilfield Chemistry held in San Antonio, USA*, 1987, pp. 319–326.

43 J. C. Lötters, W. Olthuis, P. H. Veltink and P. Bergveld, *J. Micromechanics Microengineering*, 1999, **7**, 145–147.

44 J. Kuncová-Kallio and P. J. Kallio, *Annu. Int. Conf. IEEE Eng. Med. Biol. - Proc.*, 2006, 2486–2489.

45 A. L. Larsen, K. Hansen, P. Sommer-Larsen, O. Hassager, A. Bach, S. Ndoni and M. Jørgensen, *Macromolecules*, 2003, **36**, 10063–10070.

46 A. G. Bejenariu, L. Yu and A. L. Skov, *Soft Matter*, 2012, **8**, 3917–3923.

47 F. Prabowo, A. L. Wing-keung and H. H. Shen, *Adv. Mater. Res.*, 2015, **1112**, 410–413.

48 C. E. Cooke, in *SPE-AIME 47th Annual Fall Meeting held in San Antonio, USA*, 1973, pp. 1101–1107.

49 S. L. Bryant, M. Bartosek and T. P. Lockhart, *J. Pet. Sci. Eng.*, 1997, **17**, 197–209.

50 W. T. Shi, M. Böhmer, A. Van Wamel, M. Celebi, A. L. Klibanov, C. T. Chin, C. Chlon, M. Emmer, K. Kooiman and C. S. Hall, in *IEEE Ultrasonics Symposium*, 2007, pp. 773–776.

51 Y. Jing, Y. Zhu, X. Yang, J. Shen and C. Li, *Langmuir*, 2011, **27**, 1175–1180.

52 E. M. Rosenbauer, M. Wagner, A. Musyanovych and K. Landfester, *Macromolecules*, 2010, **43**, 5083–5093.

53 S. E. Paramonov, E. M. Bachelder, T. T. Beaudette, S. M. Standley, C. C. Lee, J. Dashe and J. M. J. Fréchet, *Bioconjug. Chem.*, 2008, **19**, 911–919.

54 A. Abbaspourrad, S. S. Datta and D. A. Weitz, *Langmuir*, 2013, **29**, 12697–12702.

55 M. Volz, P. Walther, U. Ziener and K. Landfester, *Macromol. Mater. Eng.*, 2007, **292**, 1237–1244.

56 Q. Li, A. K. Mishra, N. H. Kim, T. Kuila, K. T. Lau and J. H. Lee, *Compos. Part B Eng.*, 2013, **49**, 6–15.

57 S. R. White, B. J. Blaiszik, S. L. B. Kramer, S. C. Olugebefola, J. S. Moore and N. R. Sottos, *Annu. Rev. Mater. Res.*, 2010, **40**, 179–211.

58 E. S. Araújo, H. J. Khoury and S. V. Silveira, *Radiat. Phys. Chem.*, 1999, **53**, 79–84.

59 Z. A. Kadir, F. Yoshii, K. Hosoi, K. Makuuchi and I. Ishigaki, *J. Appl. Polym. Sci.*, 1990, **40**, 799–810.

60 G. M. Vinhas, R. M. Souto-Maior, C. M. Lapa and Y. M. B. De Almeida, *Mater. Res.*, 2003, **6**, 497–500.

61 K. A. S. Aquino, E. S. Araujo and S. M. L. Guedes, *J. Appl. Polym. Sci.*, 2010, **116**, 748–753.

62 K. J. Miller, J. H. Hellman and J. A. Moore, *Macromolecules*, 1993, **26**, 4945–4952.

63 P. P. Vaishnava, R. Tackett, A. Dixit, C. Sudakar, R. Naik and G. Lawes, *J. Appl. Phys.*, 2007, **102**, 63914.

64 A. Tomitaka, K. Ueda, T. Yamada and Y. Takemura, *J. Magn. Magn. Mater.*, 2012, **324**, 3437–3442.

65 R. Regmi, A. Naik, J. S. Thakur, P. P. Vaishnava and G. Lawes, *J. Appl. Phys.*, 2014, **115**, 17B301.

66 M. Suto, Y. Hirota, H. Mamiya, A. Fujita, R. Kasuya, K. Tohji and B. Jeyadevan, *J. Magn. Magn. Mater.*, 2009, **321**, 1493–1496.

67 A. Carovac, F. Smajlovic and D. Junuzovic, *Acta Inform. Medica*, 2011, **19**, 168–171.

68 S. Salem, *Radiat. Phys. Chem.*, 1984, **24**, 405–417.

69 F. Chemat, Zill-E-Huma and M. K. Khan, *Ultrason. Sonochem.*, 2011, **18**, 813–835.

70 L. S. Ferreira and J. O. Trierweiler, *Aiche J.*, 2009, **57**, 2025–2035.

71 D. G. Shchukin, E. Skorb, V. Belova and H. Möhwald, *Adv. Mater.*, 2011, **23**, 1922–1934.

72 A. A. Dehghan, R. Kharrat and M. H. Ghazanfari, *Pet. Sci. Technol.*, 2010, **28**, 176–189.

73 A. Kumar and R. Okuno, *Ind. Eng. Chem. Res.*, 2014, **53**, 440–455.

74 R. Arshady, *J. Microencapsul.*, 1992, **9**, 187–190.

75 Y. Ma, Y. Zhang, Y. Wang, Q. Wang, M. Tan, Y. Liu, L. Chen, N. Li, W. Yu and X. Ma, *J. Biomed. Mater. Res. - Part A*, 2013, **101 A**, 1007–1015.

76 M. Ina, A. P. Zhushma, N. V Lebedeva, M. Vatankhah-varnoosfaderani, S. D. Olson and S. S. Sheiko, *J. Colloid Interface Sci.*, 2016, **478**, 296–302.

77 I. M. Martins, S. N. Rodrigues, M. F. Barreiro and A. E. Rodrigues, *Ind. Eng. Chem. Res.*, 2011, **50**, 13752–13761.

78 B. Andrade, Z. Song, J. Li, S. C. Zimmerman, J. Cheng, J. S. Moore, K. Harris and J. S. Katz, *ACS Appl. Mater. Interfaces*, 2015, **7**, 6359–6368.

79 S. Freitas, H. P. Merkle and B. Gander, *J. Control. Release*, 2005, **102**, 313–332.

80 A. Loxley and B. Vincent, *J. Colloid Interface Sci.*, 1998, **208**, 49–62.

81 S. Torza and S. G. Mason, *J. Colloid Interface Sci.*, 1970, **33**, 67–83.

82 F. M. Lavergne, D. Cot and F. Ganachaud, *Langmuir*, 2007, **23**, 6744–6753.

83 G. Baum, R. Bachmann and W. Sliwka, United States patent US 3872023 A, 1974.

84 L. Gonzalez, M. Kostrzewska, M. Baoguang, L. Li, J. H. Hansen, S. Hvilsted and A. L. Skov, *Macromol. Mater. Eng.*, 2014, **299**, 1259–1267.

85 K. Lunkwitz, U. Lappan and U. Scheler, *J. Fluor. Chem.*, 2004, **125**, 863–873.

86 M. A. Rauf and I. C. Mcneil, *Polym. Degrad. Stab.*, 1993, **40**, 263–266.

87 E. H. Lee, G. R. Rao and L. K. Mansur, *Radiat. Phys. Chem.*, 1999, **55**, 293–305.

88 J. Choi, D. J. T. Hill, K. Y. Kim, J. H. O'Donnell and P. J. Pomery, *Polym. Adv. Technol.*, 1998, **9**, 52–61.

89 J. Colombani, G. Herbette, C. Rossi, C. Joussot-Dubien, V. Labed and V. Gilardi, *J. Appl. Polym. Sci. Sci.*, 2009, **112**, 1372–1377.

90 M. I. Re, *Dry. Technol.*, 1998, **16**, 1195–1236.

91 A. Gharsallaoui, G. Roudaut, O. Chambin, A. Voilley and R. Saurel, *Food Res. Int.*, 2007, **40**, 1107–1121.

92 C. Yu, W. Wang, H. Yao and H. Liu, *Dry. Technol.*, 2007, **25**, 695–702.

93 R. M. Ferguson, A. P. Khandhar, C. Jonasson, J. Blomgren, C. Johansson and K. M. Krishnan, *IEEE Trans. Magn.*, 2013, **49**, 3441–3444.

94 E. Lima, T. E. Torres, L. M. Rossi, H. R. Rechenberg, T. S. Berquo, A. Ibarra, C. Marquina, M. R. Ibarra and G. F. Goya, *J. Nanoparticle Res.*, 2013, **15**, 1–11.

95 S. C. N. Tang and I. M. C. Lo, *Water Res.*, 2013, **47**, 2613–2632.

96 M. S. Kim, C. S. Kim, H. J. Kim, K. H. Yoo and E. J. Hahn, *J. Korean Phys. Soc.*, 2013, **63**, 2175–2178.

97 A. G. Roca, B. Wiese, J. Timmis, G. Vallejo-Fernandez and K. O'Grady, *IEEE Trans.*

Magn., 2012, **48**, 4054–4057.

98 Q. Zhao, L. Wang, R. Cheng, L. Mao, R. D. Arnold, E. W. Howerth, Z. G. Chen and S. Platt, *Theranostics*, 2012, **2**, 113–121.

99 J. Liu, Z. Sun, Y. Deng, Y. Zou, C. Li, X. Guo, L. Xiong, Y. Gao, F. Li and D. Zhao, *Angew. Chemie*, 2009, **121**, 5989–5993.

100 W. Jingjing and L. Dengxin, *Energy Procedia*, 2011, **11**, 4794–4802.

101 L. Zhang, R. He and H. C. Gu, *Appl. Surf. Sci.*, 2006, **253**, 2611–2617.

102 H. M. Santos, C. Lodeiro and J. L. Capelo-Martinez, *Ultrasound Chem. Anal. Appl.*, 2009, **1**, 1–16.

Experimental methods

Optical microscopy

Optical microscopy analysis was performed using a Leica DMIB confocal microscope. The determination of microcapsule size distribution was done using Uthsca Imagine Tool 3.0 software.

Scanning electron microscopy (SEM)

Scanning electron microscopy images were recorded on FEI Inspect S on samples that were dried and metallised with gold, using a Cressington 208HR Sputter Coater. Scanning electron microscopy with X-ray microanalysis was used to confirm the presence of encapsulated magnetic nanoparticles inside the microcapsules.

Infrared spectroscopy (FTIR)

A Fourier transform infrared (FTIR) analysis in attenuated-total-reflection mode (ATR-FTIR) was carried out using Perkin Elmer Spectrum One apparatus. The spectra were recorded in the range 4 000–600 cm^{-1} with a 4 cm^{-1} resolution.

Differential Scanning Calorimetry (DSC)

A TA Instruments Differential Scanning Calorimeter (DSC) Q1000 was used to determine the thermal behaviour of the samples. The glass transition temperatures were calculated by means of a second heating scan as the temperature of the halfway point of the jump in heat capacity when the material changed from a glassy to a rubbery state.

Thermogravimetric analysis (TGA)

Thermal stability was assessed through thermogravimetric analysis (TGA), employing a TGA Q500 instrument (TA Instruments) ranging from 20 up to 900°C with a heating rate of 10°C min^{-1} under nitrogen flow.

Size exclusion chromatography (SEC)

Size size exclusion chromatography was performed on a Viscotek GPCmax VE-2001 instrument equipped with a Viscotek TriSEC Model 302 triple detector, using two PLgel mixed-D columns from Polymer Laboratories. Samples were run in tetrahydrofuran at room temperature at a rate of 1 ml min^{-1}.

Rheological characterisation

Frequency sweep and time sweep tests were performed on either a TA Instrument AR2000 rheometer or an ARES G2 rheometer from TA Instruments, with parallel plate geometry with a diameter of 25 mm and a controlled strain of 2%. The frequency sweep tests were performed in the frequency range 100-0.01 Hz.

Nuclear magnetic resonance (NMR)

^{1}H NMR characterisation was performed on a Bruker 250 MHz spectrometer, using $CDCl_3$ as a solvent. All spectra were recorded across 32 scans.

Gamma irradiation experiments

Each sample weighed approximately 1 g, and these were irradiated at room temperature with various doses of gamma rays by using a $Cobalt^{60}$ gamma cell at the Center for Nuclear Technologies, Danish Technical University, Risø Campus. The dose rate was approximately 1 Gy s^{-1}. Nominal doses were given as doses to water, and the maximum dose was 10 kGy.

Appendices

Appendices to Chapter 2

'Preparation and Characterization of Silicone Liquid Core/Polymer Shell Microcapsules via Internal Phase Separation' published in *Macromolecular Materials and Engineering Journal*.

Preparation and Characterization of Silicone Liquid Core/Polymer Shell Microcapsules via Internal Phase Separation[a]

Lidia González, Malgorzata Kostrzewska, Ma Baoguang, Li Li, Jens Henrik Hansen, Søren Hvilsted, Anne Ladegaard Skov*

Microcapsules with a silicone liquid core surrounded by a polymeric shell were synthesised through the controlled phase separation. The dispersed silicone phase consisted of the shell polymer PMMA, a good solvent for the PMMA (dichloromethane, DCM) and a poor solvent (methylhydrosiloxane dimethylsiloxane) for the PMMA. The morphology of the PMMA microcapsules was investigated by ATR-FTIR and by optical microscopy. Microcapsules were prepared with different emulsifiers and different concentrations of acetone and PMMA in the oil phase. The thermal stability of the PMMA microcapsule and the content of the silicone oil core were assessed by TGA. ^{1}H-NMR spectroscopy and an extraction method were also used to determine the content of the silicone liquid core in the microcapsules.

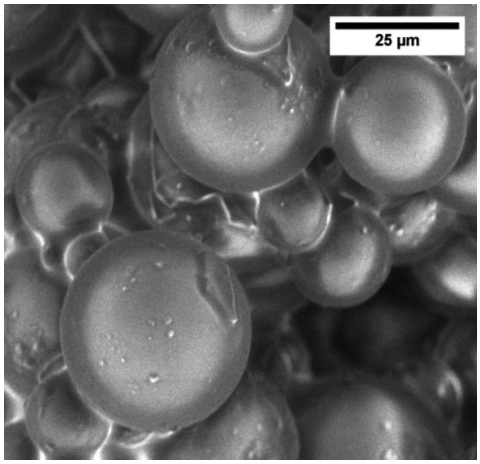

1. Introduction

In recent years, the use of several types of colloidal systems for encapsulating active substances has received considerable scientific attention and interest due to the numerous advantages of encapsulated systems.[1] Microencapsulation is a process by which solids, liquids, or even gases are enclosed in a thin coating of material. The process started in the late 1930s as a way of producing a cleaner substitute for carbon paper and ribbons. A microcapsule is a system that contains a well-defined core and a well-defined envelope. The core can be solid, liquid, or gas, while the envelope is made from a continuous, porous, or non-porous polymeric phase. The substance can be dispersed inside the microcapsule as solid particulates with regular or irregular shapes. In the case of microcapsules with a liquid core, other shapes may exist such as a pure or dissolved solution, suspension or emulsion, or the combination of a suspension and an emulsion.

In contrast, a microsphere is a structure made from a continuous phase of one or more miscible polymers in which particulate substance is dispersed at either the macroscopic (particulates) or the molecular (dissolution) level.[2] We[3] recently prepared PMMA-coated cured poly-

L. González, M. Kostrzewska, M. Baoguang, L. Li, S. Hvilsted, A. L. Skov
Department of Chemical and Biochemical Engineering, Danish Polymer Centre, DTU, Søltofts Plads 227, DK-2800 Kgs, Lyngby, Denmark
E-mail: al@kt.dtu.dk
J. H. Hansen
Maersk Oil Research and Technology Centre, Education City, P.O. Box 210112, Doha, Qatar

[a]**Supporting Information** is available from the Wiley Online Library or from the author.

DOI: 10.1002/mame.201400020

(dimethyl siloxane) microspheres by causing an emulsion polymerization reaction in a continuous aqueous phase. Baoguang et al.[4] also prepared and characterized PDMS microspheres with a PMMA coating, including a modeling study to predict the observed phenomena. Several methodologies for the preparation of microcapsules have been described, such as interfacial polymerization reactions utilizing emulsions[5–8] and microemulsions,[9] solvent extraction,[10] spray drying,[11] layer-by-layer addition,[12] phase separation from the continuous phase, and solvent evaporation,[13] including the use of multiple emulsions.[14] Encapsulation technologies cover a great assortment of applications in fields such as printing, cosmetics, perfumery, detergency, food technology, drug delivery, and agriculture.[15] Esser-Kahn et al.[16] introduced several methods for encapsulation and release, triggering and mechanisms for chemically-induced activation, while Sari et al.[17] prepared and characterized PMMA microcapsules containing *n*-octacosane as a phase change material (PCM) for thermal energy storage. They also prepared and characterized PMMA *n*-heptadecane microcapsules as an example of a novel solid–liquid micro-PCM.[18] Furthermore, Sánchez-Silva et al.[19] studied the microencapsulation of PCMs with a styrene-methyl-methacrylated copolymer shell through suspension-like polymerization, and Loxley and Vincent[20] prepared poly(methyl methacrylate) (PMMA) microcapsules with liquid cores through controlled phase separation and by using different solvents as liquid cores (hexadecane, decane, octanol, or tetrachlorometane). Figure 1, in which the basis of the method used for preparing the microcapsules is depicted schematically, illustrates that the dispersed oil phase involves dissolving the wall-forming polymer in a mixture of a volatile good solvent and a high boiling point poor solvent. When the good solvent is removed, the previously dissolved polymer separates from the remaining poor solvent, following which the polymer creates a shell at the oil droplet/water interface when the balance of interfacial tensions is correct.

Several papers describe in different ways how to prepare microcapsules with aqueous cores.[21–24] Commonly, the

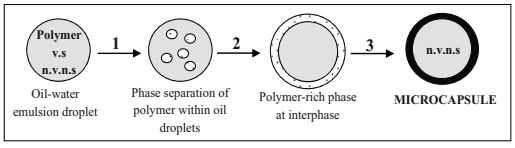

Figure 1. Schematic diagram of the shell formation mechanism: 1) evaporation of the volatile solvent (v.s.); 2) migration of the polymer-rich phase; 3) evaporation of all volatile solvents (v.s.), and the formation of a microcapsule with a non-volatile, non-solvent (n.v.n.s.) core.

encapsulation of water-soluble active components in microcapsules is achieved through the use of water-in-oil-in-water multiple emulsions. By considering different interfacial tensions between the polymeric shell (p), the oil phase (o), and the continuous water phase (w), i.e., γ_{op}, γ_{ow}, and γ_{pw}, conditions required for microcapsule formation can be determined. Torza and Mason[25] evaluated the possible equilibrium morphologies adopted by droplets of immiscible liquids (oil (o) and polymer (p) phases) when brought into contact with a third mutually immiscible liquid (water phase (w)), in terms of the various interfacial tensions between the phases (γ_{ow}, γ_{wp}, and γ_{op}). The spreading coefficients for each phase can be determined by applying the following equation:

$$S_i = \gamma_{jk} - (\gamma_{ij} + \gamma_{ik}) \quad (1)$$

and defining the oil phase (o) to be that for which $\gamma_{ow} > \gamma_{op}$, in which case the spreading coefficient for the oil phase (S_o) is $S_o < 0$. In this way, there are only three possible combinations of S_i:

$$S_o < 0;\ S_w < 0;\ S_p > 0 \quad (2)$$

$$S_o < 0;\ S_w < 0;\ S_p < 0 \quad (3)$$

$$S_o < 0;\ S_w > 0;\ S_p < 0 \quad (4)$$

Core–shell morphology particles will form when Equation (2)'s conditions are satisfied, with the oil phase being the core within a polymer phase shell. Particles with an acorn-shaped morphology will be formed when Equation (3) is satisfied. And finally, when Equation (4) is satisfied, two separate droplets, so-called "hetero-aggregates," will be formed.

Our work focuses on: i) preparing PMMA microcapsules with methylhydrosiloxane dimethylsiloxane (HMS-301) as a liquid core and ii) evaluating the content of a cross-linking agent (HMS-301) in the microcapsules.

2. Experimental Section

2.1. Materials

Commercially available PMMA ($\overline{M}_w \approx 15\,000$ Da (GPC), $T_g = 100\,^{\circ}C$, 99%) was purchased from Aldrich. Methylhydrosiloxane dimethylsiloxane (HMS-301, $\overline{M}_w \approx 1\,900$–$2\,000$ Da, 25–35 Pa s) was purchased from Gelest, Inc. and was employed as the core oil. Dichloromethane (DCM; >99.8%) was purchased from Aldrich and used as a solvent for the polymer. Acetone (99.9%) was also purchased from Aldrich and used to aid emulsification, while poly(vinyl alcohol) (PV; 22 000 Da, degree of hydrolysis 97.5–99.5 mol%) was purchased from Fluka and poly(methacrylic acid sodium salt) (PMAA; $\overline{M}_w \approx 9\,500$ Da (GPC), 30 wt% solution in

water, 110 000–375 000 cps at 25 °C) from Aldrich, both of which were used as polymeric emulsifiers. Heptane (>99%, Aldrich) and distilled water were used as solvents for washing the microcapsules.

2.2. Preparation of the Microcapsules

Different conditions used for preparing PMMA microcapsules are summarized in Table 1 (see numbers 1–12). As can be seen in Table 1, we studied five parameters necessary for preparing microcapsules, namely: i) the type of emulsifier used (PVA or PMAA); ii) the addition or not of acetone into the oil phase; iii) the concentration of a PMMA (polymer shell) in the DCM used (1, 2.4, and 3.3%); iv) the concentration of a cross-linker (HMS-301) in the DCM used (1.5, 3.7, and 5.0%), and v) the concentration of acetone used (2.5 and 5%).

PMMA microcapsules were prepared according to this specific description: PMMA (1 g) was dissolved in a DCM (75 mL) and then HMS-301 (1.5 g) was added. Next, approximately 77 mL of aqueous surfactant solution (1% PVA) was charged to a 250 mL conical flask. The aqueous phase was stirred mechanically at 2 000 rpm for 2–5 min (Eurostar Digital Ika Labortechnik, Bie & Berntsen A/S) and the oil phase was added drop-wise over 60 s to form an oil-in-water emulsion. The agitation was kept at around 750 rpm for 1 h, before pouring the emulsion into another 120 mL of aqueous surfactant solution (1% PVA). The diluted emulsion was rotary-evaporated for 25 min (20 and 65 °C), and then the vacuum was turned off and the dispersion was kept at 65 °C for a further 1 h. The rotary speed was 250 rpm. The dispersion of microspheres was filtered by using a filtration pump and qualitative filter paper 413 (particle retention: 5–13 μm). The product was washed with distilled water (≈1.5 L) and subsequently with heptane (≈400 mL), following which it was dried at room temperature in the fume hood (0.96 g).In Table 1 the conditions are specified for all systems investigated.

2.3. Characterization

Contact angle measurements (CA) and surface tension measurements were performed on a Contact Angle System OCA 20. Contact angles of HMS-301, and aqueous solutions of 1% PVA and 1% PMAA, were measured at room temperature with the sessile drop method.[26] The pendant drop method was used to estimate surface tension.[27] Scanning electron microscopy (SEM) images were recorded on FEI Inspect S on samples that were dried and metallized with gold using Cressington 208HR Sputter Coater. Optical microscopy was performed using a Leica DMIB confocal microscope in transmission mode (L50 × /0.55 PI Fluotar and 20 × / 0.1 PH1 objectives were used). Used technique of determining the microcapsules size distribution by Uthsca Imagine Tool 3.0 software was described by Lavergne et al.[28] Fourier transform infrared in the attenuated-total-reflection mode (ATR-FTIR) analysis was carried out using Perkin Elmer Spectrum One apparatus. The spectra were recorded in the range of 4 000–600 cm^{-1} with a 4 cm^{-1} resolution. Thermal stability was assessed through thermogravimetry analysis (TGA) employing a TGA Q500 instrument (TA Instruments) ranging from 20 up to 800 °C with a heating rate of 10 °C min^{-1} under nitrogen flow. In the following, we focus on a TGA-based method to determine cross-linker content in the microcapsule samples. Considering that pure commercial PMMA decomposes completely at 430 °C, we establish a method that allows correlating the residues of microcapsules at this temperature (430 °C) with cross-linker content in microcapsules. Firstly, several binary PMMA and cross-linker physical mixtures with known cross-linker concentrations (10, 24, 28, 46, and 69%) were prepared. Secondly, we made standard curves for the binary physical mixtures (Equation 5), in order to interpret data from the microcapsule samples. We define k as a proportional factor given by:

$$r_{(430^\circ C)}k = c_0 \quad (5)$$

Table 1. Different conditions used for preparing PMMA microcapsules.

Number	Formulation	m_0 DCM [g]	m_0 PMMA [g]	m_0 HMS-301 [g]	m_0 E [mL]	[PMMA] (%)	[E] (1%)	[Acetone] (5%)	m_f capsules [g]	Yield [%]
1	Capsules	100	1	1.5	77	1	PVA	No	0.96	38
2	Capsules	100	1	1.5	77	1	PVA	No	1.0	40
3	Capsules	100	1	1.5	77	1	PVA	No	1.8	72
4	Capsules	100	1	1.5	77	1	PVA	Yes	1.9	74
5	Capsules	100	2.55	3.9	77	2.4	PVA	No	3.7	57
6	Capsules	100	2.55	3.9	77	2.4	PVA	Yes	5.9	91
7	Capsules	100	1	1.5	77	1	PMAA	Yes (2.5)	1.16	46
8	Capsules	100	1	1.5	77	1	PMAA	No	1.1	44
9	Capsules	100	1	1.5	77	1	PMAA	Yes	1.3	21
10	Capsules	100	2.55	3.9	77	2.4	PMAA	No	4.0	44
11	Capsules	100	2.55	3.9	77	2.4	PMAA	Yes	1.4	54
12	Capsules	7.05	0.255	0.386	8	3.3	PMAA	Yes	0.138	22

where r is the residue percentage of the PMMA and cross-linker binary physical mixture at 430 °C and c_0 is the original cross-linker concentration (HMS-301) (%). Therefore, by substituting the known values (r and c_0) of the binary physical mixtures we can determine the value of k for each of the standard binary physical mixtures. Thirdly, by plotting k against r (residue as a percentage at 430 °C) we get a calibration line ($k = -0.023r + 2.7391$), which can be inserted into Equation (5) to give the following equation:

$$r_{(430^\circ CC)}(-0.023r_{(430^\circ C)} + 2.7391) = c_0 \quad (6)$$

The content (%) of the cross-linker (HMS-301) in the microcapsule systems can be calculated by multiplying the residue (%) at 430 °C of each microcapsule sample by k, assuming that the physical blends behave in a way similar to the microcapsules. Additionally, two other methods of determinating core content were investigated, namely NMR and extraction method. NMR spectrum were recorded using Bruker 300 MHz spectrometer. The PMMA (15 000 g mol^{-1}), cross-linker (≈2 000 g mol^{-1}) and every microcapsule samples were dissolved in $CDCl_3$, respectively. In the ^{1}H NMR spectrum for the pure commercial cross-linker, two resonances around 4.7 and 0.1 ppm were observed. The first resonance can be attributed to the hydrides attached to the silicon atom and the second resonance corresponds to the methyl groups' protons linked to the silicone atom. By integrating the area of these two signals and from the molecular weight of the cross-linker, the degree of polymerization for both repetitive units can be calculated. In the case of the ^{1}H NMR spectrum of the purely commercial PMMA, four resonances were observed. Signals at 0.7 and 1 ppm correspond to the methyl groups' protons attached to carbon in the backbone of the PMMA. The peak at 1.7 ppm is attributed to the methylene groups' protons from the backbone, while at ≈3.5 ppm the protons of the methyl groups attached to the ester groups of the side chains of PMMA were observed. Once the spectra for the PMMA and cross-linker had been analyzed, cross-linker content in every microcapsule sample could be calculated by integrating the area of the peaks with the chemical shift at 4.7 ppm (corresponding to Si—H, cross-linker) and 3.5 ppm (corresponding to CH_3—O—CO, PMMA). The core content of the prepared microcapsules was also evaluated via an extraction method using heptane as the extracting solvent.[29,30] In this case, only two microcapsule samples were investigated. The microcapsules (0.06 g) were ground with a pestle on a filter paper and then inserted into an oven for 5 h at 120 °C. Thereafter, microcapsules were crushed again to ensure the PMMA shell was broken. A fatty spot on the filter paper was observed, which could be related to the release of a cross-linker. The crushed microcapsules were collected and washed with heptane (100 mL) and dried overnight in an oven at 80 °C. The shell (W_{shell}) and core (W_{core}) contents of the microcapsules could be calculated by knowing the initial weight of intact microcapsules (W_i) and the weight of the residual shell (W_s) (see Equation 7 and 8):

$$W_{shell} = \frac{W_s}{W_i} \times 100\% \quad (7)$$

$$W_{core} = \left(1 - \frac{W_s}{W_i}\right) \times 100\% \quad (8)$$

3. Results and Discussion

3.1. Interfacial Tensions

In order to investigate the theoretical morphology of the PMMA microcapsules, the contact angles and the interfacial tensions of the emulsifiers were measured using the pendant drop method. The results are shown in Table 2.

In order to acquire core–shell morphology, the spreading coefficients must be $S_o < 0$, $S_w < 0$, and $S_p > 0$, as defined in Equation (2), where S_o is the spreading coefficient for the oil phase. S_w and S_p are the spreading coefficients for water and polymer (PMMA), respectively, and as a rule of thumb $\gamma_{ow} > \gamma_{pw}$.

Both emulsifiers were used at a concentration of 1% against the weight of the aqueous solution. The type of emulsifier and/or core oil determines interfacial tensions, which were also measured (Table 3) between the cross-linker (HMS-301) and the aqueous phase (that contains PVA or PMAA, respectively) (γ_{ow}), the cross-linker and the polymer (PMMA) (γ_{op}), and the polymer (PMMA) and the aqueous phase (γ_{pw}).

The acorn morphology particles in the HMS-301/PVA system should be obtained according to theory, but nevertheless spherical core–shell particles are observed by SEM microscopy (Figure 2). However, deviations between theory and experiments are to be expected, since the modeling relies on accurate determination of the contact angles, which is not an easy task.

Once again, core–shell morphology particles were obtained (Figure S1, Supporting Information) when using higher concentrations of PMMA in DCM (2.4%), with and without acetone and with PVA as an emulsifier (see numbers 4 and 5, Table 1).

The particles prepared from emulsions containing 1% of PMAA with no acetone exhibited core–shell morphology. This result was in good agreement with the predicted morphology from the spreading coefficients analysis. In addition, it was also observed that the addition of 5% acetone resulted in core–shell morphology particles, while with 10% of acetone added to the system, no core–shell morphology microcapsules existed. This phenomenon may be due to too strong a disturbance in the oil phase. Figure S2, in the Supporting Information, shows phase

Table 2. Contact angles (θ) and interfacial tensions (γ) for the different emulsifiers employed between o-oil, w-water, and p-polymer phases.

Emulsifier [E]	θ_{op} [°]	θ_{pw} [°]	$\gamma_{o\text{-air}}$ [mN m^{-1}]	$\gamma_{E\text{-air}}$ [mN m^{-1}]
1% PVA	<5	64.8	29.7	42.7
1% PMAA	<5	52.5	29.7	66.5

Table 3. Measured interfacial tensions (γ) and calculated spreading coefficients (S) for the different systems according to Equation (2)–(4) as well as the predicted and observed morphologies.

Oil (o)	Aq. emulsifier [w]	γ_{ow} [mN m^{-1}]	γ_{op} [mN m^{-1}]	γ_{pw} [mN m^{-1}]	S_o	S_w	S_p	Predicted morphology	Observed morphology
HMS-301	1% PVA	18.1	11.5	23.1	<0	<0	<0	Acorn	Core–shell
HMS-301	1% PMAA	31.4	11.5	18.9	<0	<0	>0	Core–shell	Core–shell

*Loxley and Vincent.[20]

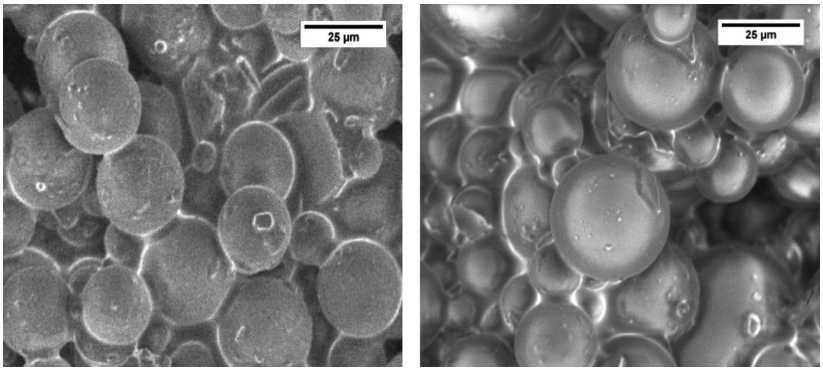

Figure 2. SEM photomicrographs of the PMMA microcapsules prepared with 1% PMMA in the DCM and 1% PVA as an emulsifier (numbers 1, 2, and 3, as shown in Table 1).

separation between the cross-linker and PMMA in a 5% PMAA solution. PMMA forms droplets and the cross-linker forms droplets on its own as well, which means that there is no coalescence and that they are immiscible at that point. The reason for such an event may be related to a decrease in interfacial tension between the cross-linker and the water, which eventually leads to phase separation.

Baum et al.[31] reported that the addition of a water-soluble co-solvent (such as acetone) to an oil phase resulted in smaller droplets when the solution was emulsified. They also found that the addition of acetone not only reduced average droplet diameter, but also caused a narrowing of droplet size distribution.

Nevertheless, we observed that addition of acetone into an oil phase and type of emulsifier do not influence significantly on the microcapsules size. Diameter of all microcapsules formulations falls between 3 and 40 μm with the average diameter around 20 μm. Figure 3 shows size distribution of microcapsules formulations 1–3 from Table 1.

3.2. ATR-FTIR Study

The formation of PMMA microcapsules with a silicone liquid core was confirmed by employing ATR-FTIR spectroscopy. In Figure 4, the spectra for commercial PMMA, commercial HMS-301 and the PMMA microcapsules synthesized by using 1% PVA as an emulsifier are shown. In the PMMA microcapsule spectrum, a carbonyl-stretching absorption band at 1 726 cm^{-1} of the ester group of PMMA is observed. Bands at 1 483, 1 435, and 1 387 cm^{-1} are also related to PMMA as well as the band at 1 146 cm^{-1}, which corresponds to the C—O (ester bond) stretching vibration of PMMA. We also observe a peak at 2 156 cm^{-1}, which is attributed to hydride vibrations (Si—H) and corresponds to the silicone liquid core (HMS-301).[29] In addition, the bands at 1 412 and 1 259 cm^{-1} are related to the asymmetric and symmetric deformations of the methyl group attached to the silicone atom (Si—CH_3) of the HMS-301, respectively. Finally, the peak at 1 024 cm^{-1} corresponds to Si—O—Si stretching vibrations, and the peak at 797 cm^{-1} is ascribed to Si—C stretching vibrations. Through ATR-FTIR spectroscopy, variations in the intensity of the bands related to PMMA and HMS-301 were also investigated, with different forces applied on the same PMMA microcapsule sample (see Supporting Information, Figure S3). No evidence of hydroxyl groups (OH) in the region of 3 300 cm^{-1} from the emulsifier (PVA) was detected via IR spectroscopy. The cross-linker is supposed to be inside the capsules, so in order

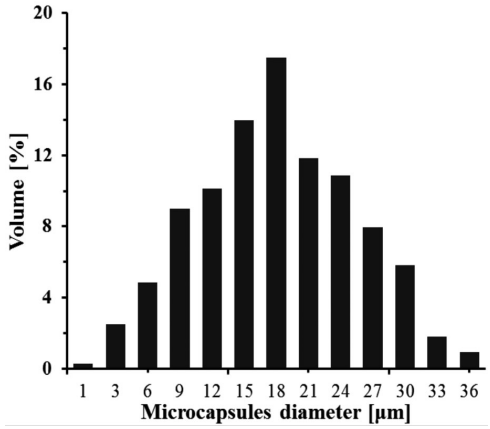

Figure 3. Size distribution of microcapsules (Table 1, sample numbers 1–3).

to verify this morphology, a force was applied gradually to the PMMA microcapsules to evaluate if a stronger cross-linker (Si—H peak at 2 156 cm^{-1}) signal could be detected.

The FT-IR spectrometer has a maximum force gauge of ≈115 N. Unexpectedly, we observed that for absorption bands related to PMMA (at 1 724, 1 483, 1 435, 1 387, and 1 146 cm^{-1}) the higher the force applied, the higher the intensity of the bands. The opposite result was observed for peaks ascribed to the cross-linker (HMS-301) (at 2 156, 1 259, 1 024, and 797 cm^{-1}), meaning that the higher the force applied, the lower the intensity of the absorption bands (Figure S3, Supporting Information). This indicates that the PMMA does indeed cover the cross-linker (HMS-301) and achieves this so efficiently that the cross-linker is not squeezed out of the capsules at high forces.

In addition, the fact that we observe the peak related to the cross-linker (Si—H) in the PMMA microcapsule

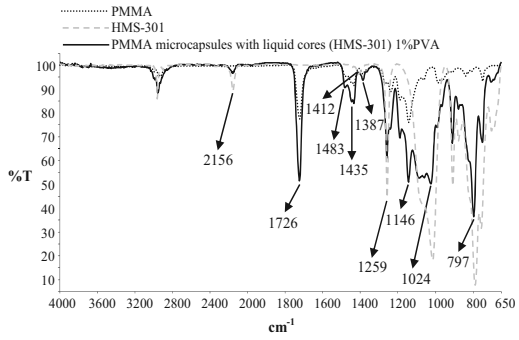

Figure 4. ATR-FTIR spectra of PMMA, HMS-301, and PMMA microcapsules with silicone liquid cores (HMS-301), obtained when using 1% PVA as an emulsifier.

spectrum for any force applied might be due to the limited effective thickness of the shell. This means that either the shell is quite thin – and therefore light can penetrate the PMMA shell – or/and the PMMA is so porous that it also allows the penetration of the light. However, from the results, we may also suspect that the silicone oil core (HMS-301) might be partially distributed on the PMMA surface. Therefore, according to these results, it cannot be concluded from IR studies that the cross-linker resides solely in the interior of the capsule. In order to investigate if the silicone oil core (HMS-301) is partially on the PMMA surface or fully encapsulated by the PMMA shell, microcapsules were washed with heptane. Possible HMS-301 on the PMMA shell should be removed by heptane due to the high solubility of HMS-301 in the liquid, but PMMA will remain since is not soluble in heptane. In Figure S4, Supporting Information, the spectra for PMMA microcapsules, before and after washing with heptane, are shown. From Figure S4, Supporting Information, we observe that the band at 2 156 cm^{-1}, corresponding to the hydride vibrations (Si—H) of HMS-301, is still present, which indicates that HMS-301 is in the core of the capsule and possible traces on the PMMA surface are removed efficiently upon washing with a suitable solvent. In order to determine the content of HMS-301 in the microcapsules after washing, the area of the peak attributed to the hydride vibrations (Si—H) of the cross-linker (at 2 156 cm^{-1}), and the area of the peak at 1 724 cm^{-1} related to the carbonyl stretching absorption of the PMMA's ester group, were integrated (see Table S1, Supporting Information). Areas obtained from the peak attributed to the cross-linker (Si—H) were normalized with those areas obtained from the peak related to PMMA (C═O). The results show that, for all samples, washing removes significant amounts of cross-linker (between 10 and 60%).

Figure S5, Supporting Information highlights spectra for commercial PMMA, commercial HMS-301, and the PMMA microcapsules synthesized from 1% PMAA as an emulsifier. From the spectra, we observe that after washing microcapsules with heptane, the peak at 2 156 cm^{-1} ascribed to the cross-linker was still present, as seen previously.

3.3. Thermal Stability Study

The thermal stability of microcapsules under nitrogen was evaluated via thermogravimetric analysis (TGA). Figure 5a and b shows data for commercial PMMA and HMS-301, as well as microcapsules prepared with 1% PVA and 1% PMAA, respectively.

From the figures, we can observe that PMMA decomposition starts around 289 °C (weight loss ≈5%) and is completed at 430 °C (see also Table 4, entry 1). All thermogravimetric analysis results for the different samples are gathered in Table 4.

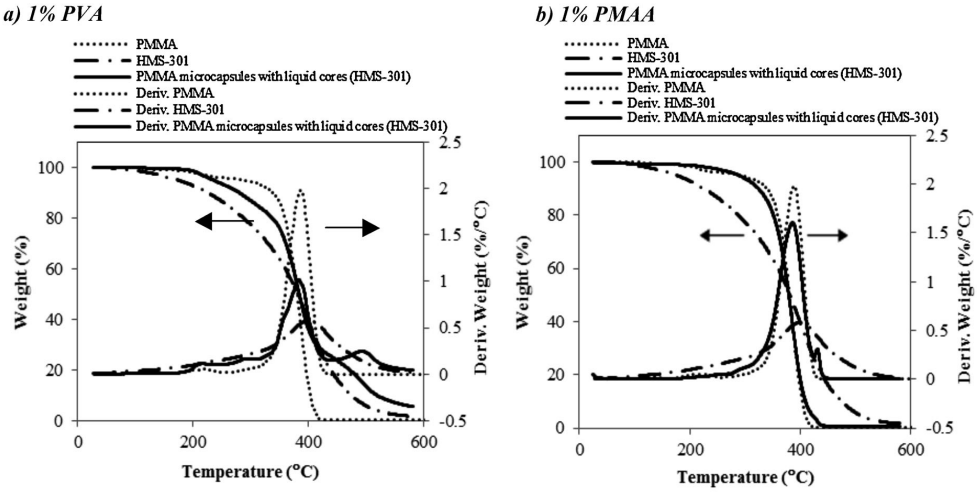

Figure 5. TGA of PMMA, HMS-301, and PMMA microcapsules with a liquid core a) 1% PVA and b) 1% PMAA) during heating at 10 °C min^{-1} in N_2. Both weight loss (←) and first derivative weight loss (→) are shown.

Different decomposition temperatures at a weight loss of 5% were obtained for the microcapsules (see Table 4; entries 4–15). Temperature T_{max}, for the maximum PMMA degradation rate and the cross-linker, occurs at 385 and 400 °C, respectively (see Table 4; entries 1 and 2). The microcapsules showed similar T_{max} values, and moreover temperatures for the maximum degradation rate of microcapsules obtained from PVA or PMAA varied between 380 and 440 °C, with the exception of the sample corresponding to entry 4, where the maximum degradation

Table 4. Thermogravimetric data for the systems studied under N_2.

Entry	Formulation	[PMMA in DCM] [%]	[HMS-301] (%)	[E] (1%)	[Acetone] (5%)	$T_{5\%}$ [a)] [°C]	T_{max} [b)] [°C]	Weight loss at 430 °C [%]	Residue at 430 °C [%]	Residue at 600 °C [%]
1	PMMA	–	–	–	–	289	385	99.7	0.3	0.3
2	HMS-301	–	–	–	–	165	400	69.1	30.9	3.6
3	HMS-301 *(under air)*	–	–	–	–	157	414	63.0	37.0	1.0
4	Capsules	1	1.5	PVA	No	235	382–493	73.2	26.8	5.3
5	Capsules	1	1.5	PVA	No	258	390–441	83.7	16.3	4.5
6	Capsules	1	1.5	PVA	No	246	384	76.6	21.4	5.1
7	Capsules	1	1.5	PVA	Yes	248	380–438	76.9	23.1	11.2
8	Capsules	2.4	3.7	PVA	No	256	385	82.6	17.4	7.1
9	Capsules	2.4	3.7	PVA	Yes	240	386–439	77.4	22.6	4.9
10	Capsules	1	1.5	PMAA	Yes (2.5%)	287	387–431	96.7	3.3	0.7
11	Capsules	1	1.5	PMAA	No	282	387–421	96.3	3.7	0.9
12	Capsules	1	1.5	PMAA	Yes	275	387–432	91.8	8.2	0.7
13	Capsules	2.4	3.7	PMAA	No	257	387–437	85.4	14.6	1.3
14	Capsules	2.4	3.7	PMAA	Yes	284	385–437	89.9	10.1	1.7
15	Capsules	3.3	5.0	PMAA	Yes	246	386–436	94.1	5.9	1.5

E, emulsifier. [a)]Temperature at 5% of weight loss. [b)]Temperature at the maximum degradation rate.

Table 5. Residues at 430 °C for the different binary physical PMMA and cross-linker mixtures.

Entry	[HMS-301] [%]	Residue at 430 °C [%]
1	10	3.5
2	24	9.9
3	28	12.1
4	46	20.1
5	69	35.5

rate varied between 380 and 490 °C. Additionally, the first derivative weight loss curves for both microcapsule samples (prepared with PVA or PMAA) show two separate weights loss processes. These two mechanisms are suggested to be attributed to: i) the degradation of the PMMA shell and ii) the degradation of the cross-linker. Nevertheless, it can also be seen from Figure 5b that these two mechanisms were somewhat overlaid when PMAA was used as an emulsifier. Moreover, the fact that the second mechanism can be attributed to the degradation of the cross-linker could demonstrate that the cross-linker is inside the PMMA shell. Microcapsules obtained from PVA as an emulsifier had higher residues at 430 °C as well as at 600 °C, indicating better thermal stability. Thus, the emulsifier contributes not only to particle formation.

For the TGA study of the content of cross-linker and PMMA as described in the experimental section, the bindary physical mixtures are first analyzed. Residues at 430 °C for the binary physical mixtures are shown in Table 5.

The further analysis of the TGA data (given in Table 6) shows that microcapsules obtained from 1% of PVA had higher cross-linker content than those obtained from 1% of PMAA. Cross-linker content in the microcapsules was also investigated by using additionally two methodologies: ^{1}H NMR spectroscopy and an extraction method. This was done to ensure that the TGA results were not interfered by polymerization, since polymerization reactions caused by radicals may occur. Results from the NMR spectroscopy are gathered in Table 6, according to which we can conclude, in general, that cross-linker content in microcapsules prepared with PVA is higher (ranging from 40 up to 58%).

The data of the contents determination from the extraction method are shown in Table 7, where all three methods are compared. Results for NMR and extraction methods are in good agreement, however, in both microcapsule samples cross-linker content is slightly higher when the extraction method is used.

From these results, we decided to analyze the supposed "empty" microcapsules through IR spectroscopy. From the spectrum, we were able to observe the peak attributed

Table 6. Residues at 430 °C (*r*), *k* values, content of PMMA, and HMS-301 (%) of the systems studied.

n°	Formulation	m_0 PMMA [g]	m_0 HMS-301 [g]	[E] (1%)	Yield of capsules [%]	Residue at 430 °C [%]	*k*	(%) of HMS-301 in capsules (TGA)[a)]	(%) of HMS-301 in capsules (NMR)[b)]
1	PMMA	–	–	–	–	0.3	–	–	–
2	HMS-301	–	–	–	–	30.9	–	–	–
3	HMS-301 (air)	–	–	–	–	37.0	–	–	–
4	Capsules	1.00	1.50	PVA	38	26.8	2.1	56	–
5	Capsules	1.00	1.50	PVA	40	16.3	2.4	39	40
6	Capsules	1.00	1.50	PVA	72	21.4	2.2	48	53
7	Capsules	1.00	1.50	PVA	74	23.1	2.2	51	55
8	Capsules	2.55	3.9	PVA	57	17.4	2.3	41	42
9	Capsules	2.55	3.9	PVA	91	22.6	2.2	50	58
10	Capsules	1.00	1.50	PMAA	46	3.3	2.7	9	16
11	Capsules	1.00	1.50	PMAA	44	3.7	2.7	10	26
12	Capsules	1.00	1.50	PMAA	21	8.2	2.6	21	43
13	Capsules	2.55	3.9	PMAA	44	14.6	2.4	35	50
14	Capsules	2.55	3.9	PMAA	54	10.1	2.5	25	32
15	Capsules	0.26	0.39	PMAA	22	5.9	2.6	15	36

[a)]Percentage (%) of HMS-301 in capsules determined by TGA; the % is calculated by multiplying the residue at 430 °C obtained by TGA by the *k* factor. [b)]Percentage (%) of HMS-301 in capsules determined by ^{1}H NMR spectroscopy.

Table 7. Comparison of the content of PMMA and HMS-301 (%) using the three methods applied in this article: TGA, ^{1}H NMR spectroscopy, and an extraction method.

n°	Formulation	[E] (1%)	Yield of microcapsules [%]	(%) of HMS-301 in capsules (TGA)	(%) of HMS-301 in capsules (NMR)	(%) of HMS-301 in capsules (extraction method)
8	Capsules	PVA	57	41	42	47
13	Capsules	PMAA	44	35	50	51

to the hydride vibrations (Si—H) from the cross-linker, meaning that even after crushing and washing microcapsules with heptane, some cross-linker remained.

4. Conclusion

Microcapsules with a silicone oil core (methylhydrosiloxane dimethylsiloxane, HMS-301) surrounded by a polymeric shell, PMMA have been synthesized by the controlled phase separation of a polymer dissolved within the silicone oil droplets of an oil-in-water emulsion. The theoretical morphology of the micro-particles was investigated by analyzing the contact angles (θ) and interfacial tensions (γ) of two emulsifiers (PVA and PMAA). Interfacial tensions (γ) between the core oil, the polymer shell, and the continuous phase were also investigated. SEM microscopy revealed that all microcapsules prepared in this work exhibited core–shell morphology. Microcapsules prepared from different emulsifiers were characterized by ATR-FTIR. Similar results were observed for the two emulsifiers applied herein (PVA and PMAA). IR spectroscopy also showed that the PMMA efficiently covered the cross-linker (HMS-301) and that the cross-linker was not squeezed out of the microcapsules when high forces were applied by the IR instrument. Finally, cross-linker content (HMS-301) in the microcapsules was assessed by three methods: TGA, ^{1}H NMR spectroscopy, and an extraction method. TGA turned out to be an unsuitable method for our systems, since polymerization reactions caused by formed radicals may occur from system to system. ^{1}H NMR spectroscopy was considered the most accurate technique for investigating cross-linker content in microcapsules.

Received: January 21, 2014; Revised: April 5, 2014; Published online: May 16, 2014; DOI: 10.1002/mame.201400020

Keywords: microcapsules; oil-in-water emulsion; PMMA shell; silicone liquid core

[1] *Microspheres, Microcapsules & Liposomes* (Ed., R. Arshady), Plenum, New York **1998**.
[2] E. Mathiowitz, M. R. Kreitz, L. Brandon-Peppas, *Encyclopedia of Controlled Drug Delivery. Microencapsulation*, Wiley, New York **1999**, pp. 493–504.
[3] L. González, M. Baoguang, S. Hvilsted, A. L. Skov, *Macromol. Mater. Eng.* **2013** DOI 10.1002/mame.201300319.
[4] M. Baoguang, L. González, S. Hvilsted, A. L. Skov, submitted.
[5] L. Janssen, K. Tenijenhuis, *J. Membr. Sci.* **1992**, *65*, 59.
[6] G. Lambert, E. Fattal, H. Pinto-Alphandary, A. Gulik, P. Couvreur, *Pharm. Res.* **2000**, *17*, 707.
[7] N. A. Fallouh, L. Roblot-Treupel, H. Fessi, J. Ph. Devissaguet, F. Puisieux, *Int. J. Pharm.* **1986**, *28*, 125.
[8] M. Fresta, G. Cavallaro, G. Giammona, E. Wehrli, G. Puglisi, *Biomaterials* **1996**, *17*, 751.
[9] N. Munshi, K. Chakarvorty, T. K. De, A. N. Maitra, *Colloid Polym. Sci.* **1995**, *273*, 464.
[10] N. Leelarasamee, S. A. Howard, C. J. Malanga, J. K. H. Ma, *J. Microencapsul.* **1988**, *5*, 147.
[11] E. Mathiowitz, H. Bernstein, S. Giannos, P. Dor, T. Turek, R. Langer, *J. Appl. Polym. Sci.* **1992**, *45*, 125.
[12] X. Shi, F. Caruso, *Langmuir* **2001**, *17*, 2036.
[13] K. J. Pekarek, J. S. Jacob, E. Mathiowitz, *Nature* **1994**, *367*, 258.
[14] G. Crotts, T. G. Park, *J. Control. Release* **1995**, *35*, 91.
[15] S. Benita, *Microencapsulation: Methods and Industrial Applications*, Dekker, New York **1996**.
[16] A. P. Esser-Kahn, S. A. Odom, N. R. Sottos, S. R. White, J. S. Moore, *Macromolecules* **2011**, *44*, 5539.
[17] A. Sari, A. Cemil, A. Karaipekli, O. Uzun, *Solar Energy* **2009**, *83*, 1757.
[18] A. Sari, A. Cemil, A. Karaipekli, *Appl. Energy* **2010**, *87*, 1529.
[19] L. Sánchez-Silva, J. F. Rodríguez, A. Romero, A. M. Borreguero, M. Carmona, P. Sánchez, *Chem. Eng. J.* **2010**, *157*, 216.
[20] A. Loxley, B. Vincent, *J. Colloid Interface Sci.* **1998**, *208*, 49.
[21] N. Zydowicz, P. Chaumont, M. L. Soto-Portas, *J. Membr. Sci.* **2001**, *189*, 41.
[22] A. Laguecir, Y. Frere, L. Danicher, M. Burgard, *Eur. Polym. J.* **2002**, *38*, 977.
[23] A. Bartkowiak, D. Hunkeler, *Chem. Mater.* **2000**, *12*, 206.
[24] Y. Yamaguchi, M. Takenaga, A. Kitagawa, Y. Ogawa, Y. Mizushima, R. Igarashi, *J. Control. Release* **2002**, *81*, 235.
[25] S. Torza, S. G. Mason, *J. Colloid Interface Sci.* **1970**, *33*, 67.
[26] G. L. Gaines, *Polym. Eng. Sci.* **1972**, *12*, 1.
[27] L. Yuan, G. Z. Liang, J. Q. Xie, L. Li, J. Guo, *Polymer* **2006**, *47*, 5338.
[28] F. M. Lavergne, D. Cot, F. Ganachaud, *Langmuir* **2007**, *23*, 6744.
[29] J. Coates, *Interpretation of Infrared Spectra, A Practical Approach. Encyclopedia of Analytical Chemistry*, John Wiley and Sons, Chichester **2000**, pp. 10815–10837.
[30] Q. Li, A. K. Mishra, N. H. Kim, T. Kulia, T. Lau, K. Lee, J. H. *Composites: Part B* **2013**, *49*, 6.
[31] G. Baum, R. Bachmann, W. Sliwka, *UK Patent 1,375,118*, **1974**.

Supplementary Information

Preparation and Characterisation of Silicone Liquid Core/Polymer Shell Microcapsules via Internal Phase Separation

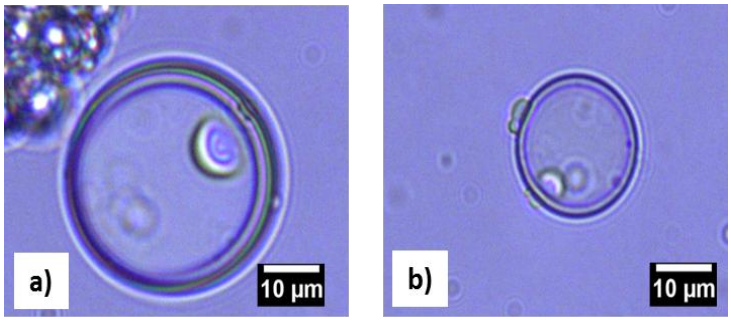

Figure A1. Optical photomicrographs of the PMMA microcapsules prepared with 2.4% PMMA in DCM and 1% PVA as an emulsifier, (a) without and (b) with 5% of acetone.

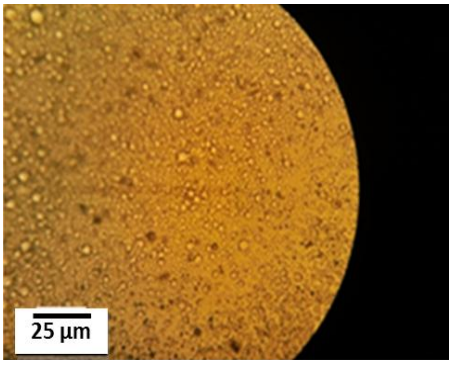

Figure A2. Optical microscope image of PMMA microcapsules, showing the phase separation of the cross-linker and PMMA.

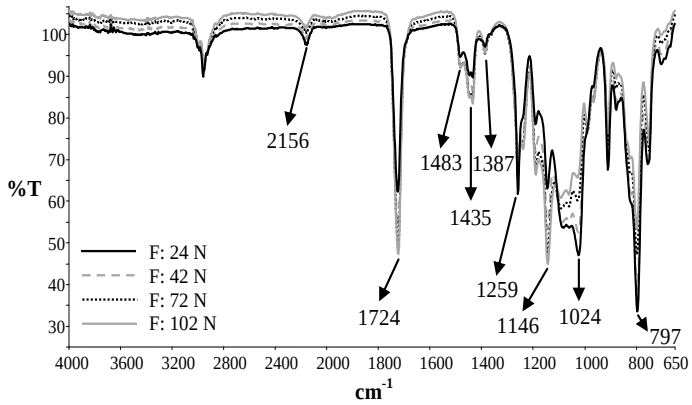

Figure A3. ATR-FTIR spectra of PMMA microcapsules with silicone liquid cores (HMS-301), with different forces applied.

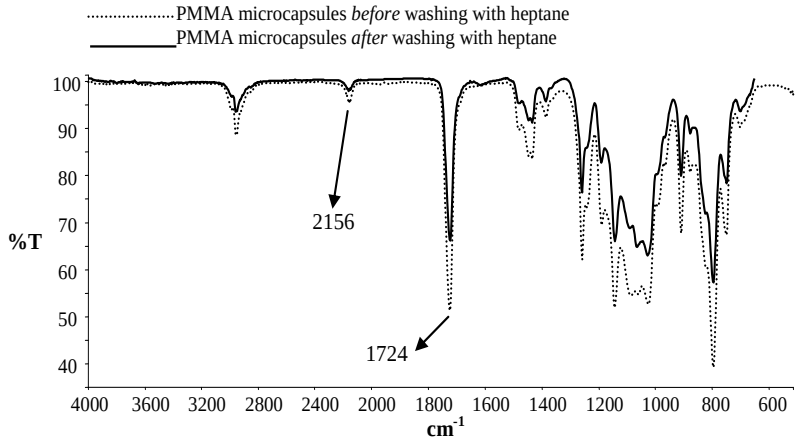

Figure A4. ATR-FTIR spectra of PMMA microcapsules with liquid cores (HMS-301), before and after washing with heptane.

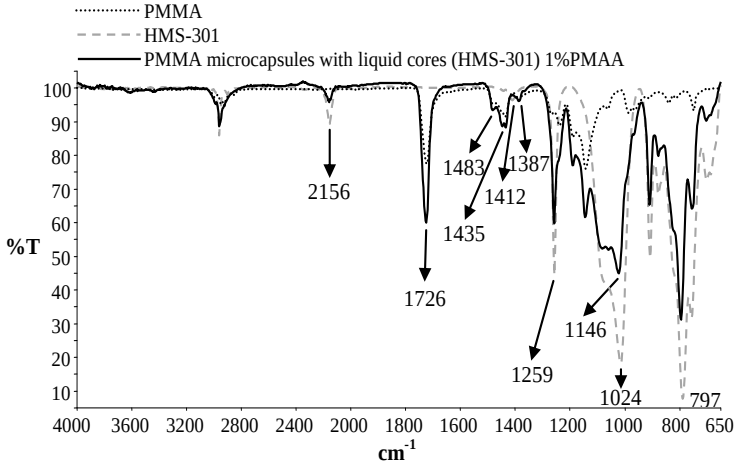

Figure A5. ATR-FTIR spectra of PMMA, HMS-301 and PMMA microcapsules with silicone liquid cores (HMS-301), obtained when using 1% PMAA as an emulsifier.

Table A1. Integration of bands related to HMS-301 and PMMA, before and after washing PMMA microcapsules (1% PVA) with heptane and with different forces (F) applied to the capsules.

	$A_{HMS-301}$ (2160 cm^{-1})*** ($A.cm^{-1}$)	$A_{HMS-301}$ (1724 cm^{-1})*** ($A.cm^{-1}$)	$\frac{A_{HMS-301}}{A_{PMMA}}$
Before*; F24**	1.15	7.66	0.15
After; F24	0.57	4.64	0.12
Before: F42	0.94	8.63	0.11
After; F42	0.55	5.61	0.10
Before; F72	0.73	10.28	0.07
After; F72	0.51	12.14	0.04
Before; F102	0.95	8.52	0.11
After; F102	0.47	12.15	0.04

*Before and after washing the product with heptane (~400ml)

**F means the force applied by ATR-FTIR, and the number indicates the strength of the force applied.

***Limits of the integrated peaks are taken from 2291 up to 2054 cm^{-1} (Si-H band) and from 1814 up to 1571 cm^{-1} for (C=O band).

Appendices to Chapter 3

'Controlled release in hard to access places by poly(methyl methacrylate) microcapsules triggered by gamma irradiation' published in *Polymers for Advanced Technologies.*

Research article

polymers advanced technologies

Received: 28 December 2014, Revised: 18 March 2015, Accepted: 21 March 2015, Published online in Wiley Online Library: 4 May 2015

(wileyonlinelibrary.com) DOI: 10.1002/pat.3532

Controlled release in hard to access places by poly(methyl methacrylate) microcapsules triggered by gamma irradiation

Malgorzata Kostrzewska[a], Baoguang Ma[a], Irakli Javakhishvili[a], Jens H. Hansen[b], Søren Hvilsted[a] and Anne L. Skov[a]*

Gamma irradiation was investigated as a triggering stimulus for the activation of poly(methyl methacrylate) (PMMA) microcapsules. PMMA was exposed to varying doses of irradiation and analyzed by differential scanning calorimetry, size-exclusion chromatography, and nuclear magnetic resonance. It was found that the glass transition temperature (T_g) of the polymer decreases at low irradiation doses. Additionally, T_g can be physically adjusted by adding a plasticizer, and both kinds of microcapsules were successfully prepared with non-plasticized and plasticized PMMA shell. Finally, impermeable microcapsules were shown to become permeable after irradiation and release an encapsulated cross-linker, which enables the remotely controlled formation of polydimethylsiloxanes in traditionally unavailable places. Therefore, the activation method has significant implications for industrial application. Copyright © 2015 John Wiley & Sons, Ltd.

Supporting information may be found in the online version of this paper.

Keywords: microcapsules; controlled release; gamma irradiation

INTRODUCTION

Microencapsulation attracts attention mainly because of the way in which it controls release.[1,2] The technique allows for the preparation of innovative materials appearing more frequently in commercial products. For example, medicines programmed to release active substances reduce harmful side effects and frequency of use.[3] Similarly, many cosmetics contain microcapsules in order to achieve prolonged action, for instance, encapsulated volatile fragrances last longer. Other examples of applications and benefits include the masking of unpleasant tastes by the food industry, the controlled release of nutrients in soil for farming, textiles, and self-healing materials.[4,5]

To obtain the desired release rate from microcapsules, the correct form of activation must be chosen. Activation in this case is a process in which the properties of a microcapsule's shell change in order to deliver enclosed material into the surrounding environment. Various sorts of stimuli, such as light, mechanical, thermal, or magnetic exposure, can trigger this release. Hence, the choice of the shell material is dictated by the type of triggering stimulus. For instance, a light-triggered release from a capsule is achieved through the usage of photo-responsive or photo-cleavable groups.[6,7] By adjusting the concentration of photosensitive material in the shell structure, different release rates are achieved. Moreover, mechanical activation is often employed in self-healing resins,[8] where the self-healing mechanism is triggered through the release and reaction of the healing agent in the region of damage. Another example is thermal activation, which leads to the melting of the shell at higher temperatures, thereby resulting in capsule collapse.[9] Furthermore, the activation of magnetically triggered capsules, the most frequently used in drug delivery systems,[10] occurs only in tissues subjected to oscillating magnetic fields, thus allowing for accurate navigation of the drug due to the presence of magnetic nanoparticles.

Poly(methyl methacrylate) (PMMA) has been used widely as a shell material for encapsulating liquid compounds.[11–13] PMMA is brittle and hard below the glass transition temperature (T_g), but it becomes soft and flexible at higher temperatures. Heating microcapsules above the T_g of PMMA leads to the shell melting and thus acts as a triggering stimulus; for instance, the formation of an elastomer network in reservoir rocks may be delayed through the encapsulation of the polydimethylsiloxane (PDMS) cross-linker. In order to use the microcapsules in the oil industry, where temperatures in reservoir rock often reach 50°C, the T_g of the polymer shell should be higher than 50 °C. However, phase change transition should not appear at too high temperatures, in order to ensure fast microcapsule response. As a result, PMMA with the T_g of 60°C seems to be a reasonable choice for such a system. In addition, exposure to another

* *Correspondence to: Anne L. Skov, Danish Polymer Centre, Department of Chemical and Biochemical Engineering, Technical University of Denmark, Søltofts Plads Building 227, 2800 Kongens Lyngby, Denmark. E-mail: al@kt.dtu.dk*

a *M. Kostrzewska, B. Ma, I. Javakhishvili, S. Hvilsted, A. L. Skov*
Danish Polymer Centre, Department of Chemical and Biochemical Engineering, Technical University of Denmark, Søltofts Plads Building 227, 2800, Kongens Lyngby, Denmark

b *J. H. Hansen*
Mærsk Oil Research and Technology Centre, Education City, P. O. Box 210112, Doha, Qatar

external stimulus, which decreases the T_g of the shell, makes microcapsules permeable at lower temperatures.

In this study, gamma irradiation was investigated as a triggering stimulus, because it penetrates through many materials and thus allows for the remote activation of microcapsules in inaccessible places. Moreover, gamma irradiation changes the structure of polymers and consequently influences their T_g. PMMA generally undergoes chain degradation at low irradiation doses, but cross-linking can take place when higher doses are delivered to the material.[14] As a result, the T_g may decrease or increase, respectively. Furthermore, polymers with purposely low M_w designed were examined, because the glass transition temperature of short chain polymers is known to depend strongly on their molecular weight.[15] Chemical and physical modifications were also tested with the aim of promoting chain scission, i.e. to increase the response for a given dose.

EXPERIMENTAL SECTION

Chemicals

Hydride-functional PDMS cross-linker (HMS-301, $M_w = 2000$ g/mol, Gelest, Morrisville, PA, USA), vinyl-terminated PDMS (DMS-V35, $M_w = 49500$ g/mol, Gelest), poly(vinyl alcohol) (PVA, $M_w = 22000$ g/mol, Fluka, Buchs, Switzerland), azo-bis-isobutyronitrile (AIBN, Ventron, Karlsruhe, Germany), and the platinum cyclovinylmethyl siloxane complex (Catalyst 511, Hanse Chemie AG, Monchengladbach, Germany) were used as received. Methyl methacrylate (MMA, Aldrich, Seelze, Germany) was passed through an aluminum oxide column to remove any inhibitor. All other chemicals were acquired from Aldrich and used as received.

Preparation of materials

Non-plasticized poly(methyl methacrylate)

Two kinds of non-plasticized PMMA were examined. Sample named as PMMA_1 is a commercially available polymer, whereas sample labeled as PMMA_2 was synthesized following the procedure: 5.0 g MMA, 20.0 g toluene, 0.35 g AIBN, and 0.36 g thioglycolic acid—a chain transfer agent—were charged to a 50 ml round-bottom flask equipped with a magnetic stirrer and sealed with a rubber septum. The flask was then flushed with nitrogen at room temperature for 15 min, and the reaction was run at 60°C for 24 h under a nitrogen atmosphere. The round-bottom flask was then cooled, and the toluene was removed by a rotary evaporator at room temperature. The material left in the flask was then dissolved in dichloromethane (DCM) and precipitated by hexane. Finally, the precipitated PMMA was washed additionally by hexane until all impurities had been removed.

Fluorinated derivatives—poly (2,2,2-trifluoroethyl methacrylate) with various molecular weights were also synthesized, and the preparation details are described in the supplementary information.

Plasticized poly(methyl methacrylate)

Firstly, PMMA_1 was dissolved in DCM, and various amounts of DBP were added to the solution. After evaporating DCM at room temperature for 2 days, the T_g of plasticized samples were evaluated. The sample with the most suitable T_g was chosen for further analysis and denoted as PMMA_3.

Poly(methyl methacrylate) microcapsules containing a polydimethylsiloxane cross cross-linker

The preparation of microcapsules with PMMA_1 as a shell and a cross-linker core was studied extensively in our research group.[11,16] The phase separation technique was employed as briefly described here: an oil phase was prepared by adding the PDMS cross-linker HMS-301 (1.5 g) to DCM (75 ml), preceded by dissolving PMMA (1 g) in an organic solvent. Afterwards, approximately 77 ml of aqueous emulsifier solution (1% PVA) was charged to a 250 ml conical flask. The aqueous phase was mechanically stirred at 2000 rpm for 2–5 min (Eurostar Digital Ika Labortechnik, Staufen, Germany), and the oil phase was added drop-wise over 60 s to form an oil-in-water emulsion. The agitation was kept for 1 h at around 750 rpm before pouring the emulsion into another 120 ml of the aqueous surfactant solution (1% PVA). The diluted emulsion was rotary evaporated, in order to remove residual DCM. The dispersion of microcapsules was filtered by use of a filtration pump and qualitative filter paper, 413 (particle retention: 5–13 μm). Finally, the product was washed with distilled water (~1.5 l) and dried at room temperature.

Microcapsules with plasticized PMMA shell were prepared analogously via the phase separation technique. Therefore, the oil phase consisted of DCM, PMMA, HMS-301, and DBP.

Gamma irradiation experiments

Each sample weighed approximately 1 g, and the samples were irradiated at room temperature with various doses of gamma rays by using a Cobalt 60 gamma cell at the Center for Nuclear Technologies, Danish Technical University, Risø Campus. The dose rate was approximately 1 Gy s^{-1}. Nominal doses were given as doses to water, and the maximum dose was 10 kGy.

Analytical methods

The glass transition temperature of the shell polymers was measured by employing a DSC Q1000 calorimeter (TA Instruments, New Castle, DE) at heating/cooling rates of 10°C min^{-1}. The samples weighed approximately 2–5 mg. The glass transition temperatures were calculated by means of the second heating scan as the temperature of the halfway point of the jump in heat capacity when the material changed from a glassy to a rubbery state. To investigate the chemical structure of the polymers, ^{1}H NMR characterization was performed on a Bruker 250 MHz spectrometer (Billerica, MA, USA) using $CDCl_3$ as a solvent. All spectra were recorded across 32 scans, while size-exclusion chromatography (SEC) was performed on a Viscotek GPCmax VE-2001 instrument (Worcestershire, UK) equipped with a Viscotek TriSEC Model 302 triple detector using two PLgel mixed-D columns from Polymer Laboratories (Yarnton, UK). Samples were run in tetrahydrofuran at room temperature and at a rate of 1 ml min^{-1}. Scanning electron microscopy (SEM) images were recorded on FEI Inspect S (Hillsboro, OR, USA) on samples that were metallized with gold using a Cressington 208HR Sputter Coater (Watford, UK), and the reactivity of the PMMA microcapsules was examined by using a controlled strain rheometer (Ares G2, TA Instruments). The strain amplitude was 2% and the frequency was kept at 1 Hz, which has previously been shown as a suitable frequency for tracking additional curing silicone.[16] Microcapsules were mixed with DMS-V35 at a mass ratio of 1:10, and the dynamic modulus (G') was measured at different temperatures.

polymers advanced technologies

RESULTS AND DISCUSSION

The addition of plasticizer was explored as an easy and fast method to adjust T_g.[17] Figure 1 shows the T_g of plasticized PMMA_1 with different amounts of DBP.

As expected, plasticized PMMA with DBP possess decreasing T_g with increasing amount of plasticizer. Because the sample with 15% of DBP showed a T_g closest to the desired activation temperature (60°C), it was irradiated and used in the preparation of the microcapsules and since now called as PMMA_3.

Prepared samples were exposed to different irradiation doses, and Table 1 shows the T_g, molecular weights and polydispersity indexes (PDI) of the studied polymers.

The polymers had lower glass transition temperatures after irradiation due to of induced chain scission. Scission is a two-stage process initiated at unsaturated chain ends, and it is followed by random scissions of the backbone.[18] Therefore, in the first stage, molecular weight does not change significantly because the cleavage of the pendant and the end groups takes place. Scission of the main backbone causes observable changes in chain length. Because the molecular weights of irradiated samples did not change significantly, it is assumed that end-chain degradation mainly took place. Additionally, Fig. 2 presents ^{1}H NMR spectra of sample PMMA_1 before and after irradiation. The PMMA gives four main resonances in the ^{1}H NMR spectrum.

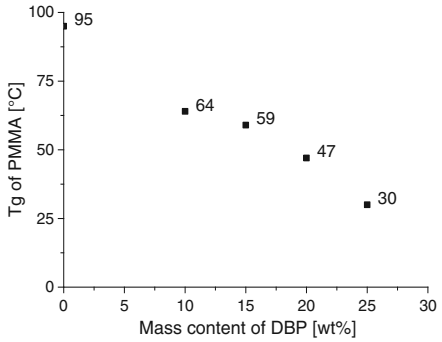

Figure 1. T_g of PMMA_1 containing various plasticizer concentrations. PMMA, poly(methyl methacrylate).

Signals at 0.7 and 1 ppm correspond to the protons of the methyl groups attached to the carbon of the backbone of the PMMA. The peak at 1.7 ppm is attributed to the protons of the methylene groups from the backbone, and the peak at ~3.5 ppm refers to the protons of the methyl groups attached to the ester groups of the side chains of the PMMA. Peaks attributed to a double bond of MMA are also observed in the spectrum at 5.5 and 6.0 ppm for both irradiated and non-irradiated samples. Integration of the signals indicated that the amount of the monomer in the sample decreased during the irradiation due to volatility of MMA. It means that presence of the residual monomer did not influence on the decrease of T_g. This could have been plausible factor for the decrease because monomers are main degradation products of PMMA.[18] Data show that the structure of PMMA did not change significantly, what confirmed our assumptions that a slight change in chain length was sufficient to influence polymer properties.

At the highest irradiation doses, T_g started to increase slightly because of a cross-linking reaction.[19] When the concentration of degradation products increases, the possibility that macroradicals will recombine with each other also increases. Since PMMA monomers are very susceptible to free radical polymerization, products formed during the degradation process cross-link with each other. Therefore, the glass transition temperature of the PMMA increased.

Irradiated sample PMMA_3 behaved similarly to the non-plasticized sample. In both cases, the lowest T_g was observed at 1.6 kGy and started to increase at higher doses. Nevertheless, the influence of irradiation was less noticeable for the plasticized samples, as plasticizers protect polymer compositions against chain scission. For instance, aromatic groups have the ability to effectively degrade absorbed energy and increase the radiation stability of a mixture.[20,21] Furthermore, plasticizers act as lubricants between adjacent polymer chains and allow for greater molecular movement. This increased mobility of chains leads to a higher rate of migration of free radicals, which in turn increases the possibility of radical collision. Therefore, the impact of irradiation on T_g was less noticeable for the plasticized sample, although PMMA degradation did take place.

Fluorinated derivatives were also exposed to gamma irradiation, but no clear relationship between the irradiation dose and T_g was observed. All experimental details are presented in the supplementary information.

Table 1. Glass transition temperatures and molecular weights of non-irradiated and irradiated polymers

Absorbed dose [kGy]	PMMA_1		PMMA_2		PMMA_3	
	T_g [°C]	M_w [g/mol]	T_g [°C]	M_w [g/mol]	T_g [°C]	M_w [g/mol]
0	95	15,000 PDI 2.3	58	2000* PDI 1.6	59	15,000* PDI 2.5
0.3	92	14,500	53		—	
0.5	90	15,000	54		—	
0.8	86	14,000	47		60	
1.6	83	13,500	46		52	
10	89	13,500	53		57	

*Size-exclusion chromatography (SEC) calibration was done for standard PMMA, poly(methyl methacrylate (PMMA) molecular weights. Therefore, SEC results are presented only for PMMA_1, because sample PMMA_2 has a very low molecular weight, and plasticized sample is a mixture of two components.

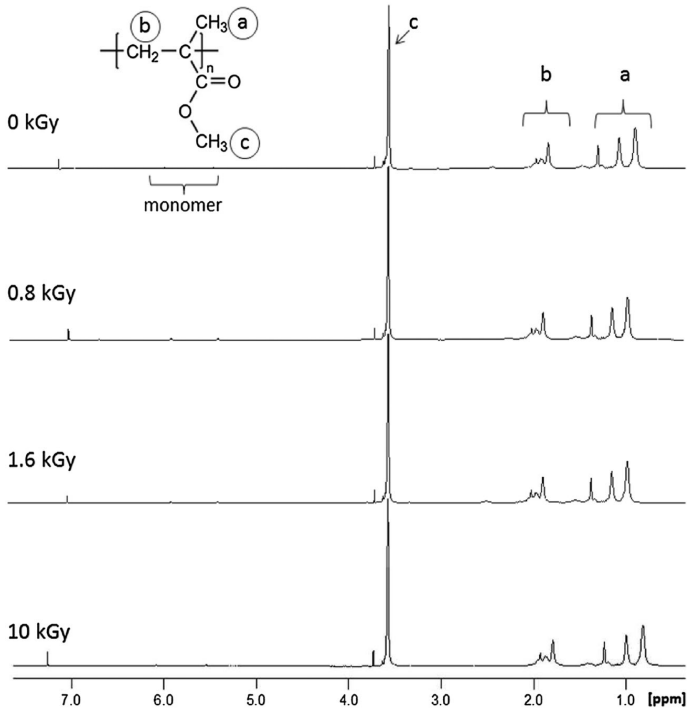

Figure 2. ^{1}H NMR spectra of PMMA_1. PMMA, poly(methyl methacrylate).

Poly(methyl methacrylate) microcapsules containing a polydimethylsiloxane cross-linker

Microcapsules with a non-plasticized PMMA_1 and a plasticized PMMA_3 shell containing a high viscosity PDMS cross-linker agent were prepared using the phase separation technique. Figure 3 presents SEM photos of the capsules. The diameter of the microcapsules falls between 3–40 μm, with the average size at around 20 μm, while the mass content of the encapsulated cross-linker, determined by the ^{1}H NMR method, was approximately 50%.[11]

The presence of DBP in the microcapsule shells was verified by ^{1}H NMR analysis, and the spectra of the microcapsules are shown in Fig. 4. The ^{1}H NMR spectrum of the plasticized microcapsules should show resonances attributed to the PMMA, cross-linker, and DBP. Peaks attributed to hydrogens in a PMMA structure were previously described. A spectrum of the cross-linker shows peak at 4.7 ppm, which is assigned to the hydrogens attached to the silicon atom, and the peak at 0 ppm corresponds to the protons of the methyl groups linked to the silicone atom. A spectrum of DBP shows six peaks. Resonances at 7.7 and 7.5 ppm are ascribed to protons in the DBP aromatic group. At 4.3 ppm, there is a signal arising from the metoxy protons of the butoxy group. Two peaks at 1.7 and 1.4 ppm come from protons in -CH_2- groups, and a resonance at 1 ppm is ascribed to the protons from the methyl group. As a spectrum of microcapsules with plasticized shell shows all these peaks, it proves that DBP was incorporated into the shell. The chemical structure of the microcapsule was also inferred from the Fourier transform infrared spectroscopy studies.[11] No evidence of hydroxyl groups in the

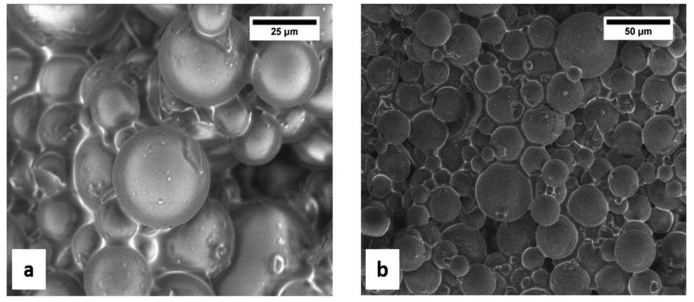

Figure 3. Scanning electron microscopy photos of microcapsules with (a) a non-plasticized and (b) a plasticized PMMA_1 shell. PMMA, poly(methyl methacrylate).

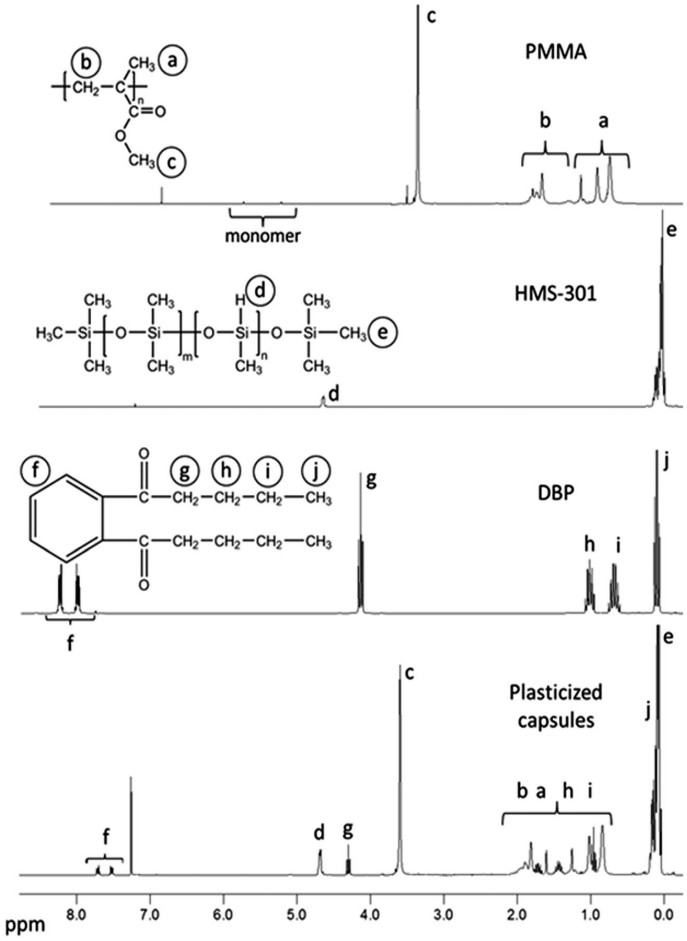

Figure 4. ^{1}H NMR spectra of microcapsules plasticized shells and the components. PMMA, poly(methyl methacrylate).

region of three 300 cm^{-1} from the emulsifier (PVA) was detected via infrared spectroscopy, meaning that all PVA was washed out during purification step.

Adding plasticizer did not influence the preparation process of the microcapsules. Because DBP is soluble in DCM and miscible with PMMA, plasticized PMMA microcapsules were successfully prepared.

Activation of the microcapsules

Microcapsules with a PMMA_1 shell were exposed to a 1.6 kGy dose, and their reactivity with DMS-V35 was examined by using a controlled strain rheometer. The dynamic moduli of the mixture were measured at different temperatures; the results of which are presented in Fig. 5. Non-irradiated microcapsules reacted with DMS-V35 at 100°C, and a significant increase in storage modulus was observed. PMMA passes through phase change transition at 95°C, and microcapsules become permeable. Below 100°C, the microcapsules were relatively stable because only minor changes in G′ were observed—the remaining cross-linker on the surface of the shell could be a reason for this result. Although the storage modulus increased below T_g of the PMMA, it is evident that the cross-linking reaction took place mainly at 100°C. On the other hand, a dramatic increase in G′ was observed at 30°C for irradiated microcapsules despite the

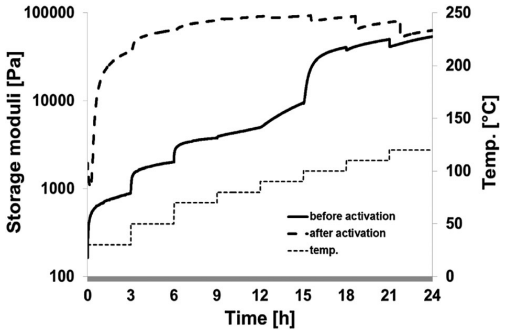

Figure 5. The reactivity of PMMA_1 microcapsules with vinyl-terminated polydimethylsiloxane before and after irradiation. The mass ratio between the compounds was 1:10, respectively. PMMA, poly(methyl methacrylate).

fact that the PMMA T_g was around 80°C, which means that not only does the T_g of polymer changes during irradiation but also local heating effects can affect the local structure of the PMMA shell.

CONCLUSIONS

This paper presents a comprehensive study of the potential application of gamma irradiation as a triggering stimulus for PMMA microcapsule remote activation. It was found that PMMA undergoes chain degradation at small doses of gamma irradiation, and therefore the glass transition temperature is decreased. The effect of chain degradation is more noticeable for PMMA with relatively low molecular weight. Moreover, physical modification of the microcapsules' shell by adding plasticizer allows for the easy and fast control of the initial T_g of the microcapsule shell.

Secondly, the reactivity of microcapsules with DMS-V35 shows that a cross-linking reaction takes place with high efficiency after γ-irradiation activation. Before activation, microcapsules are stable at a wide range of temperatures, but when they are exposed to gamma irradiation, an encapsulated cross-linker releases at lower temperatures, and an elastomer network is created. Therefore, two main advantages of the usage of the γ-irradiation stimulus are the possibility of remotely activating microcapsules in unreachable places and a significant decrease in activation temperature.

Acknowledgements

The authors would like to thank Arne Miller and Jim Thorslund Andersen from the Center for Nuclear Technologies at DTU for helping with the radiation experiments. This project was financially supported by Mærsk Oil & Gas Research, Qatar.

REFERENCES

[1] A. Abbaspourrad, S. S. Datta, D. A. Weitz, *Langmuir* **2013**, *29*, 12697–12702.
[2] S. Zhang, Y. Zhou, W. Nie, L. Song, J. Li, B. Yang, *J. Mater. Chem.* **2013**, *1*, 4331–4337.
[3] S. H. Hu, C. H. Tsai, C. F. Liao, D. M. Liu, S. Y. Chen, *Langmuir* **2008**, *24*, 11811–11818.
[4] A. P. Esser-Khan, S. A. Odom, N. R. Sottos, S. R. White, J. S. Moore, *Macromolecules* **2011**, *44*, 5539–5553.
[5] Y. Taguchia, N. Saitoa, K. Fuchigamib, M. Tanakaa, *Polym. Adv. Tech.* **2014**, *25*, 41–47.
[6] T. Dispinar, C. A. L. Colard, F. E. Du Prez, *Polym. Chem.* **2013**, *4*, 763–772.
[7] E. M. Rosenbauer, M. Wagner, A. Musyanovych, K. Landfester, *Macromolecules* **2010**, *43*, 5083–5093.
[8] Z. Yang, Z. Wei, L. Le-ping, W. Si-jie, L. Wu-jun, *Appl. Surf. Sci.* **2012**, *258*, 1915–1918.
[9] J. Abedi-Koupai, J. Varshosaz, M. Mesforoosh, A. Hossein Khoshgoftarmanesh, *J. Plant Nutr.* **2012**, *35*, 1130–1138.
[10] D. Qiu, X. An, *Colloids Surf. B* **2013**, *104*, 326–329.
[11] L. Gonzalez, M. Kostrzewska, M. Baoguang, L. Li, J. H. Hansen, S. Hvilsted, A. L. Skov, *Macromol. Mater. Eng.* **2014**, *299*, 1259–1267.
[12] A. Loxley, B. Vincent, *J. Colloid Interface Sci.* **1998**, *208*, 49–62.
[13] M. Li, O. Rouaud, D. Poncelet, *Int. J. Pharm.* **2008**, *363*, 26–39.
[14] I. Y. Al-Qaradawi, D. A. Abdulmalik, N. K. Madi, M. Almaadeed, *Phys. Stat. Solidi* **2007**, *4*, 3727–3730.
[15] X. Lu, B. Jiang, *Polymer* **1991** *32*, 471–478.
[16] B. Ma, J. H. Hansen, S. Hvilsted, A. Skov, *RSC Adv.* **2014**, *4*, 47505–47512.
[17] G. M. Vinhas, R. M. Souto-Maior, C. M. Lapa, Y. Medeiros Bastos de Almeida, *Mater. Res.* **2003**, *6*, 497–500.
[18] M. A. Rauf, I. C. McNeillt, *Polym. Degrad. Stabil.* **1993**, *40*, 263–266.
[19] E. H. Lee, G. R. Rao, L. K. Mansur, *Radiat. Phys. Chem.* **1999**, *55*, 293–305.
[20] E. Choi, D. J. T. Hill, K. Y. Kim, J. H. O'Donnell, P. J. Pomery, *Polym. Adv. Tech.* **1998**, *9*, 52–61.
[21] E. R. Booser, W. W. Gardner, *CRC Handbook of Lubrication (Theory and Practice of Tribology), Volume I—Application and Maintenance*, Taylor & Francis Group, Boca Raton, **2006**.

SUPPORTING INFORMATION

Additional supporting information may be found in the online version at the publisher's web-site.

Supplementary Information

Controlled Release in Hard-to-access Places by PMMA Microcapsules triggered by Gamma Irradiation

1. Introduction

Polymer fluorination is known to increase sensitivity to gamma irradiation. Therefore, fluorinated derivatives of PMMA were synthesised and exposed to gamma irradiation, in order to investigate the fluorination effect on the glass transition temperature. Capsules could not be obtained from fluorinated PMMA, and thus the materials were omitted from the main manuscript.

2. Chemicals

Azo-bis-isobutyronitrile (AIBN, Ventron) was used as received, whereas trifluoroethyl methacrylate (F3EMA, Aldrich) was passed through an aluminum oxide column to remove any inhibitor. All other chemicals were acquired from Aldrich and used as received.

3. Experimental part

Samples 3F-PMMA_1 and 3F-PMMA_2, both of which have different molecular weights, are fluorinated derivatives of PMMA - poly(2,2,2-trifluoroethyl methacrylate). Preparation details for the 3F-PMMA_1 sample are described as follows. A Schlenk tube equipped with a stirring bar and a rubber septum was charged with 157g of AIBN, 4.2 mL of 2,2,2-trifluoroethyl methacrylate (F3EMA) and 6.5 mL of isoamyl acetate (IAAc). The reaction mixture was stirred and purged with nitrogen for 30 min, and then the tube was immersed in an oil bath for 3 hours at 80°C. Afterwards, the reaction mixture was exposed to air, allowed to cool down to room temperature, diluted with tetrahydrofuran (THF) and precipitated in a methanol-water (3:1) mixture. The polymer was isolated on a filter paper, washed with the methanol-water mixture and dried in a vacuum oven. Reaction conditions for sample 3F-PMMA_2: AIBN (50 mg), F3EMA (4.2 mL) and IAAc (4.2 mL), the reaction mixture, were purged with nitrogen for 45 min. Figure A6 presents the chemical structure of the fluorinated polymer.

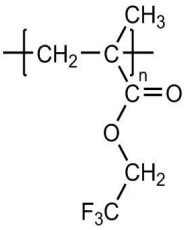

Figure A6. Chemical structure of poly(2,2,2-trifluoroethyl methacrylate).

The irradiation process and analytical methods are reported in the main part of this paper.

4. Results and discussion

In Table A2, the results of the gamma irradiation experiments are presented. The presence of fluorine atoms in a polymer's structure did not clearly enhance chain scission during irradiation.

Table A2. Glass transition temperatures and molecular weights of non-irradiated and irradiated polymers.

Absorbed dose [kGy]	**3F-PMMA_1**		**3F-PMMA_2**	
	T_g [°C]	**M_w [g/mol]**	**T_g [°C]**	**M_w [g/mol]**
0	62	10 000 PDI 2.5	71	22 000 PDI 2.1
0.8	62		63	
1.6	49		74	
10	47		74	

On the one hand, the lowest T_g for the short-chain sample 3F-PMMA_1 was observed at a dose of 10 kGy, indicating that chain scission dominated over cross-linking, even at higher doses, in contrast to non-fluorinated PMMA. On the other hand, the T_g of sample 3F-PMMA_2 decreased at lower doses, but at 10 kGy the T_g was higher than initially, meaning that cross-linking took place with higher efficiency than in the case of PMMA. In order to investigate changes in the chemical structure of the fluorinated polymer, an NMR method was used. Figure A7 presents spectra for the irradiated sample 3F-PMMA_1. Since no new peaks were observed, it was assumed that gamma irradiation did not affect the structure of the polymer significantly. Therefore, there is no conclusive evidence that the fluorination process increases the sensitivity of PMMA to chain scission during gamma irradiation.

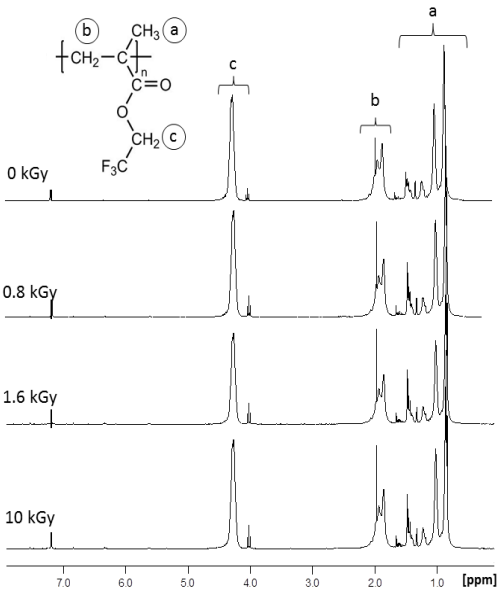

Figure A7. ^{1}H NMR *spectra of the non-irradiated and irradiated 3F-PMMA_1 sample.*

Additionally, some attempts were made to prepare microcapsules with a fluorinated PMMA shell. Fluorinated derivatives are highly hydrophobic and cause significant changes in the oil phase. Since surface tension between the two phases changed agglomerations, lumps or microcapsules with an acorn morphology formed. Although various types and concentrations of surfactants were used for adjusting surface tension, the preparation of capsules with a fluorinated shell was not achieved.

5. Conclusions

Fluorinated derivatives of PMMA with various molecular weights were synthesised. It was found that the presence of a fluorine atom in a polymer chain does not influence chain scission in an unambiguous way. Additionally, microcapsule preparation with a fluorinated shell was not achieved, due to the high hydrophobicity of the polymer. Thereafter, it was concluded that fluorinated PMMA is not a good candidate as a shell material for our purposes.

3.2.4 Microcapsule preparation via a spray technique

Since microcapsules with a fluorinated shell were not obtained via the phase separation technique, another method was applied. A spray technique is a method where an organic phase containing core (HMS-301) and shell materials (3F-PMMA_1) is sprayed directly into methanol, which results in rapid PMMA precipitation and the formation of microcapsules. Table A3 summarises the systems studied herein.

Table A3. Studied organic solutions of the fluorinated 3F-PMMA_1 polymer. The solutions were tested with aim of obtaing microcapsules via spray technique.The HMS-301 concentration was equal to 7.5%.

	Organic solvent	**3F-PMMA_1 concentration [wt%]**
1	DCM	5
2	THF	5
3	Chloroform	5
4	Chloroform	10

Three organic solutions were tested: DCM, THF and chloroform. When 5wt% solutions of 3F-PMMA were used, microcapsules did not form. In all experiments, PMMA precipitated from methanol, creating lumps and aggregations. Single microcapsules were observed only when a chloroform solution was used, but encapsulation efficiency was not sufficient and microcapsules were collected. Since single microcapsules were observed when chloroform was employed, a 10wt% of 3F-PMMA solution in chloroform was examined. Again, single microcapsules were created, but further analysis was not possible, due to a very low yield. Optical microscopy images of the methanol mixtures are presented in Figure A8.

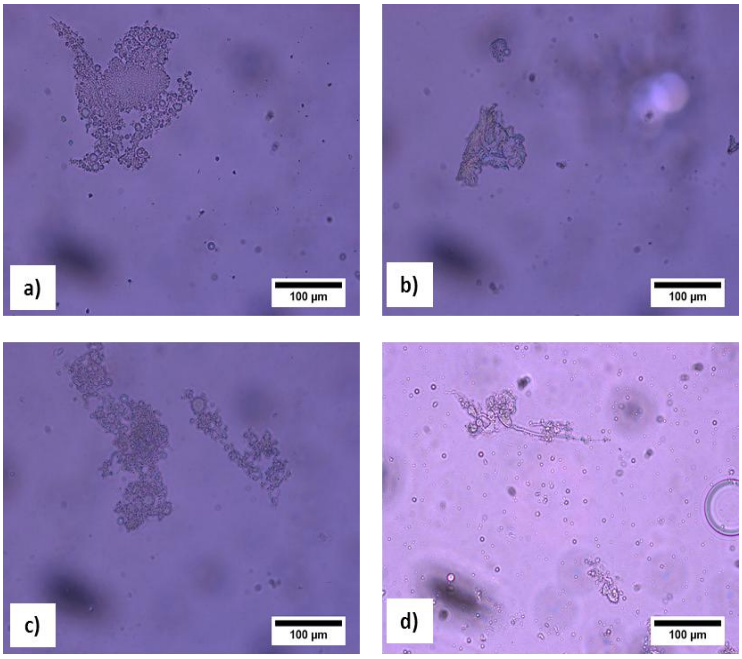

Figure A8. Optical microscope photos of precipitated 3F-PMMA_1 when polymeric solutions were used: a) 5 wt.% in DCM, b) 5 wt.% in chloroform, c) 5 wt.% in THF and d) 10 wt.% in chloroform.

Appendices to Chapter 4

4.1 Preparation of magnetic nanoparticles

Monodispersed Fe_3O_4 nanoparticles were synthesised according the reported reference[97]. Briefly, 0.65 g $FeCl_3$ and 0.20 g trisodium citrate were first dissolved in 20 mL ethylene glycol. Subsequently, 1.2 g NaAc was added under vigorous stirring for 30 min. Then, the dark-yellow mixture was transferred into a Teflon-lined stainless-steel autoclave with a capacity of 50 mL. The autoclave was sealed and heated at 200°C for 10 hours, and then cooled to room temperature. The black products were washed with ethanol and deionised water several times. Finally, the as-prepared Fe_3O_4 nanoparticles were dispersed in deionised water by ultrasonication, to obtain a dispersion of 1 mg/mL. For PDMS modification, a 100 mL Fe_3O_4 dispersion was added into a 250 mL round-bottomed flask. Then, 0.1 g PEG-12 dimethicone (XIAMETER® OFX-0193) was added via mechanical stirring and the reaction proceeded at 30°C for 2 hours in an N_2 atmosphere. Finally, the solution was removed by using a rotary evaporator along with subsequent vacuum drying at 60°C for 24 hours, giving a black solid.

4.3 Preparation and characterisation of microcapsules containing $MnFe_2O_4$ nanoparticles

Microcapsules containing $MnFe_2O_4$ nanoparticles were prepared as follows. An oil phase was prepared by adding 0.25 g of the PMMA, 0.37 g of the HMS-301 and 0.037 g of the $MnFe_2O_4$ magnetic nanoparticles to 20 mL of the DCM. The mixture was then sonicated for 2 hours in an ultrasound bath. Subsequently, the oil phase was added to 150 mL of a 1% PVA emulsifier solution. The oil-in-water emulsion was mechanically stirred for a further 2 hours at around 750 rpm. Thereafter, microcapsules consisting of a PMMA shell and a liquid HMS-301 core with the magnetic nanoparticles were washed with 1L of DI water and dried in a fume hood overnight. Figure A9 presents optical microscopy images of the microcapsules, whereas Figure A10 shows TGA analysis results.

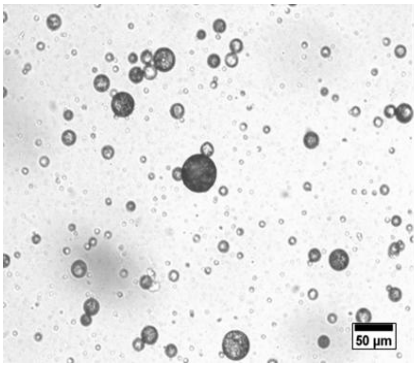

Figure A9. Optical images showing microcapsules with encapsulated $MnFe_2O_4$ nanoparticles.

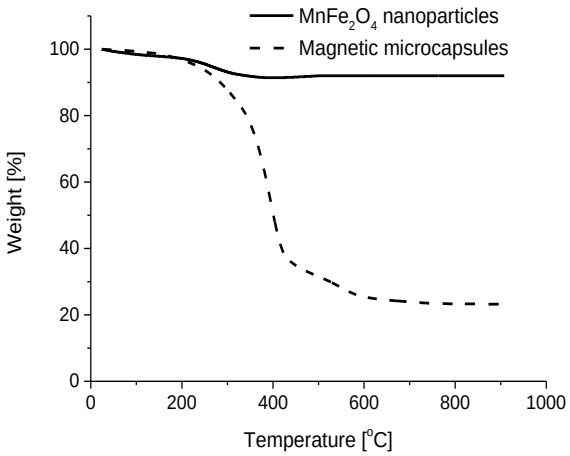

Figure A10. TGA curves of pure $MnFe_2O_4$ nanoparticles and magnetic microcapsules with encapsulated $MnFe_2O_4$.

The mass content of the magnetic nanoparitcles was found to be 23%, while PMMA and HMS-301 content was found to be 43% and 57%, respectively. The NMR method was applied. Taking into consideration TGA and NMR analysis, it was established that 1 g of the microcapsules consisted of 0.23 g of MNP, 0.33 g of PMMA and 0.44 g of HMS-301.

When the microcapsules were exposed to the AMF at various frequencies, the PMMA shell remained intact, and the microcapsules were not magnetically activated.

Appendices to Chapter 6

6.2 Preparation of core samples

Firstly, an aluminum phosphate gel (APG) was prepared according to the following procedure. In total, 50 g of aluminum hydroxide was dispersed in 100 g of 85% phosphoric acid solution in a 500 mL beaker to create a suspension. The suspension was then cured in an oven at 120°C for 1 hour to obtain the APG. After cooling to room temperature, the APG was ready for further use. Subsequently, synthetic core samples were prepared as follows. A mixture composed of 200 g sand and 120 g APG was thoroughly mixed and placed in a 500 mL beaker at 80°C for 24 hours, to remove residual water from the APG. Afterwards, the mixture was poured into a cylindrical iron tube and, when the tube was filled, it was heated to 50°C. The mixture in the iron tube was then subjected to uniaxial pressure of 3 MPa to 5 MPa by means of a hydraulic piston. Pressure was maintained on the mixture for 30 minutes, to ensure that it would bind into a solid that would not disintegrate upon removal from the iron tube. Upon releasing the pressure, the mixture was ejected from the iron tube. The mixture was then further sintered at 500°C for 10 hours to obtain the synthetic core samples. The resulting core samples were then machined at both ends to make flat, smooth surfaces.

Danish Polymer Centre
Department of Chemical and Biochemical Engineering
Technical University of Denmark
Søltofts Plads, Building 229
2800 Kgs. Lyngby
Denmark

Phone: +45 45 25 28 00
Web: www.kt.dtu.dk/